

Utah State University

DigitalCommons@USU

All Graduate Theses and Dissertations

Graduate Studies

5-2006

Lower Paleozoic Sequence Stratigraphy, Deposystems and Paleogeography of Northwestern Ordos Basin, North China

Benjamin J. Kessel
Utah State University

Follow this and additional works at: <https://digitalcommons.usu.edu/etd>



Part of the [Geology Commons](#)

Recommended Citation

Kessel, Benjamin J., "Lower Paleozoic Sequence Stratigraphy, Deposystems and Paleogeography of Northwestern Ordos Basin, North China" (2006). *All Graduate Theses and Dissertations*. 6743.

<https://digitalcommons.usu.edu/etd/6743>

This Thesis is brought to you for free and open access by the Graduate Studies at DigitalCommons@USU. It has been accepted for inclusion in All Graduate Theses and Dissertations by an authorized administrator of DigitalCommons@USU. For more information, please contact digitalcommons@usu.edu.



LOWER PALEOZOIC SEQUENCE STRATIGRAPHY, DEPOSIT SYSTEMS AND
PALEOGEOGRAPHY OF NORTHWESTERN ORDOS BASIN,
NORTH CHINA

by

Benjamin J. Kessel

A thesis submitted in partial fulfillment
of the requirements for the degree

of

MASTER OF SCIENCE

in

Geology

UTAH STATE UNIVERSITY
Logan, Utah

2006

Copyright © Benjamin Kessel 2006

All Rights Reserved

ABSTRACT

Lower Paleozoic Sequence Stratigraphy, Depositional Systems
and Paleogeography of Northwestern
Ordos Basin, North China

by

Benjamin J. Kessel, Master of Science
Utah State University, 2006

Major Professor: Dr. Bradley D. Ritts
Department: Geology

The Ordos basin rests upon the North China Block and is one of the largest sedimentary basins in north China, with more than 15 km of Phanerozoic strata. Published estimates suggest that over 2000 m of carbonates and lesser amounts of siliciclastics were deposited on the North China Carbonate Platform (NCCP) from the Lower Cambrian through the Middle Ordovician. However, lower Paleozoic facies successions and depositional systems of northwestern Ordos basin remain poorly represented in western literature. This paper constrains depositional environments, lithologies, facies relationships and sea-level history of the northwestern part of the North China block (NCB) in an effort to further document the Early Paleozoic geologic history of western Ordos basin.

New stratigraphic data come largely from measured sections in the Zhuozi Shan and Helan Shan in northwest Ordos basin. Strata in the mountains of

northwestern Ordos are divided into eleven lithofacies assemblages, distinguished by lithology, stacking patterns and sedimentary structures. Lithofacies assemblages in northwest Ordos are grouped into four lithostratigraphic units that make up the composite type section. Unit A is dominantly composed of shale and mudrock lithofacies, Unit B is dominantly composed of thin-bedded lime mudstone and banded and bioturbated lime mudstone to wackestone, Unit C is dominantly composed of quartz sandstone and dolostone and Unit D is dominantly composed of fossiliferous packstone. These four units were observed in all lower Paleozoic sections of the Helan Shan and Zhuozi Shan. Deposition of Middle Cambrian through lowermost Lower Ordovician strata in northwest Ordos basin occurred on a storm-influenced, mixed siliciclastic and carbonate, shallow-water ramp. Lateral trends in quartz sandstone, paleokarsts, thrombolites and section thickness suggest that accommodation space increased to the south. The depositional architecture changed in the Middle Ordovician to a carbonate shelf environment. The sea-level history of northwest Ordos shows transgression through the Late Cambrian, regression in the Early Ordovician, followed by a Middle Ordovician transgression, corresponding with North American sea level signatures.

Lower Paleozoic sections in northwest Ordos basin are broadly similar to those previously described in western literature. However, based upon stratigraphic data, shoreline trends of the NCCP model are proved inapplicable to northwest Ordos. There is no evidence for lower Paleozoic tectonics such as aulacogen-controlled subsidence and platform tilting as described by previous workers. The sea-level history interpreted for northwest Ordos basin is more similar to North American

curves than to the North China Carbonate Platform model, suggesting a eustatic control on lithofacies stacking patterns in northwest Ordos basin.

(139 Pages)

CONTENTS

	Page
ABSTRACT.....	iii
ACKNOWLEDGMENTS	vii
LIST OF TABLES.....	viii
LIST OF FIGURES	ix
INTRODUCTION	1
BACKGROUND GEOLOGY	5
Generalized Stratigraphy of Western Ordos Basin.....	5
Tectonic Setting	5
Tectonic History.....	7
Previous Work-Lower Paleozoic	11
Biostratigraphy.....	13
DATA AND RESULTS	16
Study Localities	16
Outcrop and Petrographic Lithologic Observations and Interpretations	17
Stratigraphy.....	55
Age Assignments	70
Paleokarst: Description, Stratigraphic Position and Interpretation.....	74
DISCUSSION.....	79
Depositional Environments and Models.....	79
Sequence Stratigraphy	87
Paleogeography and Lower Paleozoic Tectonic Events	89
Paleokarsts	95
Comparison to the Meng et al. (1997) Model.....	96
Sea Level.....	99
Uncertainties	101
CONCLUSIONS.....	103
REFERENCES	105
APPENDICES	111

APPENDIX A-SOUTHWEST ORDOS RECONNAISSANCE.....	vii
APPENDIX B-DETAILED STRATIGRAPHIC COLUMNS.....	112
	125

ACKNOWLEDGMENTS

This material is based upon work supported by the National Science Foundation under Grants No. EAR-0346816 and EAR-0604443. Additional funding came from generous grants from the American Association of Petroleum Geologists Grants-In-Aid program, and the Evolving Earth Foundation.

I owe many thanks to my advisor Brad Ritts, for the direction in China, and the helpful discussions, guidance, and support back in the United States. I would like to thank W. David Liddell and Peter Kolesar for their questions, comments and helpful reviews throughout this project, which helped immensely. Special thanks go to Carol Dehler (USU), Russell Shapiro (GAU), Charles Mitchell (SUNY-Buffalo), and J. Keith Rigby (BYU) for fossil identification. Undergraduate field support was provided by Kevin Randall and Dustin Keele (both of Utah State University). The most special, field-work “thank you” goes to Scott Friedman for unending support, insightful questions and hard work in the field (and for putting up with constant China-techno, armed forces encounters, dynamite and daily near-death experiences on Chinese highways).

I would like to thank Mindy Lloyd for driving me in the right direction throughout this experience; I couldn’t have done it without you! Last and certainly not least, I would like to thank the USU Geology Department for providing a wonderful environment for graduate students to get together and study what they are passionate about.

Ben Kessel

LIST OF TABLES

Table		Page
1	North China Carbonate Platform Biostratigraphy (Meng et al. 1997).....	14
2	Lithofacies Assemblages, Descriptions and Interpretations	56
3	Quartz Sandstone and Dolomitic Limestone Ratios Per Units C and D.....	66
4	Lithofacies Assemblage Transition Matrices.....	84

LIST OF FIGURES

Figure	Page
1	Shaded region shows the extent of the lower Paleozoic North China Carbonate Platform (NCCP) 2
2	Chronostratigraphic columns for Ordos basin 3
3	Map of Ordos basin and surrounding orogenic belts 6
4	The interpretation that a large, left-lateral, strike-slip fault has dissected the WOFTB, effectively translating the Zhuozi Shan ~60 km north to its present position..... 10
5	Outcrop map of the Zhouzi Shan and Helan Shan of northwestern Ordos Basin, showing field locations of measured sections..... 18
6	A) Mudrock/shale packages with interbedded thin-bedded lime mudstone and intraclastic conglomerate. B) Mudrock/shale lithofacies from WZA section with interbedded, nodular, thin-bedded calcareous siltstone 20
7	A) Argillaceous limestone from WZA section B-Photomicrograph of similar facies showing numerous silt-sized grains of quartz, opaques and one large trilobite fragment 23
8	A) Cross stratification in quartz arenite strata from Xima section. B) Photomicrograph from Suhaitu section 25
9	A) Intraclastic conglomerate lithofacies assemblage from Suhaitu section; note imbricated clasts. B) Intraclastic gutter within thin-bedded lime mudstone beds 27
10	Cartoon depicting the effects of storms on sedimentation 30
11	A) Granule/pebble paleokarst surface with a reddish-brown matrix from Unit C of Suhaitu section. B) Paleokarst breccia in a microbially-laminated lime mudstone from the base of WZA section in Unit A 32
12	A) Thick paleokarst from Unit B at Suhaitu section; hammer is circled for scale. B) Paleokarst below the Middle Ordovician-Middle Carboniferous contact observed ~20 km northeast of WZA section..... 33

13	A) Typical outcrop appearance of thin-bedded, fossiliferous grainstone, from Suhaitu section. B) Photomicrograph of thin-bedded fossiliferous packstone facies assemblage showing oolite content, echinoid plates and trilobite fragments.....	35
14	A) Typical thin-bedded lime mudstone outcrop character from WZA section. B) The association of thin-bedded lime mudstone with banded and bioturbated units and intraclastic conglomerate (I.C.)	37
15	Microbial mounds of northwestern Ordos basin. A) Microbial mound in thin-bedded lime mudstone from unit B of WZA section. B) Large microbial mound within thin-bedded lime mudstone from Unit B of Xima section	40
16	A) Association of banded and bioturbated facies with scoured intraclastic conglomerate and thin-bedded lime mudstone. B) and C) Typical banded and bioturbated outcrop character from Suhaitu and WZA sections, respectively	43
17	A) Bedding-plane view of fossiliferous, massive, packstone to grainstone with gastropod, bryozoan, and brachiopod fossil fragments. B) Photomicrograph of blue-gray fossiliferous packstone to grainstone facies with abundant pelloids, intraclasts and quartz silt grains.....	45
18	Bedding plane photos of <i>Craterospongia sinica</i> , a new genus and species of Middle Ordovician sponge. A) Individual specimen. B) Two individuals; note cross section	47
19	A) Outcrop of glauconitic, oolitic grainstone, younging direction is to the left. B) Photomicrograph showing glauconite (g) “roses”, ooids nucleating upon trilobite fragments and a silty matrix	49
20	A) Typical outcrop appearance of dolomitic lithofacies from Xima section. B) Bedding plane view of dolomitized intraclastic conglomerate, also from Xima	52
21	A) Laminated, totally recrystallized, dolostone. B) Grain-rich bed in which dolomitization is occurring along the periphery of larger, hyolithid grains and micritic intraclasts.....	54
22	Composite type section of northwestern Ordos basin.....	57
23	Measured section data from most complete (primary) sections	60

24	A) Cycle of thin-bedded lime mudstone capped by intraclastic conglomerate from Suhaitu section. B) Intraclastic conglomerate overlain by thin-bedded lime mudstone. Bedding is parallel to vertical direction of the photo	61
25	A) Large-scale sequence from Xima section showing more argillaceous units capped by strata rich in oolitic grainstone. B) Sequences from Suhaitu section showing an upward progression from thin-bedded lime mudstone and intraclastic conglomerate to banded and bioturbated units.....	63
26	A) Meter scale cycle of sandstone, and sandy limestone, capped by limestone as exposed at Xima section. B) Larger scale example of similar transition from WZA section	68
27	A) <i>Rafinesquina sp.</i> brachiopods which indicate Middle Ordovician age. B) Graptolites from a black shale unit in the southern Zhuozi Shan	72
28	A-Angular relationships between Middle(?) Ordovician and Carboniferous. B-Sub-unconformity paleokarst character	75
29	Depositional models proposed for carbonate ramp environments of northwest Ordos basin	81
30	Block diagrams depicting depositional environments and platform architecture	86
31	Map of Ordos basin showing shoreline positions through the lower Paleozoic ..	90
32	Comparison of 2nd and 3rd order sea-level curves of North America	100
A1	Geologic map of the central and southern Zhouzi Shan and Liupan Shan...	113
A2	A) Ordovician strata exposed in Helan Shan. Note person in lower left for scale. B) Rugose coral in Ordovician blue-gray fossiliferous packstone in the Helan Shan	114
A3	A) Thrust contact juxtaposing Ordovician limestone on top of Silurian (?) sandstone near Zhongning. B) Blue gray fossiliferous packstone lithofacies assemblage containing gastropod shells (G) near Zhongning	117
A4	A) Shale and mudrock lithofacies capped by cross-stratified oolitic grainstone in Unit A at the Green Dragon section. B) Cross-stratified oolitic grainstone	119

A5 A) Lower and Middle Ordovician dark brown shales and fine sandstones exposed near Langshia in the southern Liupin Shan. B) Folded and faulted Ordovician strata, west of Langshia 122

A6 Geologic map of the southern Liupan Shan and Zhangjia Shan in southwestern Ordos (Modified from Ma, 2002)..... 123

INTRODUCTION

The Ordos basin rests upon the North China Block (NCB) and is one of the largest sedimentary basins in north China, containing more than 15 km of Phanerozoic strata (Fig. 1) (Sun et al., 1989; Yang et al., 2005). The geology of Ordos is an important indicator of the geologic history of the entire North China Block. Economically, Ordos basin is one of the largest hydrocarbon production areas of north China, with major gas reservoirs within Ordovician paleokarst (Lee, 1986; Yang et al., 1992; Wang and Al-Aasm, 2002). Published estimates suggest that over 2000 m of carbonates and lesser amounts of siliciclastics were deposited on the North China Carbonate Platform (NCCP) from the Lower Cambrian through the Middle Ordovician (Fig. 2) (Meng et al., 1997). However, lower Paleozoic facies successions and deposystems of northwestern Ordos basin remain poorly represented in western literature.

We report a detailed sedimentologic and stratigraphic study of lower Paleozoic strata in the NW Ordos basin. Because of limited detail in previous studies, relatively simple yet fundamentally important questions still remain to be addressed. First of all, what are the lithologic units and sequences exposed in western Ordos basin? This information has not been previously reported for western Ordos, and is the foundation for interpretations such as depositional environment, paleogeography, basin history and sequence architecture. We provide detailed measured stratigraphic sections and facies descriptions from western Ordos that provide an essential stratigraphic framework for interpreting the early Paleozoic geologic history of Ordos

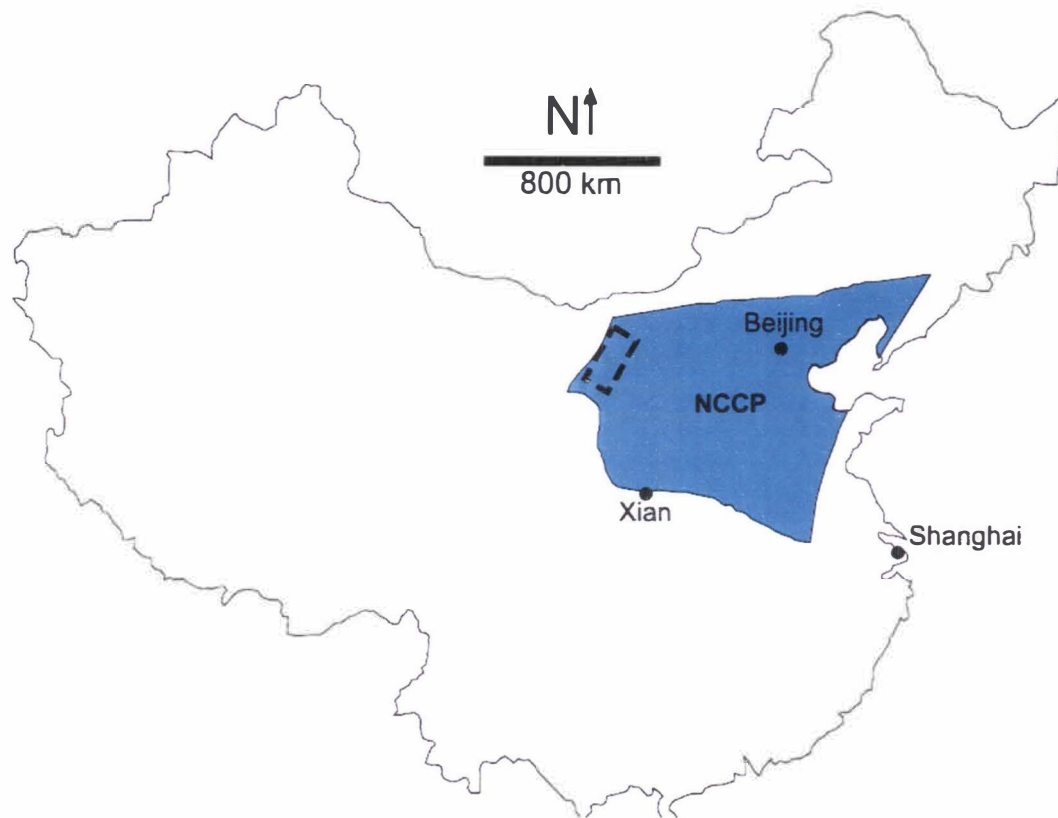


Figure 1. Shaded region shows the extent of the lower Paleozoic North China Carbonate Platform (NCCP), which was built entirely upon the North China Block (NCB). The NCB was an isolated microcontinent, located at low latitude during early Paleozoic time (Meng et al., 1997). Dashed box shows approximate location of northwestern Ordos field area (NCCP location modified from Wang and Al-Aasm, 2002; NCB boundaries from Johnson et al., 2004)

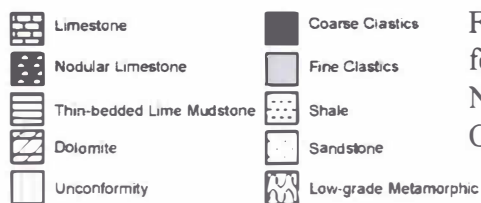
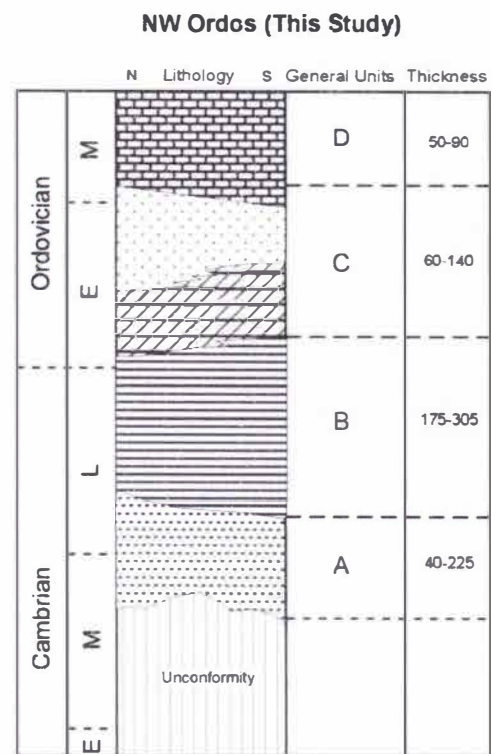
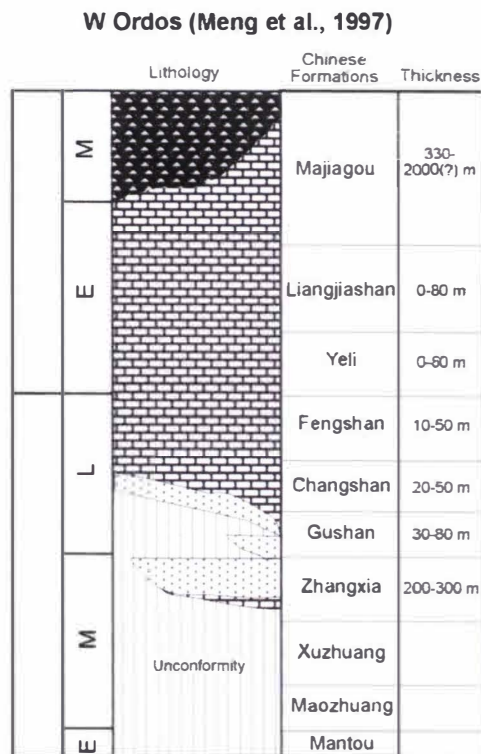
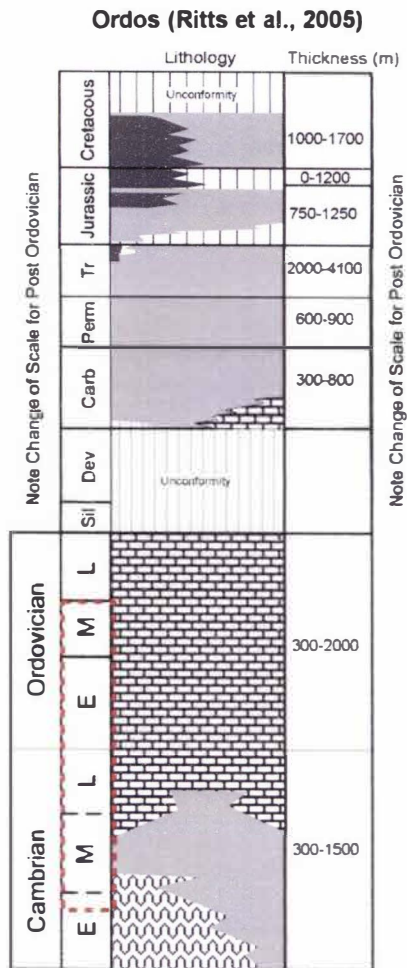


Figure 2. Chronostratigraphic columns for Ordos basin (Ritts et al., 2006b), the NCCP (Meng et al., 1997) and NW Ordos.

basin. The second question is how western Ordos lithologic stacking patterns and sequences compare with models for the whole NCCP (Meng et al., 1997) and North America analogs (Vail et al., 1977; Sloss, 1988). Third, geologic features, such as aulacogens, are commonly mentioned in the Chinese literature without substantial, descriptive evidence to support them. Fourth, paleokarsts are important reservoirs for gas within central Ordos (Wang and Al-Aasm, 2002) and are important indicators of sea level (Esteban and Klappa, 1983), yet the description and position of paleokarsts are undocumented from western Ordos. We describe the character and position of paleokarsts within the lower Paleozoic stratigraphic framework of northwestern Ordos. The last fundamental question addressed by this research is whether the post-Ordovician NCB-wide unconformity discussed in numerous papers (Meng et al., 1997; Yang et al., 1992; Yin and Nie, 1996; Huebeck, 2001) is exposed in western Ordos basin.

Huebeck (2001) implies that, although the interactions and contributions of major Asian cratonic elements are broadly understood, details such as depositional environments, paleogeography and kinematics of smaller elements remain vague. The stratigraphic record of the lower Paleozoic also may have implications for Asian tectonics as pre-existing sedimentary cover may have an effect upon younger tectonic evolution of the basin (Darby and Ritts, 2002). This paper constrains depositional environments, lithologies, facies relationships and sea-level history of the northwestern part of the North China block (NCB) in an effort to fill the lower Paleozoic data-gap of western Ordos basin.

BACKGROUND GEOLOGY

Generalized Stratigraphy of Western Ordos Basin (Fig. 2)

Basement rocks of western Ordos basin consist of Archean foliated and non-foliated granitic plutons, gneiss, schist and mafic dikes (Darby, 2003), deemed the Jinian and Urashan Groups in the north and the Luliang, Fenghe and Yeji Groups in the south (Sun et al., 1989). Archean basement rocks are unconformably overlain by Meso-Proterozoic clastic and metasedimentary rocks of the Changchenian and Jixianian Groups and Neo-Proterozoic Sinian Group siliciclastic rocks (Yang et al., 1992). Lower Paleozoic lithologies are dominantly carbonate rocks with minor siliciclastics and span the Lower Cambrian through the Middle Ordovician. A basin-wide unconformity separates Ordovician carbonate rocks of the Majiaogou Formation from Middle Carboniferous to Permian strata; Upper Paleozoic strata are dominantly clastic, non-marine with lesser marine carbonate and shale (Yang et al., 1992). Thick sequences of Triassic arkosic sandstone and shale (Ritts et al., 2004) are overlain by Middle Jurassic to Upper Cretaceous conglomerates, sandstone and shale (Darby and Ritts, 2002). Cenozoic basin fill is thin and discontinuous, and is composed of non-marine, fluvio-lacustrine clastic rocks; Quaternary wind-blown deposits are common in Ordos basin (Sun et al., 1989).

Tectonic Setting

The Ordos basin consists of an undeformed, central plateau bounded on all sides by mountain belts (Fig. 3) (Sun et al., 1989; Darby and Ritts, 2002; Ritts et al.,

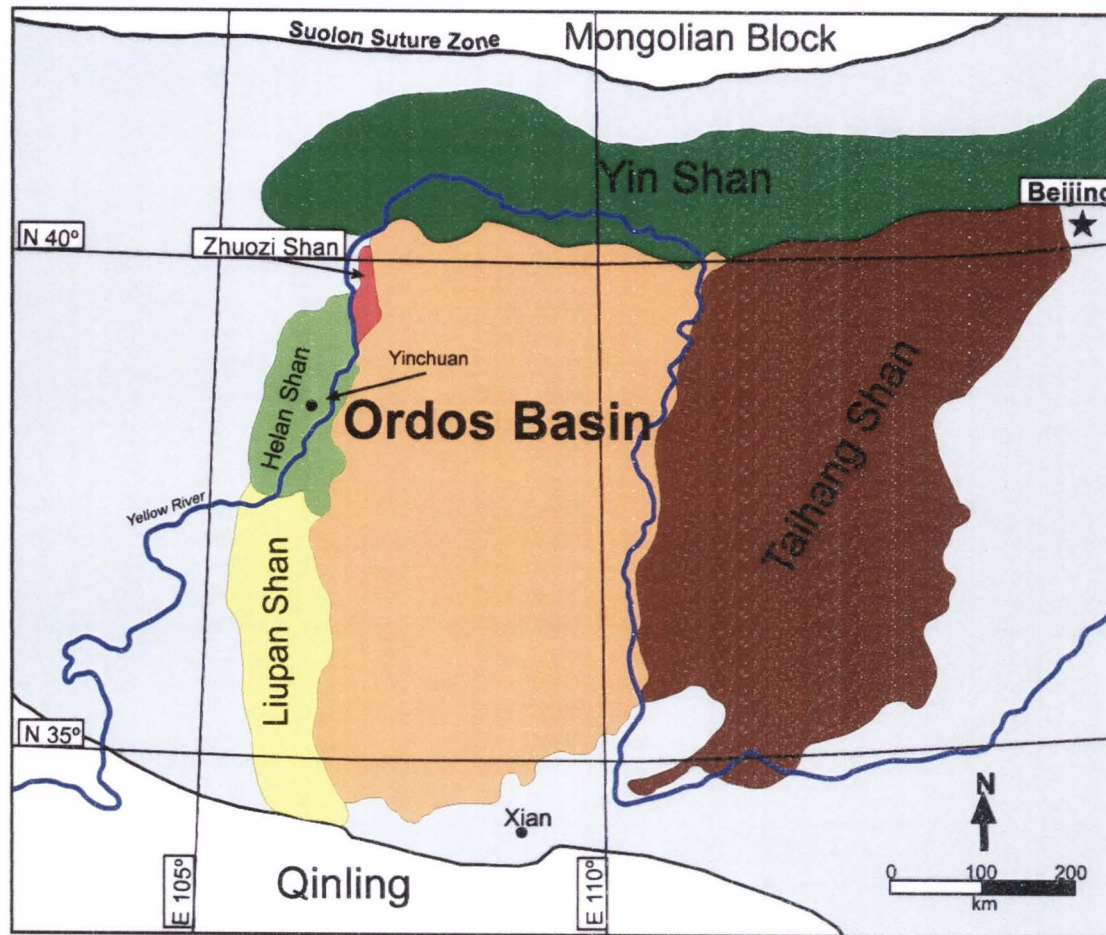


Figure 3. Map of Ordos basin and surrounding orogenic belts. Gray color indicates North China Block (NCB). (Modified from Darby and Ritts, 2002)

2006b). The northern margin of the basin is bounded by the Jurassic-Cretaceous, contractile Yinshan belt, an east-trending mountain range (Davis et al., 1998; Darby et al., 2001). North of the Yinshan marks the boundary between the NCB and Mongolian arc terranes, expressed by the Permian, Suolon suture zone (Darby et al., 2001). The eastern periphery of Ordos basin is composed of the Taihang Shan (Fig. 3), another Jurassic-Cretaceous contractile fold belt (Darby and Ritts, 2002). Southern Ordos is bounded by the Late Triassic Qinling suture zone, which separates the NCB from the South China Block (SCB) (Fig. 3) (Meng and Zhang, 2000). Western Ordos is bordered by a Late Jurassic-Early Cretaceous fold and thrust belt, well exposed in the approximately north-south trending Helan Shan and Zhuozi Shan (Darby and Ritts, 2002).

Tectonic History

Regional Tectonics

China is an amalgamation of continental blocks and accretionary orogens bounded by sutures, fold and thrust belts or large faults (Enkin et al., 1992). The NCB is one of the major tectonic elements of China, and is composed of two major Archean metamorphic continental elements (Zhao et al., 2003). Archean isolated microcontinents were fused together to form the larger NCB in the Paleoproterozoic (Meng et al., 1997). Rift basins dominated during the Late Proterozoic and are expressed by the thick sequences of Proterozoic sedimentary rocks deposited in the Ordos area (Sun et al., 1989).

The NCB persisted as an isolated microcontinent located at sub-tropical latitude through the early Paleozoic (Meng et al., 1997; Huang et al., 1999). During the early Paleozoic, the NCB was submerged under a shallow-marine, epicontinental sea on which over 2000 m of carbonates and lesser amounts of siliciclastics were deposited (Meng et al., 1997). A craton-wide unconformity separates Middle Ordovician from Middle Carboniferous strata (Fig. 2) (Sun et al., 1989). Chinese workers (Sun et al., 1989; Zhao et al., 1996) have characterized the pre-Permian history of the Ordos basin as tectonically quiescent, however the early Paleozoic history is poorly constrained. The NCB collided with arc terranes in present Mongolia in the Late Paleozoic; collision with the SCB was completed by the end of the Triassic and marked the beginning of intracratonic tectonics of the NCB (Enkin et al., 1992; Darby and Ritts, 2002).

Local Tectonics

Data reported herein come from the Helan Shan and Zhuozi Shan, located adjacent to the western margin of Ordos basin (Fig. 3), which are part of the intracratonic, Western Ordos fold and thrust belt (WOFTB) (Darby and Ritts, 2002). The strata exposed within these Mesozoic-age contractile belts are generally regarded as analogs to subsurface units within the central portion of the basin (Ritts et al., 2006a). Palinspastic reconstructions of tectonic elements of western Ordos are important for reconstructing the paleogeographic position of the lower Paleozoic NCCP.

The oldest structures known in the western Ordos belt, are pre-Carboniferous normal faults, which are exposed in both the Helan Shan and the Zhuozi Shan (Darby, 2003). Paleozoic extension is linked to: (a) continued aulacogen rifting or (b) an after-effect of the Devonian Qaidam-North China collisional event (Darby, 2003; Yin and Nie, 1996) although neither relationship is rigorously established. The early Mesozoic history of the Helan Shan has been characterized as extensional (Ritts et al., 2004). Sedimentological data from thick packages of Middle and Upper Triassic strata exposed in the Helan Shan and Zhuozi Shan suggest a north-trending half-graben with both depocenter and master fault located in the west, over part of the Helan Shan (Liu, 1998; Ritts et al., 2004). Early Jurassic, non-marine rocks within the Zhuozi Shan and Helan Shan record initiation of the WOFTB (Darby and Ritts, 2002). The WOFTB consists of east vergent thrust faults, folds and associated reverse faults exposed in the Helan Shan and Zhuozi Shan (Darby and Ritts, 2002). Both ranges show a paleocurrent reversal from west-directed to east-directed in the Lower to Middle Jurassic, suggesting onset of contraction during this time (Darby and Ritts, 2002; Ritts et al., 2006a). Late Jurassic to early Cretaceous (?) rocks are the youngest deformed rocks associated with the WOFTB in the Zhouzi Shan (Darby and Ritts, 2002).

Of great importance to this study is the Cretaceous dissection of the WOFTB. Chinese workers (e.g. Liu et al., 1990) suggest that the northern Zhuozi Shan is an along-strike equivalent thrust belt, formed penecontemporaneously with the Helan Shan (Darby and Ritts, 2002). By reconstructing fault geometries within the region, Darby and Ritts (2002) dispute this interpretation and propose that a large, northwest-

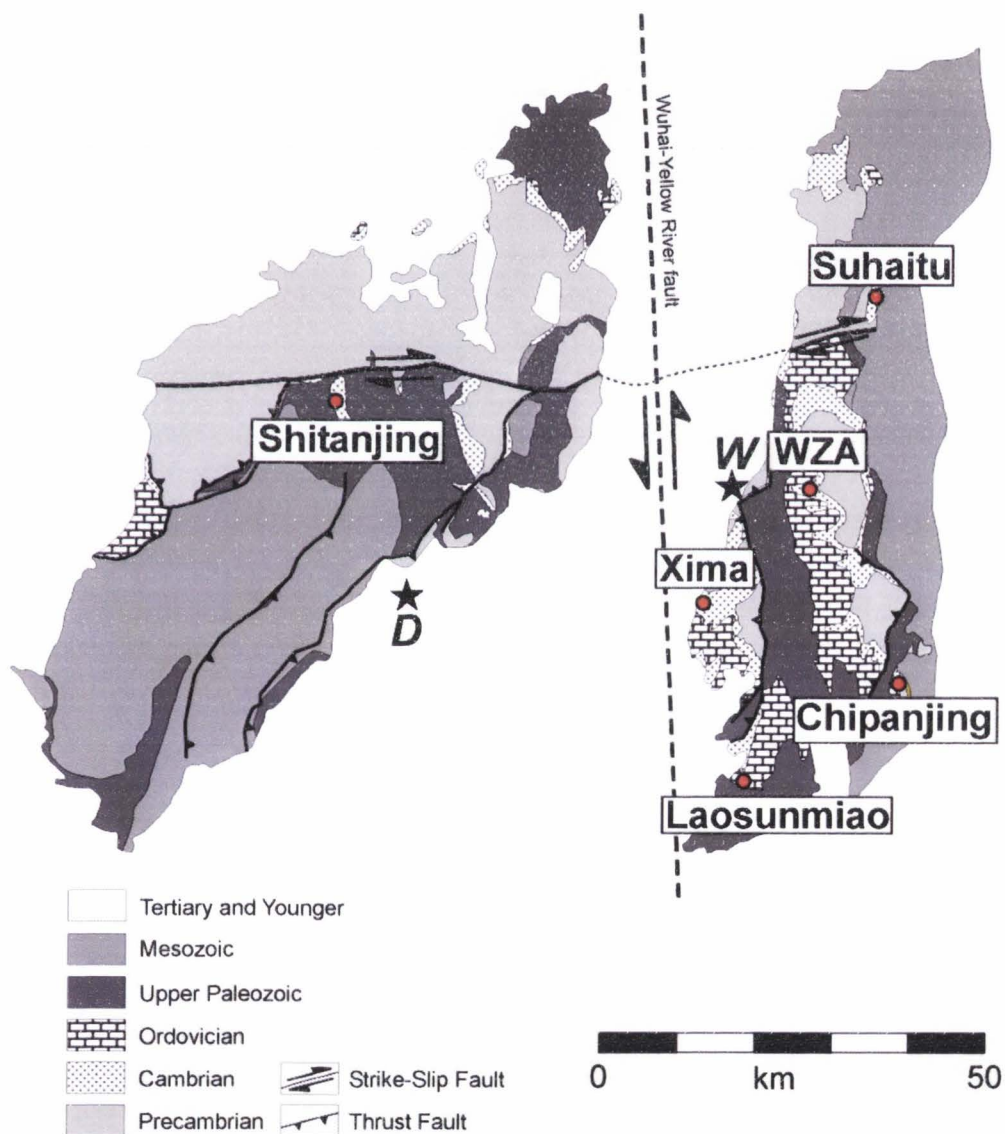


Figure 4. The interpretation that a large, left-lateral, strike-slip fault has dissected the WOFTB, effectively translating the Zhuozi Shan ~60 km north to its present position. Dotted line shows the position of the Wuhai-Yellow River fault between the Zhuozi Shan and northern Helan Shan (Darby and Ritts, 2002; Ritts et al., 2006a)

southeast trending, left-lateral strike-slip fault, the Wuhai-Yellow River fault (Ritts et al., 2006a) has dismembered the WOFTB to its current position and that the western Zhuozi Shan actually represents the frontal portion of the WOFTB (Fig. 4). This interpretation is drawn from four lines of evidence: (a) the occurrence of a large, Late Jurassic, strike-slip fault that cuts both the Helan Shan and Zhuozi Shan and is presently offset by ~60 km, (b) similar trending, along strike, left-lateral faults in the Lang Shan, northwest of the WOFTB (c) a conspicuous northwest-southeast trending straight segment in the course of the Yellow River between the Helan and Zhuozi Shan and (d) thrust belt characteristics (Darby and Ritts, 2002; Darby, 2003; Ritts et al., 2006a, 2006b).

Previous Work – Lower Paleozoic

Chinese workers have documented the lower Paleozoic stratigraphy of the Ordos region, based primarily on core analyses (e.g. Lee, 1986; Sun et al., 1989; Yang et al., 1992; Yang et al., 2005). These papers present an overview of the Phanerozoic sedimentologic and tectonic history of Ordos basin, with the main focus upon paleogeography and petroleum system architecture of the Mesozoic and Cenozoic. While petroleum-related aspects of these studies are relatively coherent, details of field relationships, outcrop locations and depositional environments are extremely broad or cryptic. For example, the Upper Cambrian of the whole of Ordos basin is described by Yang et al. (1992) as, “medium to thick bedded, silty to fine-grained dolomite, muddy dolomite with some pebbly dolomite” in which “a disconformity existed”. Paleoenvironmental interpretations in the same study are

limited to general descriptors such as “tidal flat patchy limestone” and “tidal flat wormkalk” plotted on paleogeographic maps without discussion of implications (Yang et al., 1992).

Outcrop investigations of lower Paleozoic strata in Ordos basin are limited. Wang and Al-Aasm (2002) focused on karst horizons strictly in the Middle Ordovician Majiagou Formation in the east-central portion of Ordos basin. The main focus in the Wang and Al-Aasm (2002) paper is on reservoir properties and petrographic and geochemical analyses of carbonate rocks within the Majiagou Formation. Majiagou reservoir porosity in east-central Ordos is a function of dissolution-enhanced vugs in dolomites. Wang and Al-Aasm (2002) used physical measurements of reservoir quality to show 0.5-15% porosity and 0.01-1224 md permeability in outcrop, and 0.5-8% porosity with 0.1-5 md permeability in the subsurface dolomites. Through isotopic and petrographic data, they interpreted dolomites as mixing zone-induced from both shallow-and deep-burial environments (Wang and Al-Aasm, 2002). However, Wang and Al-Aasm (2002) have not addressed the stratigraphic positions of paleokarsts elsewhere within the lower Paleozoic section.

The study of Meng et al. (1997) documented sequences of carbonate rocks in the lower Paleozoic strata of the whole NCCP, including sites near eastern and western Ordos basin. They also published a tentative correlation to North American sequences. The foundation of this paper is based upon detailed Cambrian lithologic descriptions, with depositional environment and sequence stratigraphic interpretations, resulting in a Lower to Middle Cambrian, stratigraphic column and a

general model for early Paleozoic deposition on the NCCP. However, the bulk of field data from that study was concentrated in regions situated north and south of Beijing, with inferred references to lateral changes (Meng et al., 1997). The Meng et al. (1997) model is generalized for the entire platform, which makes application to local areas, such as western Ordos basin, difficult.

By using bounding sequences of intraclastic conglomerates as relative depth indicators, Liang et al. (1993) demonstrated the cyclic nature of Middle and Upper Cambrian storm facies associations of the Helan Shan of western Ordos. The result of the Liang et al. (1993) study is a detailed, Middle and Upper Cambrian stratigraphic column for the Helan Shan showing various cycles and lithofacies associations of intraclastic conglomerate rocks. They interpreted intraclastic conglomerate abundance in west Ordos as a function of lower Paleozoic storm cyclicity.

Biostratigraphy (Table 1)

Chinese workers give lower Paleozoic age assignments for strata on the NCCP based upon trilobite, graptolite and conodont biostratigraphy (Meng et al., 1997). In China, Cambrian age designations are based primarily upon trilobite biostratigraphy. The Middle to Upper Cambrian transition is marked by the change from redlichiid to ptycopariid trilobites (Meng et al., 1997). Chinese trilobite faunal assemblages of the Cambrian are correlated to both North American and European zones (Meng et al., 1997). The Upper Middle Cambrian Zhangxia Formation of China is correlated to the *Bathyriscus-Elrathia* and *Bolasipidella* zones, while the Upper Cambrian is correlated to trilobites of the Dresbachian, Franconian and

Table 1. North China Carbonate Platform Biostratigraphy (Meng et al. 1997)

Age	Formation	Chinese Fossil Zones	North American Fossil Zones
Middle Ordovician		<i>Pterograptus elegans/Didymograptus murichisoni</i>	Whiterock
Lower Ordovician	Majiagou	<i>Ampexograptus-confetus</i>	Beekmantown
		<i>Cardiograptus</i>	
		<i>Didymograptus nexus</i>	
		<i>Oncograptus magnus</i>	
		<i>Didymograptus abnormis/Azygograptus suecicus</i>	
	Liangjiashan	<i>Didymograptus protobifidus, Didymograptus deflexus</i>	
		<i>Tetragraptus-fruticosus/Didymograptus filiformis</i>	
		<i>T. (Etragraptus)-approximatus</i>	
		<i>Adelograptus-Clonograptus</i>	
Yeli	<i>Aletograptus-Triograptus</i>	Gascondia	
	<i>Staurograptus-Anisograptus</i>		
Upper Cambrian	Fengshan	<i>Calvinella-Mictosaukia, Quadricephalus-Dictyella-Ptchaspis-Tsinania</i>	<i>Saukia</i>
			<i>Saratogia</i>
			<i>Taenicephalus</i>
	Changshan	<i>Kaolishania</i>	<i>Elvinia</i>
		<i>Changshania</i>	<i>Dunderbergia</i>
		<i>Chuangia</i>	<i>Aphelaspis</i>
	Gushan	<i>Drepanura</i>	<i>Crepicephalus</i>
		<i>Blackwelderia</i>	<i>Cedaria</i>
		<i>Damesella</i>	
Middle Cambrian	Zhangxia	<i>Amphoton-Taitzuia</i>	<i>Bolasipidella</i>
		<i>Crepicephalus</i>	<i>Bathyunsus-Elrathina</i>
		<i>Bailiella</i>	<i>Glossopleura</i>
	Xuzhuang	<i>Poriagraulos</i>	<i>Albertella</i>
		<i>Sunaspis</i>	
		<i>Kochaspis</i>	<i>Plagiura-Poliella</i>
	<i>Shantungaspis</i>		

Trempealeauan stages of North America (Meng et al., 1997). The Cambro-Ordovician boundary is placed between the *Calvinella-Mictasaukia* and *Onychopyge-Leiostegium* zones (Meng et al., 1997). A combination of graptolites and conodonts are used for dating Ordovician strata; conodonts are most effective for correlation because they are more widely distributed within carbonate platform interiors than graptolites (Meng et al., 1997). Graptolite assemblages suggest that the Ordovician Yeli, Liangjiashan and Majiagou (lower) Formations are correlative to the North American Gascondia and Beekmantown zones, respectively (Meng et al., 1997).

DATA AND RESULTS

Study Localities

Cambrian and Ordovician strata are exposed across north central and northeastern China (Meng et al., 1997). New stratigraphic data in this study come largely from measured sections in the Zhuozi Shan and Helan Shan (Fig. 5; Plate 1).

The Suhaitu section is the northernmost section in the Zhuozi Shan, located approximately 35 km northeast of Wuhai (Fig. 5). The Suhaitu section is 573 m thick from the Middle Cambrian-Proterozoic unconformity to Middle Ordovician limestone beds that cap the section. The section is overlain by upper Jurassic to lower Cretaceous conglomerate (Darby and Ritts, 2002). Lower Paleozoic strata that make up this section are bounded in the south by a late Jurassic, right-lateral, strike-slip fault (Darby and Ritts, 2002). Strata in this section have an average strike of 196° and dip of 57° SW.

The west Zhuozi Shan anticline (WZA) section is located 10 km east of Wuhai, in Wuhai Canyon (Fig. 5). The lower Paleozoic section at the WZA section is 548 m thick, spanning the Middle Cambrian through the Middle Ordovician. Units strike an average of 189° and dip approximately 11° SW.

The Xima section is 20 km southwest of Wuhai and is the thickest section encountered, at 785 m (Fig. 5). The lower contact is faulted, but is mapped by Ma (2002) as covering Middle Cambrian through Lower Ordovician strata. Lower Paleozoic units strike at an average of 250° and dip at 20° SW.

The Chipanjing section is located 35 km southeast of Wuhai and is one of the thinnest lower Paleozoic sections in the Zhuozi Shan at 200 m (Fig. 5). The lower contact is faulted upon Proterozoic quartzites and may be missing some Middle Cambrian rocks; it is mapped by Ma (2002) as spanning from the Middle Cambrian through the Lower Ordovician. The Chipanjing section strata strike 164° and dip 26° SW.

The Laosunmiao section is located 40 km south of Wuhai (Fig. 5), and is mapped as Middle Ordovician (Ma, 2002). This is the thinnest measured section at 94 m thick, and is an intact chunk of Ordovician carbonates and clastics surrounded by heavily folded and faulted lower Paleozoic section. The basal contact is covered and not mapped as a fault (Ma, 2002) yet is juxtaposed above Carboniferous rocks while the upper contact is marked by faulted and folded Ordovician rocks. Strata strike 239° and dip 40° SE.

The Shitanjin section is 30 km northwest of Dawukou City (Fig. 5), and is the only measured section from the Helan Shan. These rocks are mapped by Ma (2002) as Middle and Upper Cambrian. This section is 270 m thick. The basal contact is a thrust-fault against Carboniferous strata and the upper contact is contact to the Upper Cambrian limestone. The Shitanjin section strata have an average strike of 230° and dip 10° SE.

Outcrop and Petrographic Lithologic Observations and Interpretations

Strata in the mountains of northwestern Ordos are divided into twelve lithofacies assemblages, distinguished by lithology, stacking patterns and sedimentary

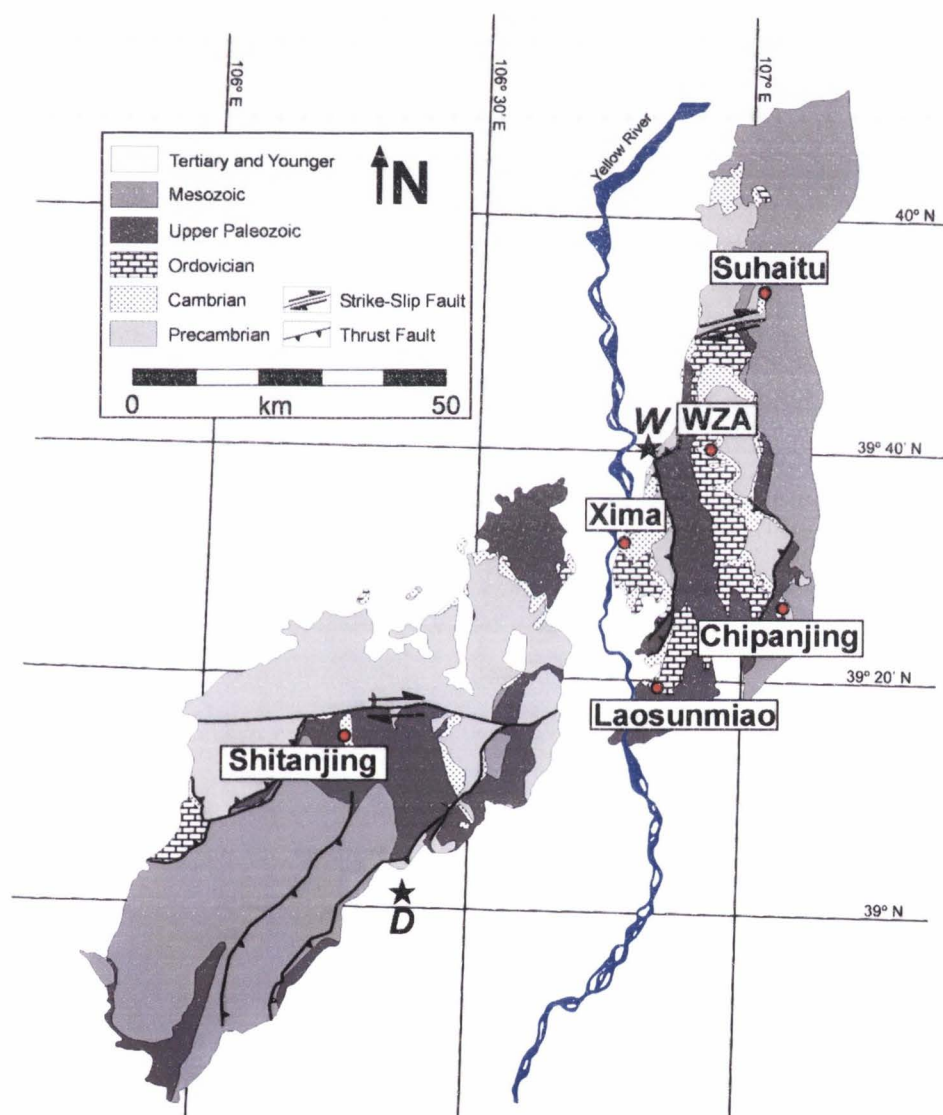


Figure 5. Outcrop map of the Zhouzi Shan and Helan Shan of northwestern Ordos Basin, showing field locations of measured sections. D=Dawukou City, W=Wuhai City. (Map locations adapted from Ma, 2002, major structural interpretations from Darby and Ritts, 2002)

structures. These lithofacies assemblages include mudrock and shale; argillaceous limestones; quartz sandstone; intraclastic conglomerate; breccia; thin, fossiliferous packstone; thin-bedded lime mudstone to wackestone; microbial mounds; banded, bioturbated lime mudstone to wackestone; fossiliferous, massive packstone to grainstone; oolitic packstone to grainstone and dolomitic limestone. These assemblages are named for their dominant lithologic component; assemblages may contain numerous lithologies and sedimentary structures.

Mudrock/Shale

The mudrock/shale lithofacies assemblage is predominantly composed of calcareous shale and mudstone with minor interbedded thin, fossiliferous packstone, oolitic grainstone and thin-bedded lime mudstone and siltstone. Mudrock and shale colors are variable between sections, ranging from tan, green, brown, purple to gray-black. Grain size in mudstone and shale units ranges from clay to silt-size; coarser grains also are present. Mudrock beds can be massive, however fissile shales are also exposed (Fig. 6A). Thicknesses range from meter-scale packages down to thin, cm-scale, interbeds. This lithofacies assemblage also includes thin shales that are interbedded in limestone packages. Interbeds within shale packages range in thickness from centimeter scale to 1 m and are composed of intraclastic conglomerate, glauconitic, cross-stratified oolitic lime grainstone, thin-bedded, hummocky cross-stratified, rippled calcareous siltstone (Fig. 6B), thin beds of shell-rich grainstone, and fossiliferous, bioturbated lime wackestone. Individual ooids within interbeds exhibit “chewed” margins while other oolitic beds are thick with



Figure 6. A) Mudrock/shale packages with interbedded thin-bedded lime mudstone and intraclastic conglomerate. B) Mudrock/shale lithofacies from WZA section with interbedded, nodular, thin-bedded calcareous siltstone.

cross-stratification. Thin (5-15 cm) limestone nodules were encountered in the lower portion of the WZA section.

Interpretation

Interpreting the depositional environment of shale and mudstone is complicated. The fundamental criterion necessary for fine particles to settle out of suspension is low-energy, quiet-water (Wignall, 1994). This type of environment is found in both deep and shallow water (Wignall, 1994).

What makes the shale of this lithofacies assemblage even more of a conundrum are the sedimentary structures contained within interbedded units. Interbedded lithofacies contain sedimentary structures found in both shallow and deep-water environments. Interbeds include thin, oolitic beds, fossiliferous packstone, and thin-bedded lime mudstone and siltstone, with ripples and hummocky cross-strata (HCS). At the base of the WZA section, shale occurs between two microbially-laminated limestone beds that are interpreted as intertidal to supratidal facies. Because distal shale models require rapid, high-magnitude sea-level changes at the base of all sections, and most shale beds are bounded by shallow-water facies, mudrock and shale lithofacies are interpreted as deposited in a near-shore, restricted lagoon rather than at a deep-water setting. Both shallow water shale and deep water shale models will be presented in the sea-level interpretation section later in the paper.

Argillaceous Limestone

The argillaceous limestone lithofacies assemblage is composed of lime mudstone to wackestone with a significant proportion of detrital siliciclastic material that gives this unit a recessive and brittle appearance (Fig. 7A). Fresh and weathered surfaces are tan to gray. Individual beds are usually thin; packages range from few cms to 1 m thick. The limestone component of the argillaceous lithofacies assemblage is dominantly mudstone to wackestone with shell grains and trilobite fragments.

Petrographic investigation of a sample of argillaceous lime mudstone from Suhaitu section indicates a more grain-rich lithology than is apparent in the field. Grains include pelloids, glauconite, trilobite fragments, echinoderm plates, tabular muscovite crystals and a large component of fine quartz silt. The matrix is composed of microspar (Fig. 7B).

Interpretation

Paucity of sedimentary structures combined with high, fine-grained, siliciclastic content suggest that this assemblage was deposited in a bioturbated, low-energy environment (Enos, 1983; Tucker and Wright, 1990; Wignall, 1994). This facies assemblage was likely deposited in a subtidal environment below normal wave base (Enos, 1983; Wilson and Jordan, 1983).

Quartz sandstone

The quartz sandstone lithofacies assemblage is more common in the Lower and Middle Ordovician portions of lower Paleozoic sections and is composed

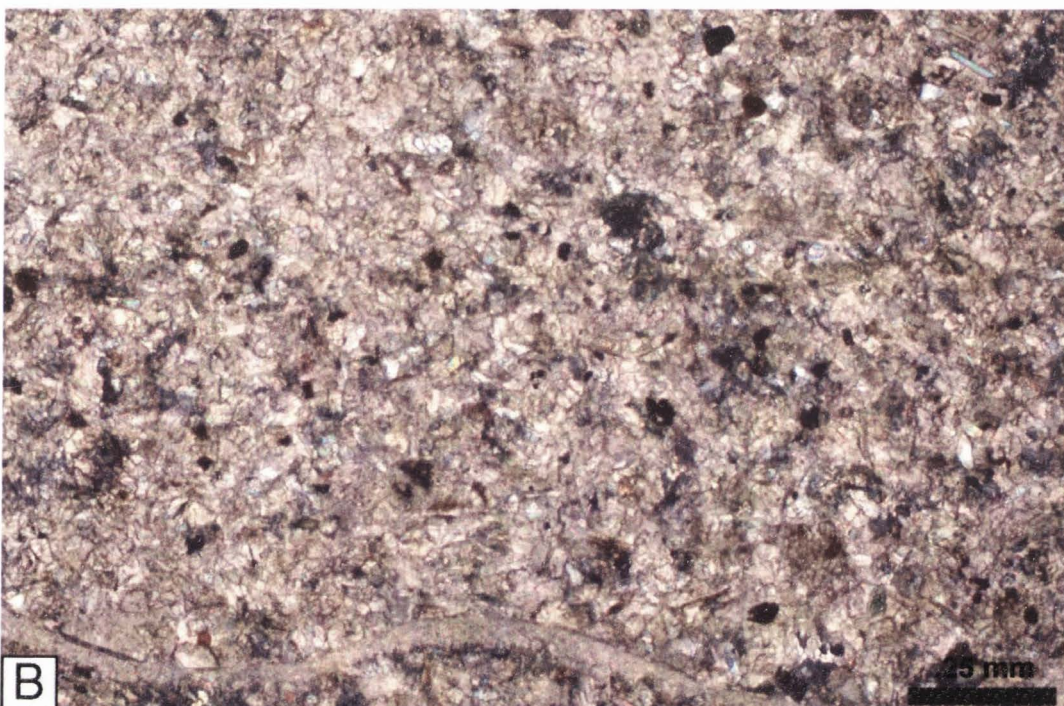


Figure 7. A) Argillaceous limestone from WZA section with thin lime mudstones and interbedded, mud-rich layers. Middle layer is composed of carbonate mud mounds and intraclastic conglomerates. Hammer is circled for scale. B) Photomicrograph of similar facies showing numerous silt-sized grains of quartz, opaques and one large trilobite fragment (bottom of photo) in a calcareous matrix.

of fine to coarse sand-sized, calcareous and quartz-cemented quartz sandstone, usually interbedded with dolomitic limestone. Fresh surfaces are tan to red-pink, and weathered surfaces are reddish-brown to dark brown. Quartz sandstone bed thickness ranges from 10 cm to 1 m. Quartz sandstone is frequently rippled, planar cross-stratified (Fig. 8A) and less commonly shows hummocky cross-stratification. Planar cross-strata foresets are on the order of 0.3-1 m in height. Coarsening upward beds of medium to coarse sand with scoured bases and cross-stratified tops outcrop at the Xima section. Contrasts in cementation of sand grains make some well-cemented, quartz-cemented quartz sandstone beds appear extremely resistant and resemble quartzite, interbedded with more friable, calcareous-cemented quartz sandstone. Thin section analyses of quartz sandstone from northwestern Ordos reveal a dominant quartz composition (Fig. 8B). Grains are subround to rounded, ranging in size from silt to medium sand sized and are poorly sorted. Most thin sections show numerous quartz grain-to-grain contacts and pressure-solved margins. Clay jackets are evident on quartz grains, however quartz overgrowth cement is the primary cement. Remaining porosity is low; pore spaces appear to have angular margins and are filled by calcite, an unidentified clay mineral and euhedral dolomite rhombs and subhedral calcite crystals. Other mineral grains include chert, rounded hornblende and small (0.01 mm) grains of mica (muscovite).

Interpretation

Quartz sandstone units of northwestern Ordos were deposited in a relatively shallow-water, shoreface environment (Tucker and Wright, 1990). Subrounded to

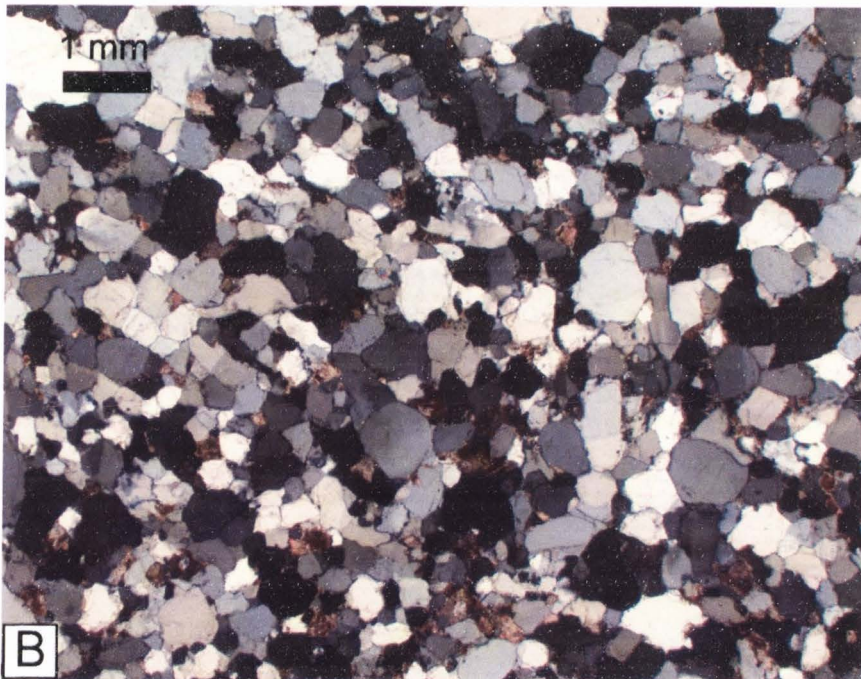


Figure 8. A) Cross stratification in quartz arenite strata from Xima section. B) Photomicrograph from Suhaitu section. Note pressure-soluted quartz grains and calcite filling pore spaces.

rounded, fine to coarse quartz grains are the dominant mineral component, indicating compositional maturity (Boggs, 2001). Planar, ripple and hummocky cross stratification all indicate traction transport in bedload (Walker, 1979; Tucker and Wright, 1990), and ripple marks and hummocky cross strata suggest, storm affected, lower shoreface deposition (Tucker and Wright, 1990). Quartz sandstone units are frequently interbedded with carbonate rocks and do not mark the end of carbonate production in the lower Paleozoic, thus siliciclastic input was not great enough to shut down the carbonate factory (James and Kendall, 1992). Sand was likely input from a continental source, and reworked into the shallow shoreface. Quartz-cemented, pressure-solved quartz sandstones resemble quartzites but are actually quartz sandstones. Based on the shape of pore spaces and pore-fill, host pores for calcite and dolomite were likely a result of dissolution of a less stable mineral (feldspar?); replacement of feldspars by clay or calcite is common in quartz sandstones (Tucker, 2001). Thin section analyses imply at least four stages of diagenesis; initial cementation, burial compaction and pressure solution resulting in quartz overgrowth cements, dissolution of an unstable framework grain and porosity filling by calcite and dolomite.

Intraclastic Conglomerate

The intraclastic conglomerate lithofacies assemblage is composed of beds of flat, granule to pebble-sized clasts of lime mudstone with a fine-to-coarse matrix (Fig. 9A). These beds are interbedded with nearly all lithofacies assemblages described

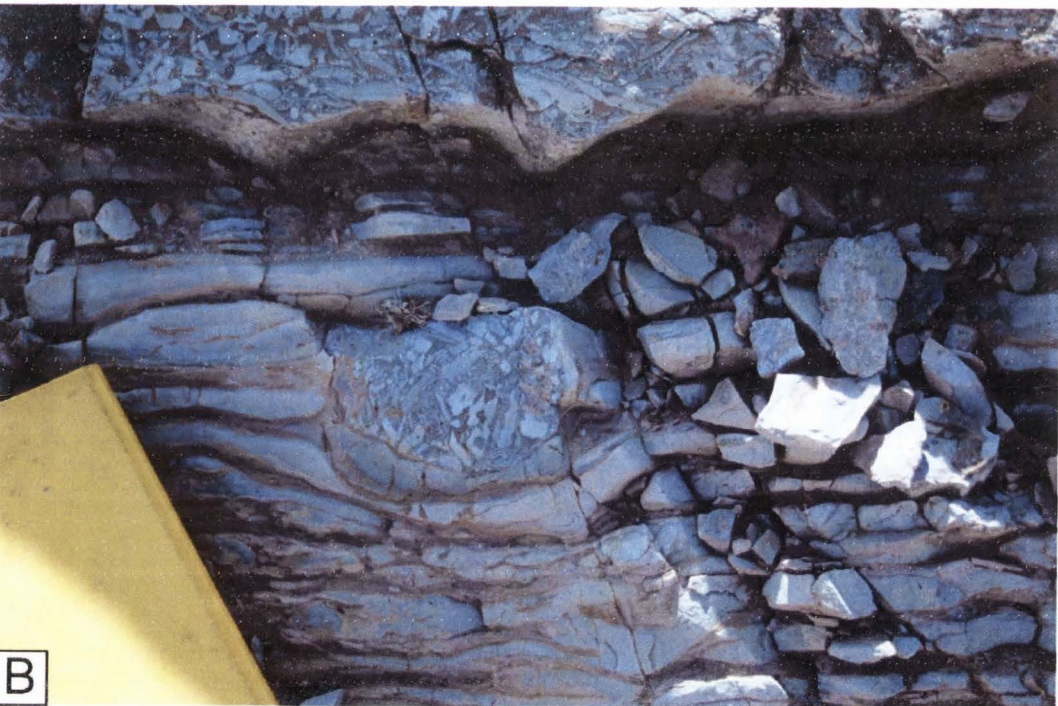


Figure 9. A) Intraclastic conglomerate lithofacies assemblage from Suhaitu section; note imbricated clasts. B) Intraclast-filled gutter within thin-bedded lime mudstone beds.

from the lower Paleozoic section. This lithofacies assemblage is one of the most pervasive lithofacies assemblages found in the lower Paleozoic section of northwestern Ordos. Fresh and weathered surfaces are gray to dark gray. Relatively minor clast components in the intraclastic conglomerate assemblage are fossiliferous material, usually thick-walled molluscan fragments (hyolithids?). Intraclasts are usually matrix supported; clast supported units were also encountered. The composition of matrix support varies from the more common lime mud matrix to, less frequent, coarse matrix containing shell fragments, quartz sand grains, ooids and oncoids. Intraclastic lithofacies assemblage bedding thickness varies from 1 cm beds to thick packages containing beds up to 50 cm thick. Intraclastic conglomerate within the lithofacies assemblage frequently have scoured bases and are laterally discontinuous with interrupted margins in bedding planes. The Suhaitu section contains excellent exposures of gutter casts, approximately 20-30 cm wide, containing both locally-derived lime mudstone clasts and coarse grainstone, preserved as isolated pods cross-cutting bedding within thin-bedded lime mudstone packages (Fig. 9B). Reddish fringes were observed on clasts at the Suhaitu section. Intraclastic conglomerate are frequently associated with thin-bedded lime mudstone, bioherms and banded, bioturbated limestone; however, intraclastic conglomerate also are found with oolitic lithofacies assemblages and as dolomitized beds within dolomitic strata.

Interpretation

The intraclastic conglomerate lithofacies assemblage represents storm deposition (Aigner, 1985; Myrow et al., 2004) and is a common component of

Cambrian and Lower Ordovician strata worldwide (Sepkoski, 1982), including northwestern Ordos (Liang et al., 1993). Myrow et al. (2004) document Upper Cambrian and Lower Ordovician intraclastic conglomerate units of the Snowy Range Formation of northern Wyoming and southern Montana that are representative of a multitude of depositional environments and processes in both shallow and deep water. Liang et al. (1993) examined Middle to Upper Cambrian lithologic associations of the Helan Shan of western Ordos and developed a cyclicity model for the Upper Cambrian by using facies associations as proxies for sea level. Intraclastic conglomerate are categorized as nearshore beach deposits, more distal mass-movement-derived and winnowed, nodular limestones based upon clast type, matrix and bounding units (Myrow et al., 2004). Although intraclastic conglomerate lithofacies assemblages are not the primary focus of this paper and, thus, were not described in the same amount of detail as in the Myrow et al. (2004) paper.

The sedimentary mechanics of intraclastic conglomerate depend on deposition and partial lithification of lime mud at a middle to outer ramp, low-energy position, which is later disturbed and transported by storm currents (Fig. 10) (Sepkoski, 1982; Myrow et al., 2004). The discontinuous bedding relationships encountered at approximately 250 m above the base of Suhaitu section exemplify storm deposition at a distal setting. Lime mud was deposited and allowed to firm slightly, and was later scoured by storm-generated bottom currents with subsequent coarser deposition within the scoured channel. Thin beds of lime mudstone, which overlie intraclastic conglomerate lithofacies assemblages in this setting, imply a return to relative quiescence and indicate the episodic nature of storm activity. Scoured bedding

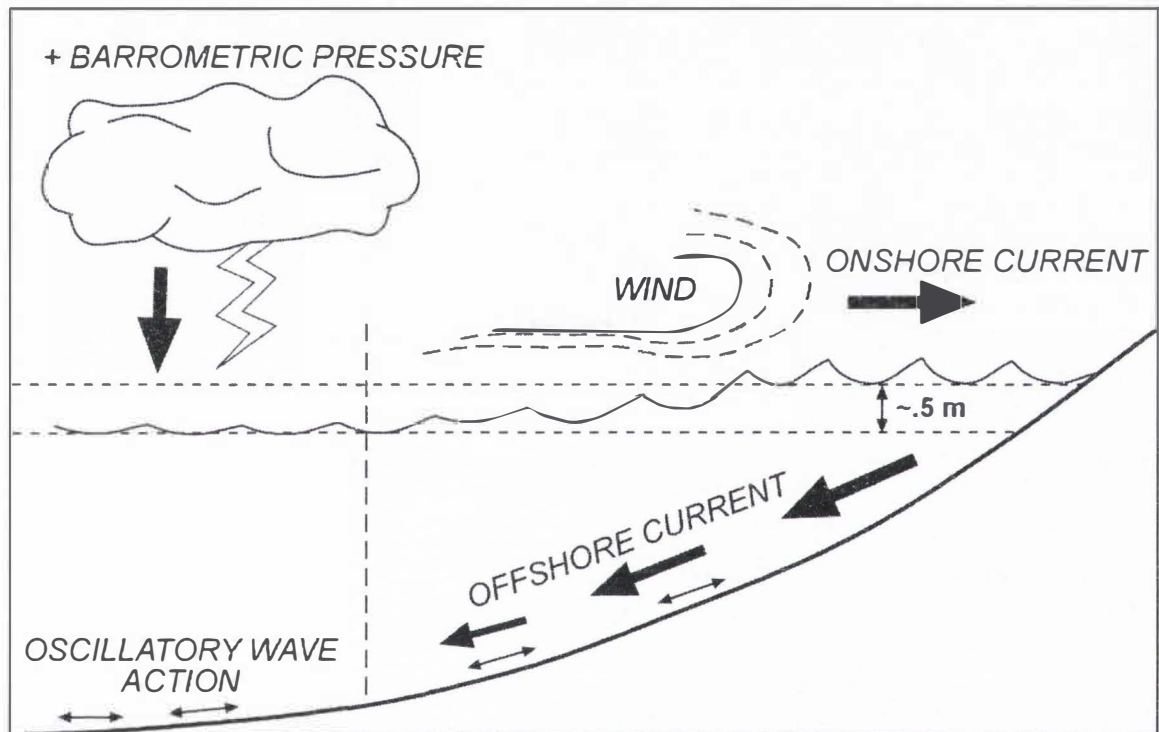


Figure 10. Cartoon depicting the effects of storms on sedimentation. This model predicts onshore material transport in shallower settings and offshore material transport in more distal facies (Aigner, 1985).

relationships of this style are exposed in nearly all sections visited in northwestern Ordos. Depositional environments of intraclastic conglomerate lithofacies assemblages are inferred from bounding units. As stated above, matrix components also are useful for interpreting depositional environment (Myrow et al., 2004), however, the details of upsection intraclastic conglomerate matrix changes were noted but not recorded in great enough detail to provide such information. For the purposes of this paper, a more simplistic method is used. Because intraclastic conglomerate lithofacies are ubiquitously interbedded with almost all units, those associated with shallower lithofacies (i.e., grainstone or microbially-laminated mudstones) are inferred to have been deposited at a shallower position, while intraclastic conglomerates occurring within more distal facies assemblages such as banded and bioturbated mudstone and wackestone and mounded strata are interpreted to be deposited at a distal position. These interpretations are generally similar to interpretations of intraclastic facies associations of the Helan Shan by Liang et al. (1993).

Breccia

The breccia lithofacies assemblage is composed of granule to boulder sized (Fig. 11) breccias (Fig. 12) with reddish-brown sandy matrix, usually associated with sand-rich limestone, dolomite and blue-gray packstone. Clast composition within the breccia lithofacies assemblage varies from banded and bioturbated limestone to sandy mudstone, quartz sandstone, whole bioherm heads and fossiliferous limestone. Breccias range in thickness from 1-10 cm to 1-2 m. The thickest breccias are



Figure 11. A) Granule/pebble paleokarst surface with a reddish-brown matrix from Unit C of Suhaitu section. B) Paleokarst breccia in a microbially-laminated lime mudstone from the base of WZA section in Unit A.

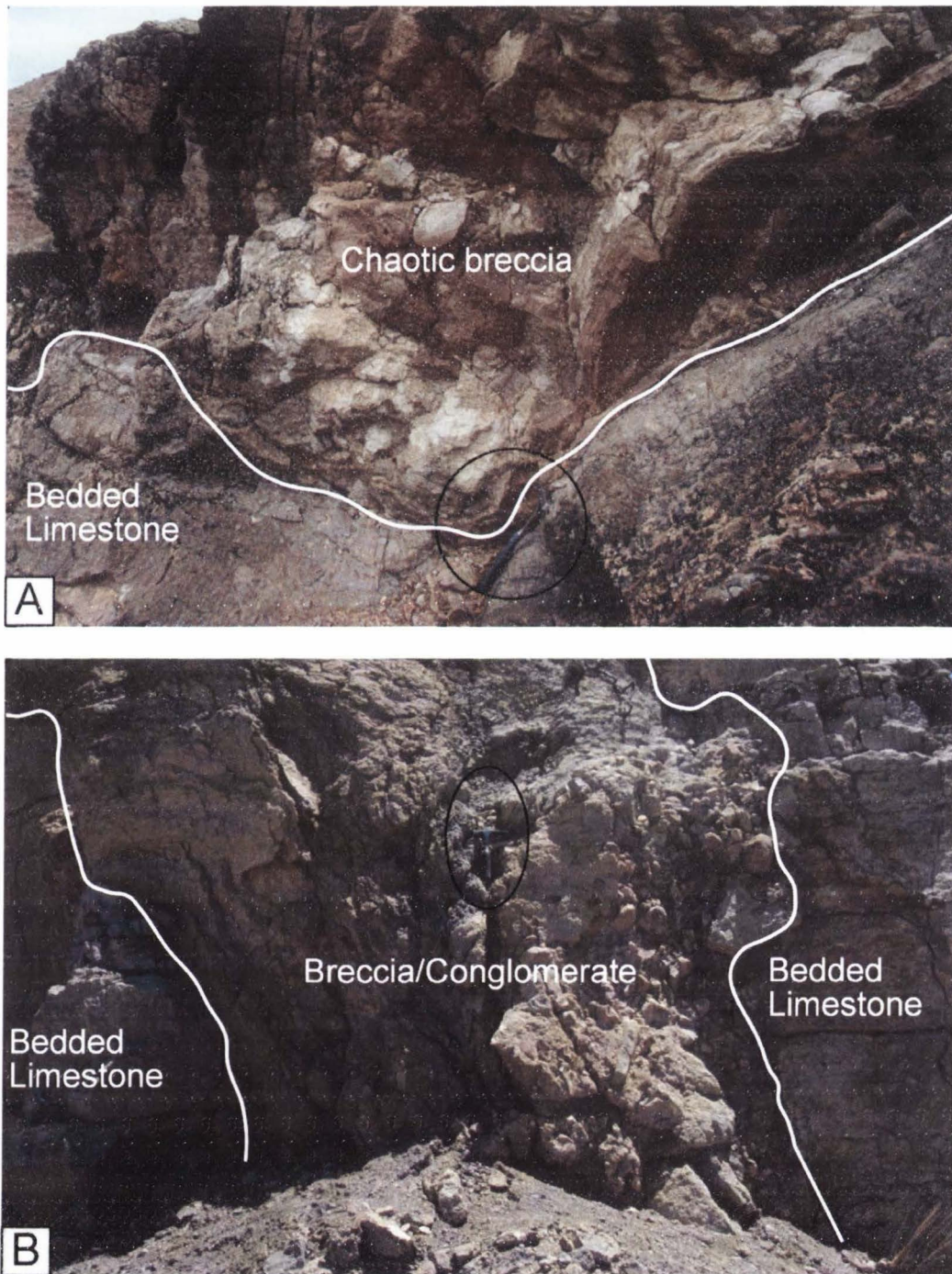


Figure 12. A) Thick paleokarst from Unit B at Suhaitu section; hammer is circled for scale. B) Paleokarst below the Middle Ordovician-Middle Carboniferous contact observed ~20 km northeast of WZA section.

concentrated near the top of stratigraphic sections, however thinner breccia intervals are distributed throughout the upper half of sections in northwest Ordos, particularly Suhaitu. Brecciation style ranges from chaotic infill to crackle type (Loucks, 1999). A mega breccia located at 320 m above the base of Suhaitu section overlies slump-folded quartz sandstone.

Interpretation

Breccia lithofacies in northwestern Ordos represent periods of subaerial exposure, which caused dissolution of carbonate material, cave formation and subsequent collapse and infill (Esteban and Klappa, 1983; Loucks, 1999).

Thin-bedded, Fossiliferous Packstone

The thin-bedded fossiliferous packstone lithofacies assemblage is composed of relatively thin, skeletal-rich beds interbedded with shale and thin-bedded lime mudstone rocks. Fresh and weathered surfaces are gray to dark gray (Fig. 13). Grains include trilobite fragments, hyolithids, brachiopod fragments, gastropods, bivalve shells, ooids, pelloids and oncoids. Thin-bedded fossiliferous packstone lithofacies assemblages at Suhaitu are associated with numerous cycles of thin-bedded lime mudstone capped by intraclastic conglomerate. Bedding thickness in thin-bedded fossiliferous packstone is commonly 2-15 cm. Sedimentary structures are not common, although planar cross-stratification was observed in one bed at WZA section. Thin sections of this thin bedded fossiliferous packstones show an abundance of trilobite fragments and ooids (Fig. 13). Trilobite thorassic segments and genal spines are present as free grains and as nuclei of ooids. Intraclasts of trilobite and



Figure 13. A) Typical outcrop appearance of thin-bedded, fossiliferous grainstone, from Suhaitu section. B) Photomicrograph of thin-bedded fossiliferous packstone facies assemblage showing oolite content, echinoid plates and trilobite fragments.

oid wackestone-packstone are present; some show multiple coating events. Infrequent pelmatozoan echinoderm plates are present. Fine sand to silt-sized, subrounded, quartz grains are an abundant component of the matrix. All ooids are replaced by microspar, leaving only faint relic exterior coatings; some ooids have been completely replaced by sparry calcite, leaving only the interior trilobite fragment nuclei remaining. Matrix has been replaced by fine crystalline calcite.

Interpretation

The lack of intact, whole fossils, combined with bounding strata composed mainly of shales and thin-bedded lime mudstone suggests two different depositional interpretations. Deposition was either by: (a) storm currents, which washed more grain-rich material into deeper water or into a quiet water lagoon (Aigner, 1985), or (b) a product of low sedimentation rates (Emery and Myers, 1996). Depositional environments in northwestern Ordos basin were heavily influenced by storms during the early Paleozoic (especially the Cambrian); thus transported, thin interbeds within thick shale (e.g. the lower Suhaitu section) is likely.

Thin-Bedded Lime Mudstone to Wackestone

The thin-bedded lime mudstone to wackestone lithofacies assemblage is composed of packages of thin (1-20 cm) lime mudstone with interbedded, banded, bioturbated mudstone to wackestone, intraclastic conglomerate, oolitic packstone to grainstone, mudstones and shale (Fig. 14). Fresh and weathered surfaces are gray to tan-gray. Grains in the thin-bedded lime mudstone lithofacies assemblage include

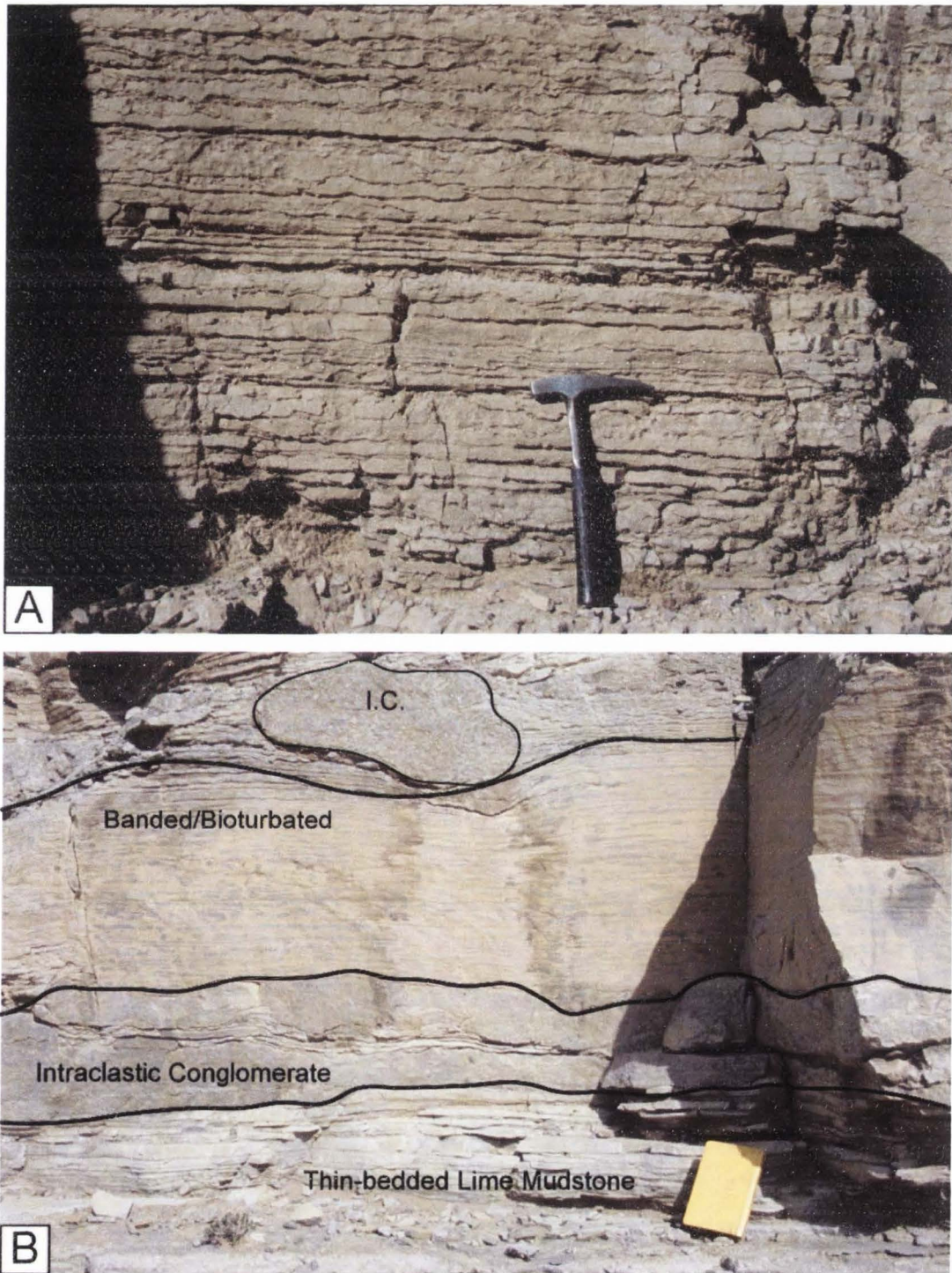


Fig. 14. A-Typical thin-bedded lime mudstone outcrop character, taken from WZA section. B-The association of thin-bedded lime mudstone with banded and bioturbated units and intraclastic conglomerate (I.C.).

trilobite, gastropod and brachiopod fragments. Average bedding thicknesses are 3-20 cm on average. Major sedimentary structures within thin-bedded lime mudstone units are laminations, ripple cross-laminae, horizontal burrows, sinuously-deformed beds and hummocky cross strata. Individual beds within larger packages of lime mudstone are sometimes discontinuous and sinuous, producing sedimentary boudinage texture. Interbeds of lime mudstone within thicker shale packages encountered at the WZA section are nodular with starved rippled tops. Thin-bedded lime mudstone at the Suhaitu, and Xima section commonly have a high quartz silt content and show hummocky cross-stratification. These rocks are usually interbedded with fine siliciclastic beds; beds with higher percentages of fines result in more recessive slopes. Outcrop character also varies with bioturbation; heavily bioturbated strata are more recessive and crumbly. Bedding contacts vary from gradational contacts with shale, to sharp, scoured bedding contacts with banded bioturbated limestone and intraclastic conglomerate.

Thin section analyses indicate that some thin-bedded lime mudstone samples are more grain-rich than initial outcrop observations, while others are dominantly composed of lime mud. One sample collected from the Xima section shows an abundance of silt-sized quartz, tabular crystals of muscovite and minor biotite and numerous trilobite fragments. An additional sample collected from a stratigraphically-higher position at the Xima section is dominantly composed of pyrite-stained lime mud with no apparent fossil materials.

Interpretation

As with other lithofacies assemblages in northwestern Ordos, thin-bedded lime mudstone and wackestone are not limited to a single depositional environment. Sedimentary structures within individual beds and bounding lithofacies aid in interpretation. With the exception of microbially-laminated lime mudstone, most thin-bedded lime mud was deposited subtidally (Cook and Taylor, 1977; Morgan, 1988; Tucker and Wright, 1990). Individual interbeds with laminations and hummocky stratification are interpreted to have been deposited more distally between fair-weather and storm wave base (Tucker and Wright, 1990), whereas thicker packages associated with ripples, mounded strata or oolitic rocks are interpreted to have been deposited more proximally, above fair-weather wave base (Tucker and Wright, 1990; Boggs, 2001).

Microbial Mounds

The microbial mound lithofacies assemblage includes mounds with either no internal structure (mud mounds) or a simple, thin vertical columns (true microbial mounds) (Fig. 15). Mud mounds are dominantly composed of lime mud, usually lacking texture; microbial mounds in the WZA, and Xima sections have internal, vertical layered columns, 2-7 cm wide. Most microbial mounds are hemispheroidal in shape and highly variable in size; widths range from 0.1 to 3 m and heights from 0.05 to 3.5 m. Mounds are commonly associated with thin-bedded lime mudstone, banded and bioturbated mudstone to wackestone and intraclastic conglomerate. Surrounding beds commonly onlap at microbial mound margins and

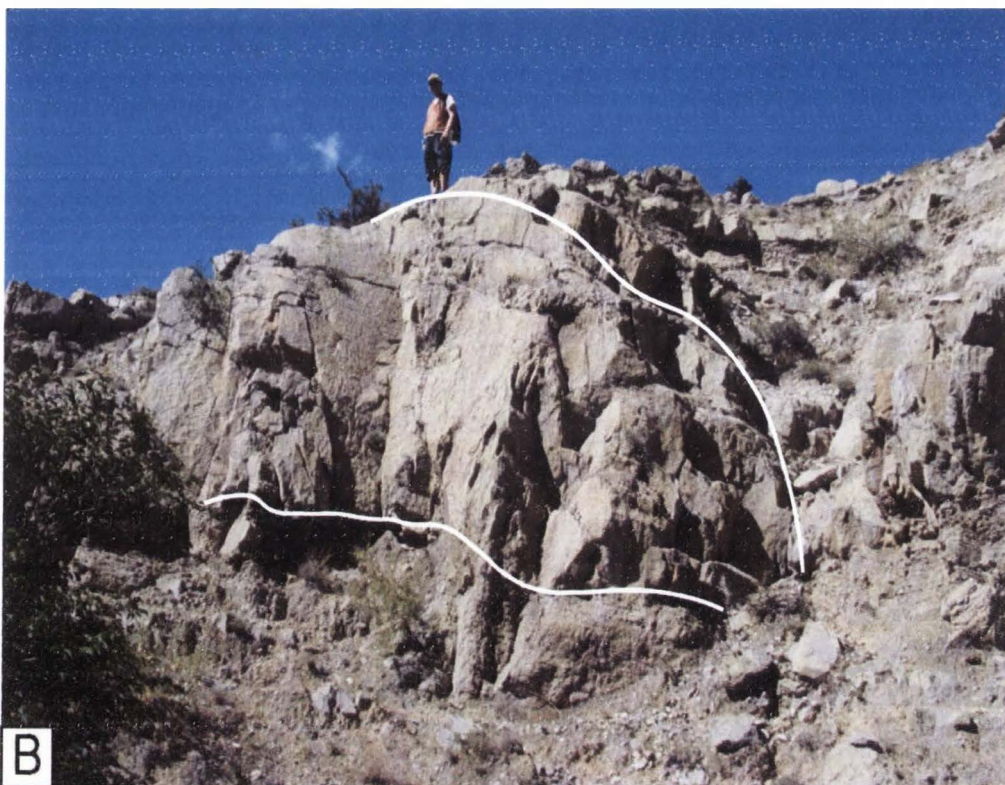
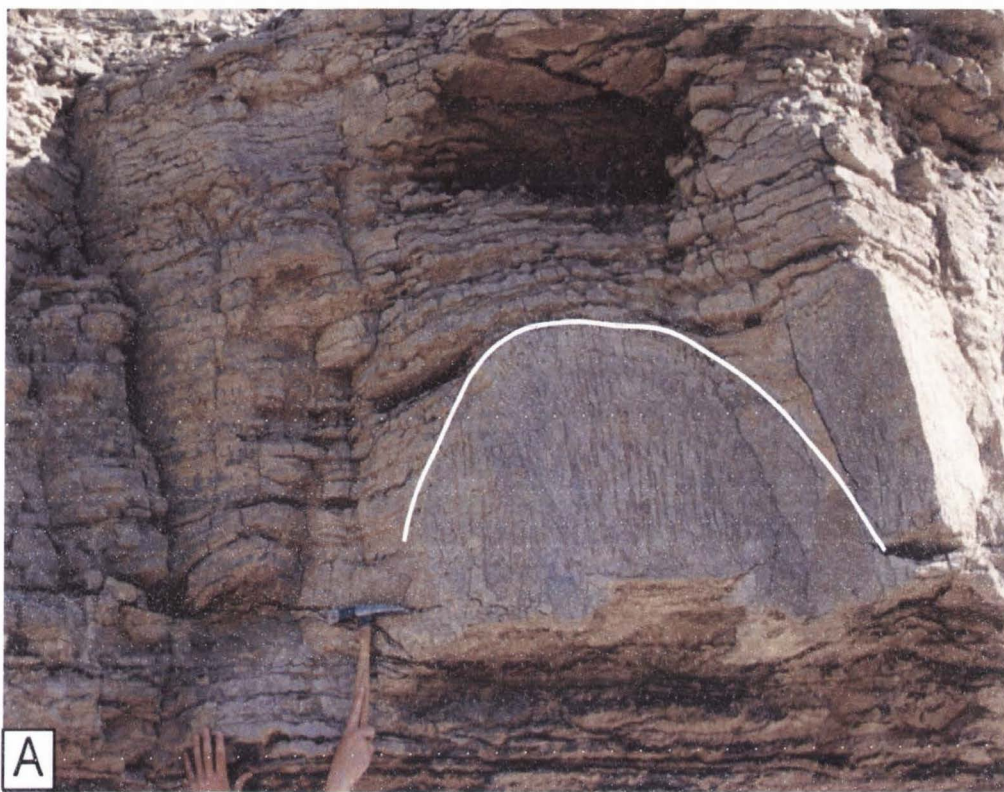


Figure 15. Microbial mounds of northwestern Ordos basin. A) Microbial mound in thin-bedded lime mudstone from unit B of WZA section. B-Large microbial mound within thin-bedded lime mudstone from unit B of Xima section

overlie the apex of the mound. One specimen at Suhaitu section exhibits a possible stromatolitic overgrowth on top of a mound; this is the only example of a stromatolite encountered in northwestern Ordos.

One thin section from a microbial mound in the WZA section was examined and is composed of lime mud; a clotted texture is apparent when the thin-section is observed under diffuse light.

Interpretation

Most carbonate mounds are formed by microbial growth trapping carbonate mud (James and Bourque, 1992). Mounds at the WZA and Xima sections are internally structured, which represents microbial growth and entrapment. Mounds without internal structure can originate hydrodynamically from concentration of carbonate mud or from mud producing organisms (James and Bourque, 1992). Mounds are rather ubiquitous within carbonate environments (Boggs, 2001). The association with microbial growth implies clear water depositional environments within the photic zone, which is roughly to 100 m depth in clear water (James and Bourque, 1992; Boggs, 2001). Most microbial mounds in northwest Ordos are domal and hemispherical in shape, which may be a high energy, wave-resistant morphology (James and Bourque, 1992) and are, therefore, interpreted as shallow, subtidal features. Sedimentological connotations of surrounding units and mound margins imply that the structure was existent at or before the time of deposition of the surrounding strata. The size of mounds is likely directly proportional to accommodation space, which, in this case, is water depth. As demonstrated by thin-

bedded lime mudstone eventually overlapping them, microbial mounds were eventually terminated as a result of sea-level outpacing growth, thus either placing the microbial mound at a sub-photic depth or causing an increase in turbidity (James and Bourque, 1992).

Banded, Bioturbated Lime Mudstone-Packstone

The banded, bioturbated lime mudstone to packstone lithofacies assemblage is composed of thick beds of bioturbated limestone and is characteristically resistant in outcrop profile. Banded and bioturbated lime mudstone to packstone lithofacies assemblages are commonly associated with shale, thin-bedded lime mudstone and microbial mounds (Fig 16). Fresh surfaces are gray to dark gray and weathered surfaces are commonly reddish and gray and mottled in texture. Grains in this lithofacies assemblage include brachiopods, gastropods, hyolithids, trilobite fragments, peloids, ooids and oncoids. Profound bioturbation and preferential dolomitization of porous material within burrows can give the banded, bioturbated lithofacies assemblage a reddish appearance. Individual beds range in thickness from 0.1-1.5 m. Within the lithofacies assemblage, bedding contacts with intraclastic conglomerates are usually scoured at the base and margins while bedding contacts with thin-bedded lime mudstone are more frequently sharp to gradational.

Thin sections range from lime mudstone to packstone. Major grain types in this lithofacies assemblage are trilobite fragments, ooids, and silt-sized, angular to subrounded quartz grains. Bioturbation is evident in both cases, and burrows are infilled with finely crystalline dolomite rhombs. Ooids frequently have pitted exterior

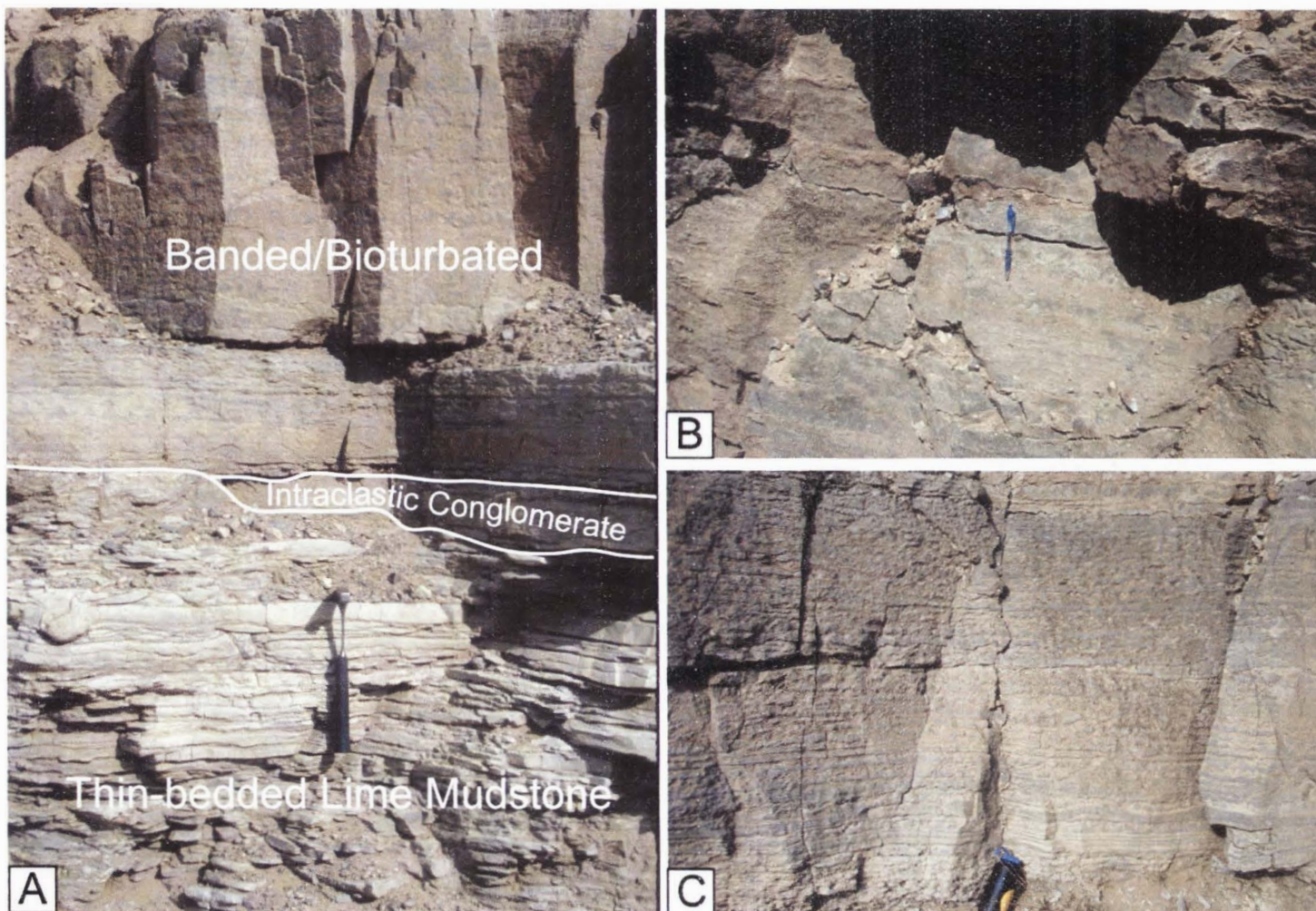


Figure 16. A) Association of banded and bioturbated facies with scoured intraclastic conglomerate and thin-bedded lime mudstone. B) and C) Typical banded and bioturbated outcrop character from Suhaitu and WZA sections, respectively.

margins. Dolomitization is also evident along stylolitic fronts. Matrix support is mainly fine crystalline calcite (microspar). A lime mudstone sample from Suhaitu section shows excellent geopetal filling of burrows.

Interpretation

Generally, this lithofacies assemblage is interpreted as a result of shallow, subtidal deposition, above storm wave-base (Tucker and Wright, 1990; Emery and Meyers, 1996). Grain content and composition, combined with elevated levels of bioturbation, suggest that these rocks were deposited adjacent to a relatively high-energy position. Increased carbonate mud content within this lithofacies assemblage reflects fluctuation to a more distal-ramp position.

Fossiliferous, Massive, Packstone to Grainstone

The massive fossiliferous packstone to grainstone lithofacies assemblage (Fig. 17) is composed of limestone, rich in both articulated and disarticulated skeletal material, interbedded at the base with sandstone and dolostone. The massive fossiliferous packstone to grainstone lithofacies assemblage crops out in the upper portions of all sections. The weathered surfaces of this lithofacies assemblage are light gray; fresh surfaces are blue-gray. This lithofacies assemblage contains numerous whole fossils. Fossil grains include straight and coiled nautiloid shells, gastropods, brachiopods, rugose corals, trilobite fragments, bivalves, pelmatozoan echinoderm fragments, sponges, bryozoans, ooids and oncoids. Large, whole nautiloid shells are frequent fossil constituents within this unit. Coiled specimens have radii up to 30 cm, whereas straight, orthocone specimens are up to 40 cm long.

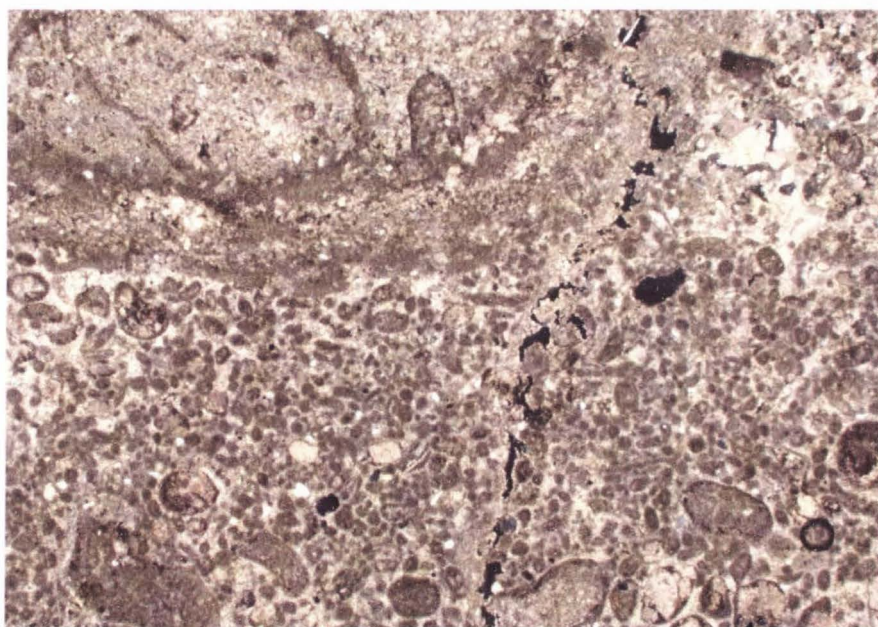
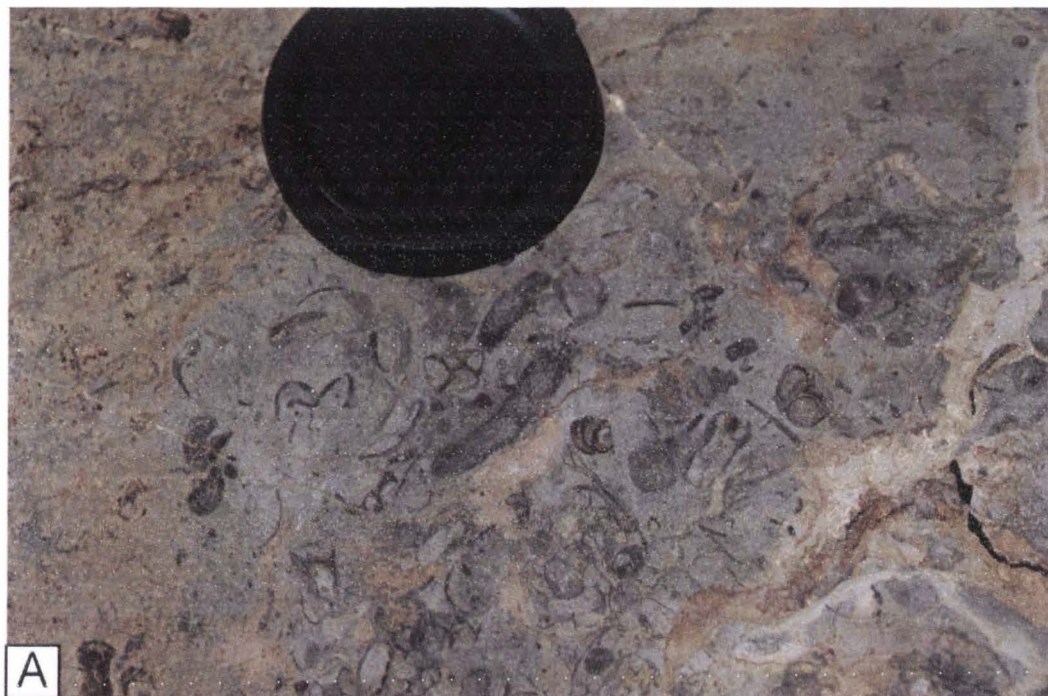


Figure 17 A) Bedding-plane view of fossiliferous, massive, packstone to grainstone with gastropod, bryozoan, and brachiopod fossil fragments. B) Photomicrograph of blue-gray fossiliferous packstone to grainstone facies with abundant pelloids, intraclasts and quartz silt grains.

Numerous *Craterospongia sinica* (new genus, new species; Rigby et al., 2006) (Fig. 18) sponges were found in this interval; sponges are dome shaped and generally 3-5 cm high and approximately 5 cm in diameter with thick, corrugated exterior walls. Individual sponges are numerous and may form small buildups. Large gastropods (6-10 cm) are also abundant and are likely *Maclurites* sp. (Liddell, personal communication). Bedding thickness ranges from 20 cm to 2 m. Most lithologies of the massive fossiliferous packstone to grainstone lithofacies assemblage are bioturbated. Some pervasively bioturbated strata are similar in appearance to banded, bioturbated strata lower in the section. Burrows in this lithofacies assemblage are preferentially replaced with reddish-pink dolomite.

In thin section, massive fossiliferous packstone to grainstone rocks are rich in intraclasts, pellets, echinoderm plates, pelmatozoan echinoderm fragments, brachiopod shell fragments, gastropod shells and ostracodes. Thin sections from this lithofacies assemblage are almost completely recrystallized, with few original textures remaining. The majority of cement is finely crystalline calcite (microspar), while pods of carbonate mud (micrite) remain. Bladed and prismatic cements are visible on the rims of clasts, and, while distinction is difficult, cements seem to rim grains in an even coating. Fine sand-to silt-sized, subround quartz grains are common constituents. Several brachiopod and molluscan grains are coated with the cyanobacterium *Epiphyton* sp. (Shoelle and Ulmer-Schoelle, 2003). Euhedral dolomite rhombs within this lithofacies assemblage are most frequently concentrated along burrowed margins or along stylolites. Small (0.2-0.5 mm) ostracode shells are also abundant grains; most are disarticulated, but otherwise intact. Pellets are small,



Figure 18. Bedding plane photos of *Craterospongia sinica*, a new genus and species of Middle Ordovician sponge. A) Individual specimen. B) Two individuals; note cross section.

ovate grains with no apparent microstructure and are the most abundant grain constituent within units. Trilobite fragments, which are very common in stratigraphically lower lithofacies assemblages, are notably lower in abundance in this portion of the stratigraphic section.

Interpretation

Massive fossiliferous packstone contains a wide variety of fossils indicative of shallow-subtidal, open marine deposition above fair-weather wave base. Fossil assemblages containing brachiopods, echinoids, crinoids and nautiloids suggest normal marine salinity (Wilson and Jordan, 1983). Variations within lithofacies, such as localized concentrations of peloids, oncoids and lime mud, may suggest deposition within a back-barrier lagoon (Enos, 1983; Tucker and Wright, 1990). Articulated, open-marine fauna within beds interpreted as lagoonal either suggest open-marine circulation (Tucker and Wright, 1990) or transport by storm currents (Aigner, 1985). Overall, this lithofacies assemblage was deposited at a shallow depth, ranging from the landward low-energy zone to locations proximal to high-energy depositional environments (Tucker and Wright, 1990; Emery and Myers, 1996).

Oolitic Packstone to Grainstone

The oolitic packstone to grainstone lithofacies assemblage consists of locally cross-stratified, oolitic limestone interbedded with shale, thin-bedded lime mudstone, and banded and bioturbated lime mudstone to wackestone. Fresh and weathered surfaces are usually gray to dark gray; however they can be reddish as well (Fig. 19). Ooids range in size from medium sand-size to greater than 2 cm (pisoid). Some ooid

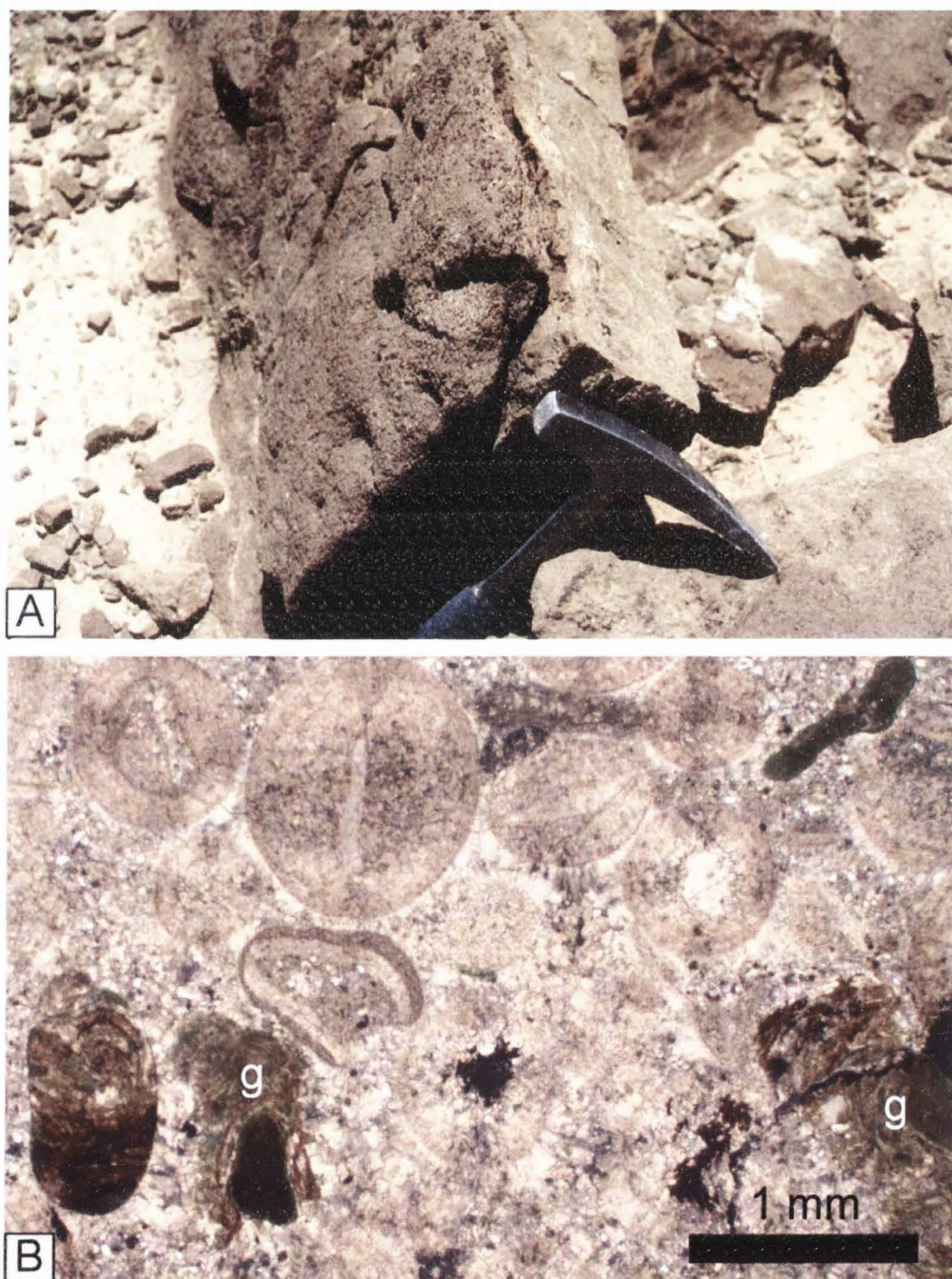


Figure 19. A) Outcrop of glauconitic, oolitic grainstone, younging direction is to the left. B) Photomicrograph showing glauconite (g) “roses”, ooids nucleating upon trilobite fragments and a silty matrix.

packages contain glauconitic grains; these packages are often oxidized, giving the entire bed a reddish-purple hue. Bed thickness is also variable from thin centimeter-scale interbeds to thick, meter-scale packages that are commonly planar cross stratified. Horizontal burrows were observed in Xima section oolitic rocks.

In thin section, oolitic microstructures are obscured by diagenetic overprints that have leached the original material and replaced it with sparry calcite. Concentric laminae are obscured, but more apparent when thin sections are viewed through diffuse light. There is a significant amount of microcrystalline calcite between grain boundaries. In addition, dolomitization has replaced the interior of ooids proximal to stylolites and fractures with zoned, dolomite rhombs, leaving only the micritic envelope. Ooid nuclei are dominantly trilobite fragments, but fine-grained, quartz sand nuclei were also observed. Trilobite thorassic fragments are abundant fossil grains within this lithofacies assemblage. The original calcite microstructure has been completely replaced; however, undulose extinction and typical “shepherd’s crook” (Tucker, 2001) morphology still remain. The matrix within oolitic lithologies is dominantly fine-grained crystalline calcite (microspar). Glauconite grains found in oolitic rocks have a pellet-shape, or a less-distinct, “rose-petal” morphology, replacing coatings in oncoids (Fig. 19). Additional grains observed are intraclasts, echinoderm plates, oncoids, trilobite genal spine fragments and reddish opaque mineral grains (hematite?). Grain-to-grain contacts are few; little pre-cement compaction occurred. Although multiple diagenetic overprints obscure original cement morphologies, Suhaitu section samples show consistent, down-side stalactitic cementation.

Interpretation

Thick oolitic lime grainstone lithofacies assemblages with cross-stratification are interpreted after Halley et al. (1983) as nearshore, high-energy deposits, deposited above fair weather wave-base. In the Read (1981) model, ooid sand shoals potentially form the primary boundary between the nearshore and offshore low-energy environments. Thin section analyses show a significant amount of recrystallized lime mud between grains, indicating that some oolitic samples are not true grainstone. Oolitic packstone beds within this lithofacies assemblage are interpreted as subtidal and more distal relative to grainstone, far enough above fair weather wave base to winnow most, but not all, carbonate mud (Halley et al., 1983; Tucker and Wright, 1990; Emery and Meyers, 1996). Glauconite is commonly formed at mid to outer ramp positions at moderate water depths (Schoelle and Ulmer Schoelle, 2003). Glauconite within a storm-affected depositional environment may have been brought up by bottom currents and worked into sand shoal bodies (Aigner, 1985). Vadose zone cements are not unexpected for this depositional environment; oolitic sand shoals may have been periodically exposed.

Dolomitic Limestones

Dolomitic limestone lithofacies assemblages in northwestern Ordos (Fig. 20A) are almost always interbedded with quartz sandstone beds in the upper half of most stratigraphic sections. Fresh and weathered surfaces are tan to brownish-gray and red-brown. Some dolostone beds are laminated, while others are massive with no apparent preserved sedimentary structures. Limestone texture varies from mudstone



Figure 20. A) Typical outcrop appearance of dolomitic lithofacies from Xima section. B) Bedding plane view of dolomitized intraclastic conglomerate, also from Xima.

to packstone, and quartz sand grains, oncoids and intraclasts were observed. Xima section observations yielded at least two horizons of completely dolomitized intraclastic conglomerate (Fig. 20B). Bedding thickness ranges from 1 cm beds, up to 1.5 m thick. Bioturbation is also apparent in dolomitic limestones, especially at Suhaitu.

Dolomitic limestone thin-sections are more variable texturally and compositionally than was observable at the outcrop. Most can be grouped into true dolomitic mudstones with little to no remaining original texture. Laminae observed at the outcrop were also observed at the microscopic scale as alternating bands of finely- and coarsely-crystalline dolomite crystals (Fig. 21A). Some dolomitic limestone samples contain superb examples of zoned dolomite crystals with a darker nucleus and euhedral, rhombic margin (Fig. 21B). Dolomite rhombs nucleated upon dark grains. Fine-sand sized, subround grains of quartz are present within dolomite samples. Diffuse light observation reveals spherical halos, some of which are completely encased in single dolomitic rhombs, likely former ooids before replacement. Calcite is also usually present, typically limited to the interstices of dolomitic rhombs. A dolomitic limestone sample from the base of WZA section shows a definite microbially-laminated structure that was not observed at the outcrop.

Interpretations

The variability in dolomitic limestone textures and sedimentary structures in northwestern Ordos basin suggests that dolomitization is a function of association. A number of relic structures are observed within dolomite thin-sections (ooids,

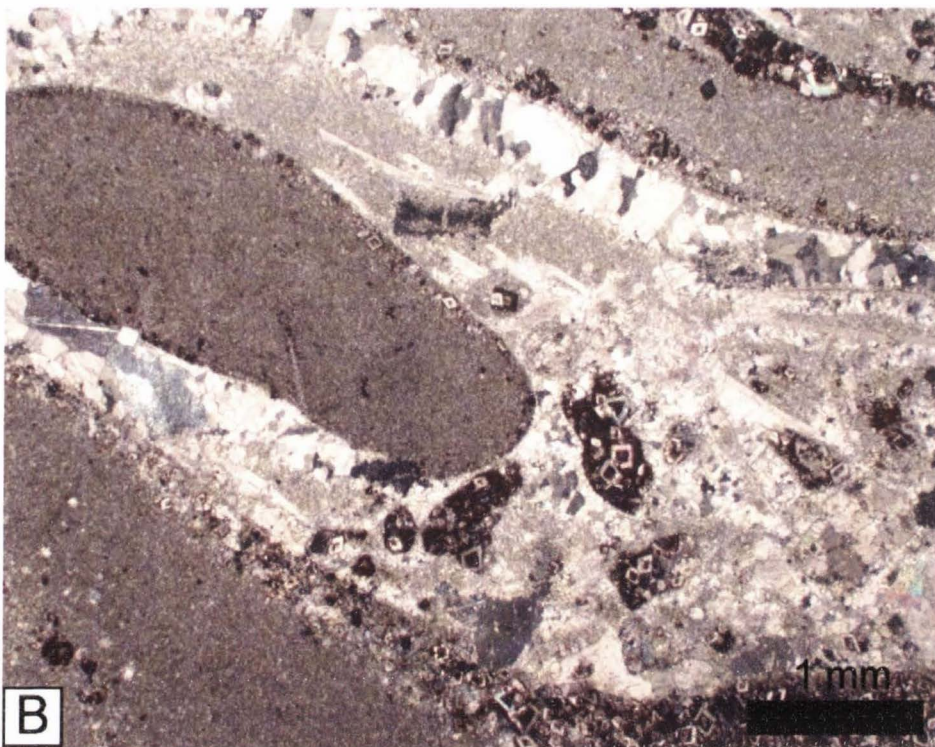
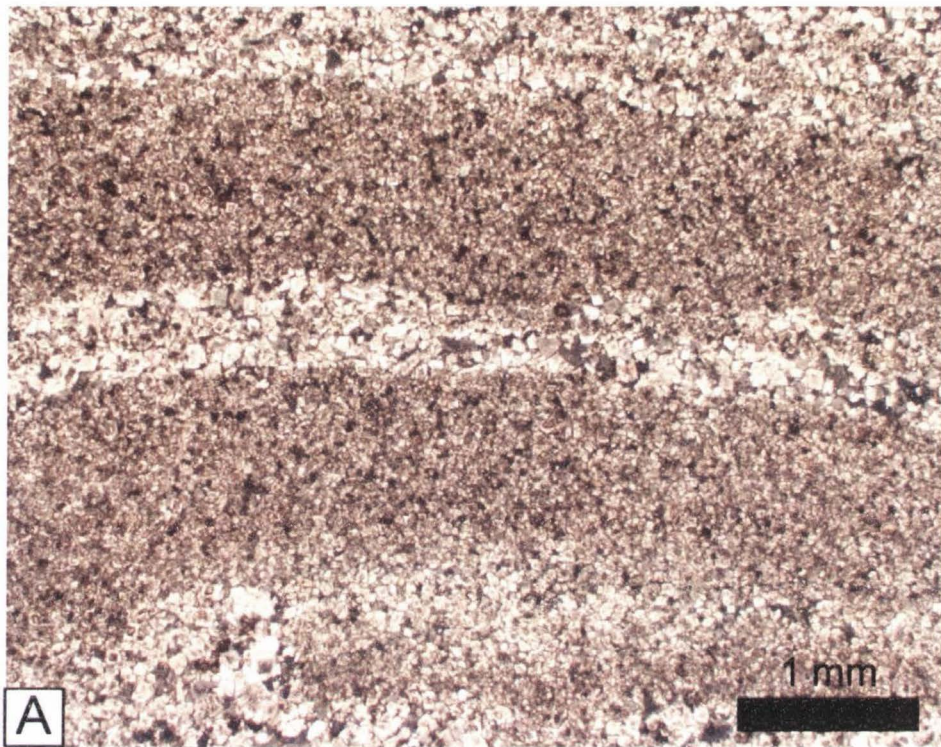


Figure 21. A) Laminated, totally recrystallized, dolostone. B) Grain-rich bed in which dolomitization is occurring along the periphery of larger, hyolithid grains and micritic intraclasts.

intraclastic conglomerate, microbial laminite), thus dolomitization in northwestern Ordos is interpreted to be a post-depositional, diagenetic process.

Dolostones in the Zhuozi Shan are nearly always associated with potentially higher porosity lithofacies, mainly quartz sandstone. Though highly debated, most models of post-depositional dolomite formation involve mechanisms for hydraulic flow through a carbonate platform (Tucker, 2001). Quartz sandstones may have acted as conduits for magnesium-rich fluid flow through the NCCP, causing dolomitization of any surrounding bed with high enough permeability to allow for the transfer of magnesium-rich fluids (Tucker, 2001). Lithofacies assemblage descriptions, interpretations that make up individual units are summarized in Table 2.

Stratigraphy

The stratigraphic succession of lower Paleozoic rocks is similar in both the Zhuozi Shan and the Helan Shan. The lack of biostratigraphic indicators in this study, coupled with the vague descriptions of the lower Paleozoic stratigraphic section of western Ordos in the literature, make applying Chinese formation names and equivalents difficult. In light of this complication and consistent lithostratigraphic successions across the study area, this study breaks away from Chinese formation divisions and subdivides the lower Paleozoic of the Helan Shan and Zhuozi Shan into 4 lithostratigraphic units that make up the composite type section (Fig. 22). The basal portion of all of the stratigraphic sections is rich in shale and is designated as Unit A. There is a distinct upsection change from shale-rich lithofacies assemblages to lime mudstone and wackestone with local microbial mounds. This marks the change from

Table 2. Lithofacies Assemblages, Descriptions and Interpretations

Lithofacies Assemblage	Field Description	Interpretation	Unit
Mudrocks/Shale	Tan, green, brown, purple, gray-black rocks in thin to thick packages, interbedded with thin-bedded lime mudstone, intraclastic conglomerate and thin fossiliferous packstone	Lagoonal	A, B
Argillaceous Limestone	Generally thin bedded and recessive, with minor shell grains and trilobite fragments	Deep Subtidal	A, B, C
Quartz Sandstone	Brown, purple, to white, fine to coarse, ripple, planar and hummocky cross stratified	Shallow Subtidal	A, B, C
Intraclastic Conglomerate	Thin to medium beds, with scoured bases, gutter casts, reddish fringes; associated with all units	All Environments	A, B, C
Thin-Bedded Fossiliferous Packstone	This lithofacies contains trilobite fragments, ooids, pelloids, gastropods, oncoids, and bivalves; rare planar cross strata	Shallow Subtidal	A
Breccia	Granule to boulder sized associated with Unit C	Paleokarst	A, B, C, D
Thin-Bedded Lime Mudstone/Wackestone	Trilobites, gastropods, brachiopods, laminations, ripple cross-strata, burrows, deformation, nodular, starved ripples	Deep Subtidal	A, B, C
Microbial Mounds	Thin, vertical internal structures, frequently associated with thin-bedded lime mudstone/banded and bioturbated mudstone/wackestone	Deep Subtidal	A, B
Banded Bioturbated Lime Mudstone, Packstone	Reddish, very resistant mudstone to packstone, with silty interbeds, and are heavily bioturbated	Deep Subtidal	A, B
Fossiliferous Massive Packstone/Grainstone	Blue-gray packstone to grainstone with abundant whole fossil content (sponges, coiled and orthocone nautiloids, gastropods); also rich in pelloids	Shallow Subtidal	C, D
Oolitic Packstone/Grainstone	Reddish/purple, with glauconite, commonly tabular cross-stratified	Shallow Subtidal	A, B
Dolomitic Limestone	Laminated, microbial, quartz sand, oncoids, intraclasts, bioturbated	Shallow (?)	C


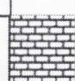




Period	Epoch	Thickness (m)		Facies	Description	
		N	S			
Ordovician	Middle			D	-Massive, blue-gray, fossiliferous lime packstone to grainstone	
		162	90(?)	C	-Sand-rich limestones -Fine to medium grained, cross-bedded quartz-cemented, quartz arenite -Thin to medium bedded dolomitic lime mudstone, dolomitized intraclastic conglomerate	
	Lower	112	246	B	-Thin-bedded lime mudstone -Banded, bioturbated mudstone to wackestone -Local mounds -Intraclastic conglomerate -Thin, fossiliferous packstone	
Cambrian	Upper	100	140	B	-Thin-bedded lime mudstone -Banded, bioturbated mudstone to wackestone -Local mounds -Intraclastic conglomerate -Thin, fossiliferous packstone	
	Middle	158	225	A	-Thick packages of brown to tan shale -Cross-bedded, oolitic lime packstones, glauconite -Thin-bedded lime mudstone, with local microbial laminae -Fossiliferous packstone -Intraclastic conglomerate	

Figure 22. Composite type section of northwestern Ordos basin

Unit A to Unit B, composed of banded and bioturbated lithofacies. Upsection gradational changes from lime mudstone and wackestone to quartz sandstone and dolostone characterizes the boundary between Unit B and Unit C. Quartz sandstone and dolostone beds are capped by Unit D, an open marine, fossiliferous limestone. This general upsection pattern is repeated in all measured sections in the Zhuozi Shan and Helan Shan and there are several lateral trends in thickness, sedimentary structures, and lithology that will be discussed below.

Unit A

The composite type section consists of a lower, shale-rich portion ranging from 40 to 225 m in thickness deemed Unit A. This unit is composed of several lithofacies assemblages, including mudrock and shale, intraclastic conglomerate, thin-bedded dominant lithofacies assemblage within Unit A is mudrock and shale, lime mudstone to wackestone, thin, fossiliferous packstone, oolitic lime packstone to grainstone and lesser banded and bioturbated mudstone to wackestone (Table 2). The which can be up to several meters thick. Thin shale beds act as interbeds in limestone packages whereas thicker mudrock packages are interbedded with numerous lithofacies assemblages. Interbeds within shale packages range in thickness from 5 cm to 1 m and are composed of intraclastic conglomerate, glauconitic, cross-bedded oolitic lime grainstone, thin-bedded, hummocky cross-stratified, rippled limestone and thin shell-rich packstone, and fossiliferous, bioturbated lime wackestone.

Unit A changes laterally from the northern Suhaitu section to the southern Xima section. Unit A at the Xima section contains banded and bioturbated units, thick

shale interbedded with thin intraclastic conglomerate, oolitic packstone and grainstone and fossiliferous packstone. Unit A at the WZA section contains microbially-laminated lime mudstone and dolostone, quartz sandstone and breccia. These lithofacies are interpreted as representing shallow, intertidal to supratidal depositional environments. The boundary between intertidal facies and overlying shales is sharp, without evidence for stagnation and development of a hardground surface. Unit A thickens to the south (Fig. 23), as the Xima section is the thickest at ~225 m and contains thick shale at the base grading into thin shale and argillaceous units upsection, with no evidence of microbial laminae or brecciation. Upsection lithofacies changes support a shallow water, lagoonal depositional environment for the shale lithofacies assemblage. Overall lateral trends place the shallowest facies in the north, and support a southward-dipping ramp model.

At the Suhaitu section, meter-scale cycles consist of lower shale and argillaceous limestone capped by thicker, more resistant beds of thin fossiliferous lime grainstone and intraclastic conglomerate (Fig. 24). This sequence is repeated several times at the meter scale; 25 individual cycles are visible at the base of the Suhaitu section. Similar sequences are present at the WZA and the Xima sections. Basal cycles again are composed of lower mudrock and shale, argillaceous limestone capped by intraclastic conglomerate. Upsection, parasequences have frequent thin-bedded lime mudstone, oolitic lime packstone and grainstone beds; intraclastic conglomerate and shale become less frequent. The progression of cycles from more proximal, argillaceous basal sequences to shoal-derived grainstone reflects transgressive sea-level changes at this point within the section.

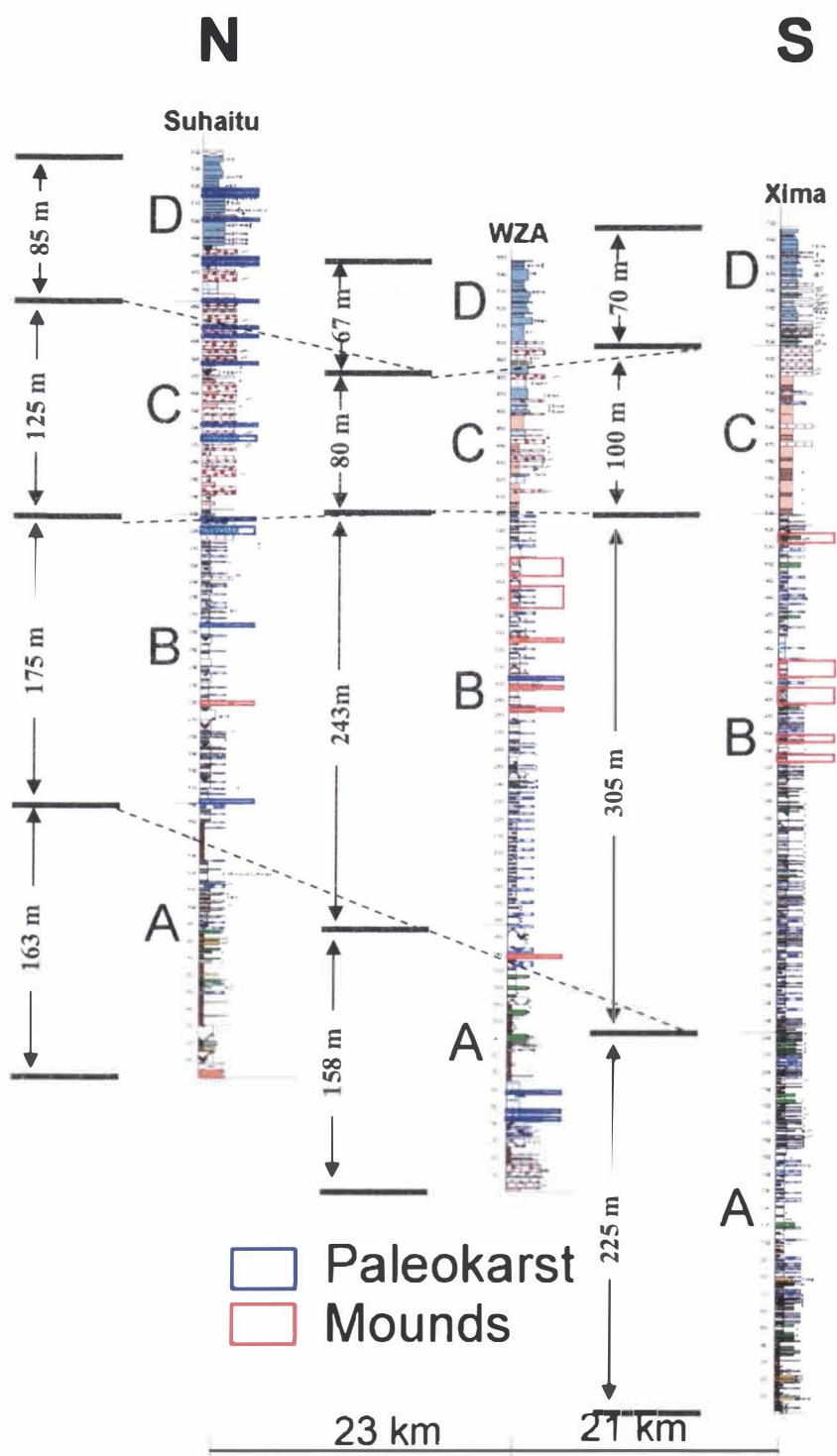


Figure 23. Measured section data from most complete (primary) sections. Sections are scaled from north to south to illustrate lateral trends in section thickness, unit thickness, paleokarsts (blue), and mud mound (red) abundances.



Figure 24. A) Cycle of thin-bedded lime mudstone capped by intraclastic conglomerate from Suhaitu section. B) Intraclastic conglomerate overlain by thin-bedded lime mudstone. Bedding is parallel to vertical direction of the photo.

Unit B

Shale and mudrock-dominated, lower portions of northwest Ordos stratigraphic sections grade into packages dominantly composed of banded and bioturbated lime mudstone to wackestone called Unit B. Other lithofacies assemblages contained within Unit B are thin-bedded lime mudstone to wackestone and thin, fossiliferous packstone. Lateral variability in Unit B is limited to thickness, microbial mound abundance and size and paleokarst abundance. Unit B thickens to the south from 175 to 243 and 305 m (Fig. 23) at the Suhaitu, the WZA and the Xima sections, respectively. North to south mound abundance and size trends are apparent across Unit B in the Zhuozi Shan. The Suhaitu section contains one mounded horizon horizon comprised of a few, relatively small (40 cm diameter) mounds and one bed containing a small microbial mound with a digitate stromatolite cap (Fig. 23). Moving south, the WZA section contains more mounds of larger size, occurring at a relatively higher stratigraphic position. The Xima section contains large microbial mounds at an even higher stratigraphic position; the Xima section microbial mounds reach up to 3 m in height and are the largest mounds encountered in northwestern Ordos (Fig. 23).

Paleokarsts are thicker and more abundant in the north at the Suhaitu section; the WZA section has one paleokarst horizon in Unit B while the Xima section has none (Fig. 23). Lateral trends in Unit B support a southward-dipping, (landward-to-the-north) ramp depositional model. Cyclicity typical of Unit B reflects a transgression relative to Unit A. At the Suhaitu section sequences are composed of thin-bedded lime mudstone, with interbedded and sometimes scoured intraclastic conglomerate beds capped by resistant, banded and bioturbated units (Fig. 25B). This

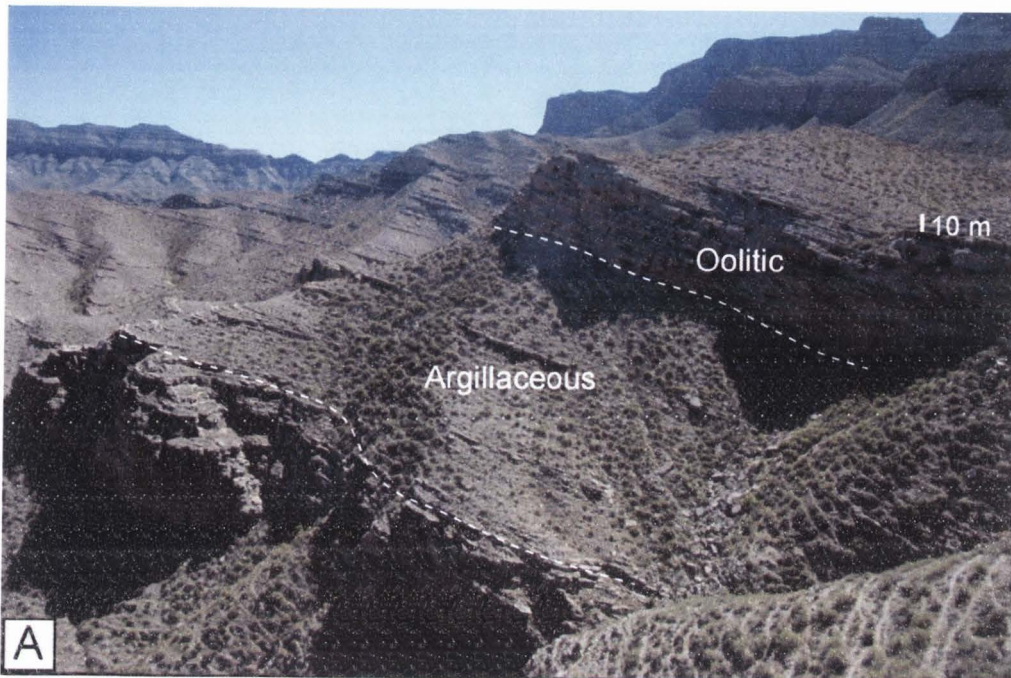


Figure 25. A) Large-scale sequence from Xima section showing more argillaceous units capped by strata rich in oolitic grainstone. B) Sequences from Suhaitu section showing an upward progression from thin-bedded lime mudstone and intraclastic conglomerate to banded and bioturbated units.

sequence is also exposed at the WZA and Xima sections. Farther upsection in Unit B, basal portions of cycles include mounds; mounds are more frequent components of sequences in the southern Zhuozi Shan at the WZA and Xima sections. These cycles represent transgressive, shallowing-upward sequences from more distal thin-bedded lime mudstones to relatively, proximal banded and bioturbated lithofacies assemblages.

Unit C

Unit C is found in the upper portion of the composite type section and contains a marked, gradational transition to a dolomitic and quartz sandstone-rich package of strata (Table 2). Intraclastic conglomerate lithofacies assemblages are nearly nonexistent above this point in the type section. Unit C varies in thickness from 60 to 140m. Dolomitic limestone lithofacies assemblages are thin to medium bedded and contain laminations, while quartz sandstone lithofacies assemblages are moderately to well cemented, and contain planar and hummocky cross stratification.

Intraclastic conglomerate is a common constituent of Cambrian through Lower Ordovician outcrops in North America (c.f., Cook and Taylor, 1977; Sepkoski, 1982; Pratt, 2002), while examples from the rest of the Paleozoic through the Recent are scarcely encountered (Myrow et al., 2004). The absence of intraclastic conglomerate in rocks younger than Lower Ordovician is attributed to an increase in diversity of infaunal dwelling organisms near the end of the Lower Ordovician that constantly agitated sediment and disrupted any potential for early sub-lithification (Sepkoski, 1982).

Cyclicity is less apparent within sandstone and dolostone of Unit C.

Parasequences are characterized by argillaceous limestone grading into dolostone and sandstone. This sequence of lithologies is interpreted as shallowing upward cycles of lagoonal, argillaceous limestone lithofacies assemblages to shallower, shoreface sandstone. At Xima section, coarsening upwards sequences are observable within sandstone, grading from fine calcareous sandstone to coarse calcareous sandstone. Coarsening upwards packages in quartz sandstone beds are likely representative of progradation of the siliciclastic system (Boggs, 2001).

A rather striking trend from north to south in the Zhuozi Shan is the percentage of quartz sandstone per section. Quartz sandstone beds are interbedded with both the dolomitic limestone of Unit C and lime packstone in Unit D. Section comparisons show that quartz sandstone is concentrated in the northernmost Suhaitu section. To demonstrate this trend quantitatively, a simple quartz sandstone to total thickness ratio was calculated (Table 3) using the total thickness of quartz sandstone beds in Units C and D to the total thickness of Units C and D. Suhaitu section has a significantly larger percentage of quartz sandstone at ~48%. The southernmost section, Xima, has less quartz sandstone (25%), while WZA section contains the least amount of quartz sandstone at ~16%. The non-linear relationship in quartz sandstone percentages between the southernmost sections (WZA and Xima) is interpreted as an offshore sand bar, which is common in shallow water carbonate systems (Halley et al., 1983). Quartz sandstone trends suggest that the northern Suhaitu section was more proximal to the source of siliciclastics and shoreline.

As in Unit B, paleokarsts in Unit C are concentrated in the north and are not

Table 3. Quartz Sandstone and Dolomitic Limestone Ratios Per Units C and D

Section	Quartz Sandstone Thickness (m)	Dolomitic Limestone Thickness (m)	Units C and D Thickness (m)	% Quartz Sandstone	% Dolomitic Limestone
Suhaitu	100	12	211	48	6
WZA	24	33	149	16	22
Xima	42	71	168	25	43

found in the south. Paleokarst horizons are more frequent at the Suhaitu section, and are not exposed in Unit C at the WZA or Xima sections. As stated for Unit B, paleokarst abundance trends suggest that lower Paleozoic landward was located north.

Unit D

Overlying the quartz sandstone and dolomite of Unit C is an interval of more massive, blue-gray skeletal packstone and grainstone lithofacies assemblage, 50-90 m thick, deemed Unit D (Table 2). Abundant articulated, whole fossil material and disarticulated fossil grains are present and consist of brachiopods, sponges, coiled and conical nautiloid shells, rugose corals and echinoderm fragments. Beds in Unit D are generally thin to medium bedded, but can contain heavily bioturbated, thick beds with a banded appearance. Other minor lithofacies assemblages contained within Unit D are quartz sandstone, dolomite, and banded and bioturbated packages. Paleokarst surfaces are locally abundant within this horizon.

The transition from Unit C to Unit D contains some of the best exposures of meter scale cycles representative of this part of the northwest Ordos composite type

section. The Xima and WZA sections contain well-exposed examples of interbedded sandstone and dolostone of Unit C grading into sand-rich limestones, and massive, blue-gray fossiliferous packstone lithofacies of Unit D in the scale of one to two meters (Fig. 26). This transition is representative of meter-scale transgressive sea-level changes affecting the basin, exemplified by lithologic contrasts of the shallow sandstone and dolostone of Unit C and the open marine packstone of Unit D. Coarsening upward sequences from pelloid-rich packstone to grainstone are likely representative of sea-level transgression, with high-energy shoals migrating over lagoonal strata.

Incomplete Sections

All measured sections in the Zhuozi Shan follow the general stratigraphic succession described above, yet lateral changes in lithofacies assemblage between sections are apparent. Measured section localities form a rough, north-south transect along the trend of the Zhuozi Shan (Fig. 5; Fig. 23). Several differences become evident when comparing stratigraphic columns, most notably the variation in section thicknesses. Complete sections (Suhaitu, WZA, and Xima) show an increase in thickness from north to south, from 540, to 550, and 700 m, respectively (Fig. 5).

One of the southernmost sections, Chipanjing, is significantly thinner at approximately 200 m; the reason for this trend is unclear. The basal and upper portions at Chipanjing show a familiar lithofacies succession, similar to the composite type section. However, a significant portion of the middle section is absent and covered. Lack of section of this magnitude is possibly the result of a depositional

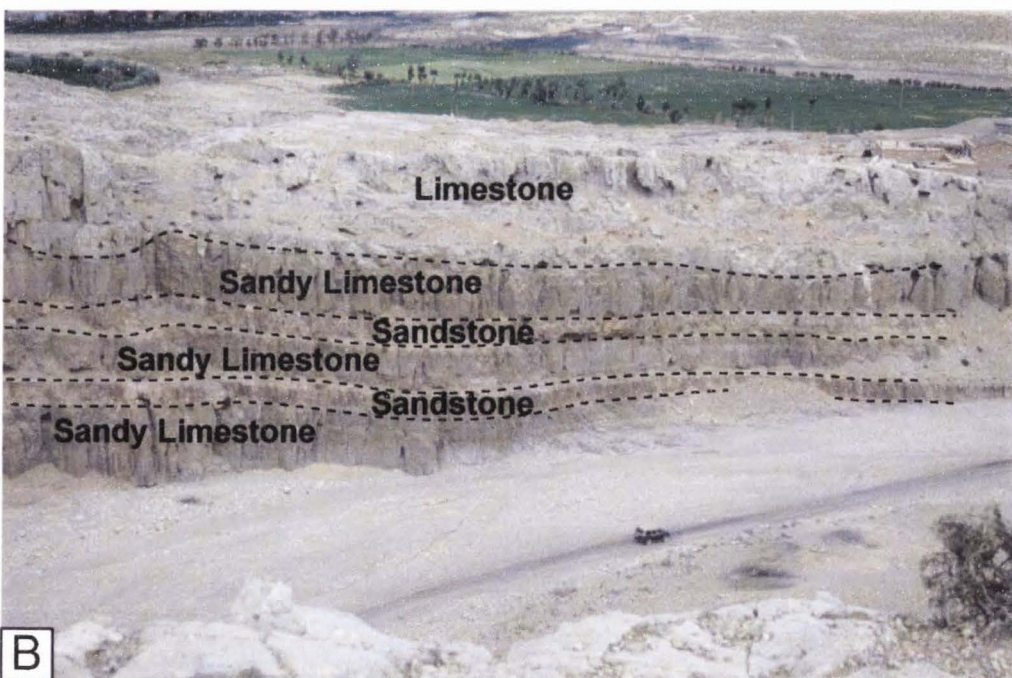
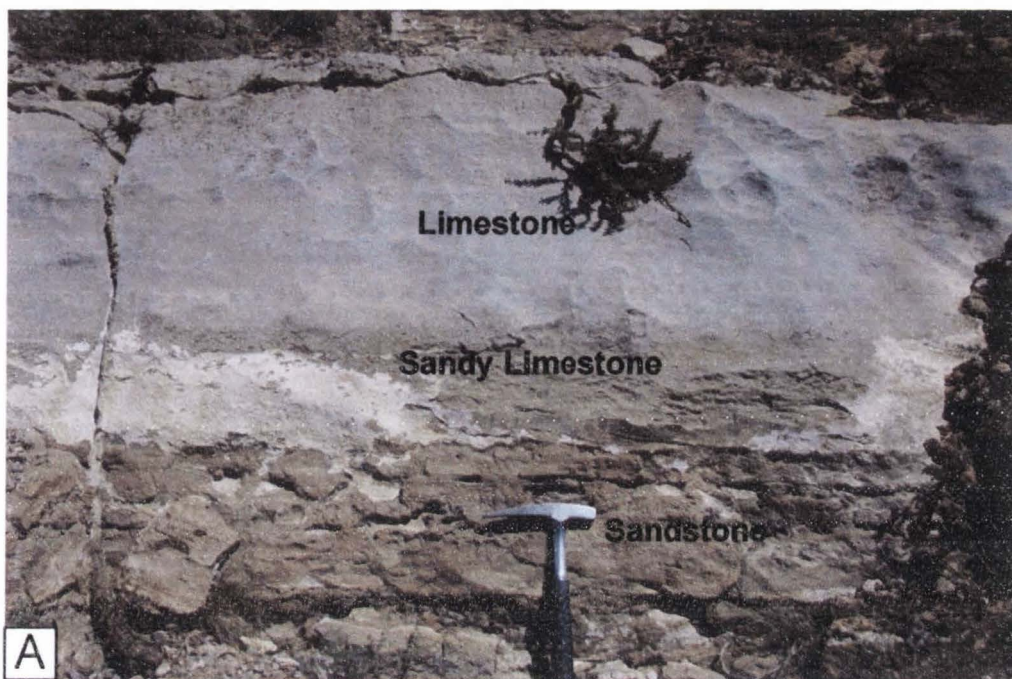


Figure 26. A) Meter scale cycle of sandstone, and sandy limestone, capped by limestone as exposed at Xima section. B) Larger scale example of similar transition from WZA section.

hiatus, low sedimentation rates, or a fault cutting out numerous units. An unconformity or depositional hiatus omitting this much section should show a paleokarst surface or major hardground, however, such a surface was not encountered. Similarly a major fault contact would be expected to be large, exposing evidence such as fault breccia, gouge, mineralization or a slip surface, which was not encountered. Without a surface to observe, the answer to this question is speculative, but given the proximity relative to other sections and to major thrusts in the vicinity, and a conspicuous covered interval in a finer-grained unit, this is most likely either a faulted contact, or a series of faults responsible for cutting out a major portion of this section. Additionally, the Chipanjing section is located in the southern part of the Zhuozi Shan. Therefore, a depositional hiatus omitting a large part of the section is not expected in this more distal part of the early Paleozoic ramp.

Black shale is exposed in the southernmost Zhuozi Shan at Laosunmiao section, which is mapped as Lower Ordovician (Ma, 2002). This is the only occurrence of black shale encountered in the Zhuozi Shan. Basal black shales are laminated, contain graptolites, are several meters thick and grade into thin-bedded, laminated lime mudstone with infrequent chert nodules. Graptolite assemblages indicate a Middle Ordovician age (Charles Mitchell, personal communication). In comparison to the Middle Ordovician, fossiliferous limestones of Unit D north of Laosunmiao, these rocks indicate a rapid change in slope to the south, and a change from shallow carbonate ramp to deeper, shelf deposition.

Age Assignments

Biostratigraphic constraints are poor for lower Paleozoic stratigraphic sections of northwestern Ordos. Index fossils, such as trilobites and graptolites, were not encountered frequently enough to gain proper age control. Meng et al. (1997) discuss formation lithologies and thicknesses for western Ordos, but these formation descriptions are vague in both location and description. By using a combination of the stratigraphic descriptions of Meng et al. (1997) and the thickness estimates of Yang et al. (1992), some preliminary formation assignments have been proposed.

The 1:500,000 map of Ordos basin interprets lower Paleozoic sections in the Zhuozi Shan as Middle Cambrian through Lower Ordovician (Ma, 2002). The stage of the Middle Cambrian is unclear. Middle Cambrian strata of western Ordos are described as three sequences of lower terrigenous clastic rocks and upper oolitic lithofacies 322-333 m thick (Yang et al., 1992; Meng et al., 1997). Literature estimates of Upper Cambrian strata of western Ordos range from 60-180 m thick, comprised of siltstone, calcareous shale, intraclastic conglomerate and bioherms capped by microbially-laminated dolomite (Meng et al., 1997). On average, strata of the Upper Cambrian are thought to be 100 m thick in Ordos (Yang et al., 1992). The Lower Ordovician is described as compositionally similar to the Upper Cambrian, except finer in texture, varying from 98-222 m (Yang et al., 1992; Meng et al., 1997). The average total thickness of Middle Cambrian through Lower Ordovician rocks is approximately 600 m (Yang et al., 1992; Meng et al., 1997). Upper Cambrian strata are variable in thickness and, in some parts of the basin, are completely eroded, juxtaposing Middle Cambrian and Lower Ordovician units (Meng et al., 1997).

Lower Ordovician rocks are possibly absent from western Ordos due to a major unconformity (Yang et al., 1992); most unconformity surfaces reported in NCCP strata are marked by irregular surfaces with visible relief (Meng et al., 1997).

The Suhaitu, WZA and Xima measured sections average 520 m thick. Units A and B are lithostratigraphically similar to Cambrian units from outcrops in eastern Ordos described by Meng et al. (1997). There is a rather thick (1.5 m) brecciated horizon, interpreted to be a paleokarst, 320 m above the base of Suhaitu section that can be traced to WZA section. NCCP literature suggests that Upper Cambrian and Lower Ordovician are bounded by a paleokarst surface (Meng et al., 1997). Thus, the major paleokarst ~320 m above the base of Suhaitu section is interpreted to represent the Upper Cambrian-Lower Ordovician boundary in northwestern Ordos. Using this boundary and Upper Cambrian thickness estimates, Suhaitu section likely reaches down to at least the upper part of the upper Middle Cambrian. Above the proposed Cambro-Ordovician boundary at Suhaitu section, there should be at least 100-200 m of Lower Ordovician rocks (Meng et al., 1997; Yang et al., 1992), which would place the Lower-Middle Ordovician boundary somewhere near the upper part of Unit C at Suhaitu. At Suhaitu, another thick paleokarst occurs approximately 485 m above the base of the section. This paleokarst likely represents the Lower and Middle Ordovician boundary.

In both WZA and Xima sections, there is a brachiopod-rich packstone horizon encountered at 420 m and 630 m, respectively, composed of concavo-convex brachiopod shells of the Rafinesquinidae family, a group no older than Middle Ordovician (Fig. 27A) (Schuchert, 1893). *Maclurites* (sp.) gastropods, found in Unit



Figure 27. A) *Rafinesquinina* sp. brachiopods which indicate Middle Ordovician age. B) Graptolites from a black shale unit in the southern Zhuozi Shan of the *Archiclimacograptus riddellensis*, and *Pterograptus elegans* biozones, which indicate a Late Middle Ordovician age (Charles Mitchell, personal communication, 2005).

D of Suhaitu and Chipanjin sections, is a Middle Ordovician gastropod (Lesueur, 1818). Outcrop evidence for a major unconformity horizon such as paleokarst or paleosol development is not present stratigraphically lower than the first appearance of the Rafinesquinidae horizon. Hence, there is no evidence to assume that these sections are missing major portions of the Lower Ordovician, as suggested by Yang et al. (1992). The age of Rafinesquinidae horizon, combined with the presence of *Maclurites* (sp.) gastropods, implies that units are at least Middle Ordovician near the top of WZA and Xima sections. Also, with no observable, major unconformities below, the sections are dominantly Upper Cambrian to Lower Ordovician. Future workers should examine more detailed biostratigraphic indicators (i.e., conodonts) as a way to refine the stratigraphic assumptions of this study. Laosunmiao section is mapped as Middle Ordovician (Ma, 2002) and is composed of black shales interbedded with dark-gray to black, thin-bedded lime mudstone. Two identifiable species of graptolites (Fig. 27B) found within black shale outcrops are *Archiclimacograptus riddellensis* and *Haddingograptus intermedius*, indicative of the *Archiclimacograptus riddellensis*, and *Pterograptus elegans* Zones (Charles Mitchell, personal communication). These zones indicate a late Middle Ordovician age for Laosunmiao section (Charles Mitchell, personal communication).

It is important to remember that these age assignments for northwestern Ordos basin are based upon a few key assumptions. First of all, literature thickness estimates are assumed to be applicable to western Ordos. Second, paleokarsts are thought to not omit significantly thick packages of strata. These assumptions for northwestern Ordos

basin are initial estimates, and further illustrate the need for additional biostratigraphic work.

Paleokarst: Description, Stratigraphic Position and Interpretation

Major hydrocarbon accumulations of central Ordos basin are reservoired in Middle Ordovician Majiagou Formation paleokarst (Wang and Al-Aasm, 2002). Occurrences of other potential paleokarst surfaces are described in the literature (Yang et al., 1992; Meng et al., 1997); however, data regarding stratigraphic positions are absent. Furthermore, the existence of the Middle Ordovician to Middle Carboniferous unconformity reported from various localities on the NCB is not documented or described in literature pertaining to northwestern Ordos basin (c.f. Yang et al., 1992; Wang and Al-Aasm, 2002).

The major, post-Ordovician, NCB-wide unconformity between the Lower and Upper Paleozoic is exposed in the Zhuozi Shan. Stratigraphic sections measured in the Zhuozi Shan did not include exposures of this unconformity; the upper portion of Suhaitu section is overlain by Jurassic pebble conglomerate, whereas lime packstones of the upper portions of the remaining sections are topographic ridge caps (WZA) or inaccessible (Xima). However, reconnaissance work along the northeastern margin of the Zhuozi Shan anticline revealed the unconformity, expressed as a covered slope-forming zone between Middle Ordovician, massive fossiliferous packstones and Carboniferous clastics (Fig. 28A). Major paleokarst horizons are below the Upper Paleozoic units and into coherent Middle Ordovician

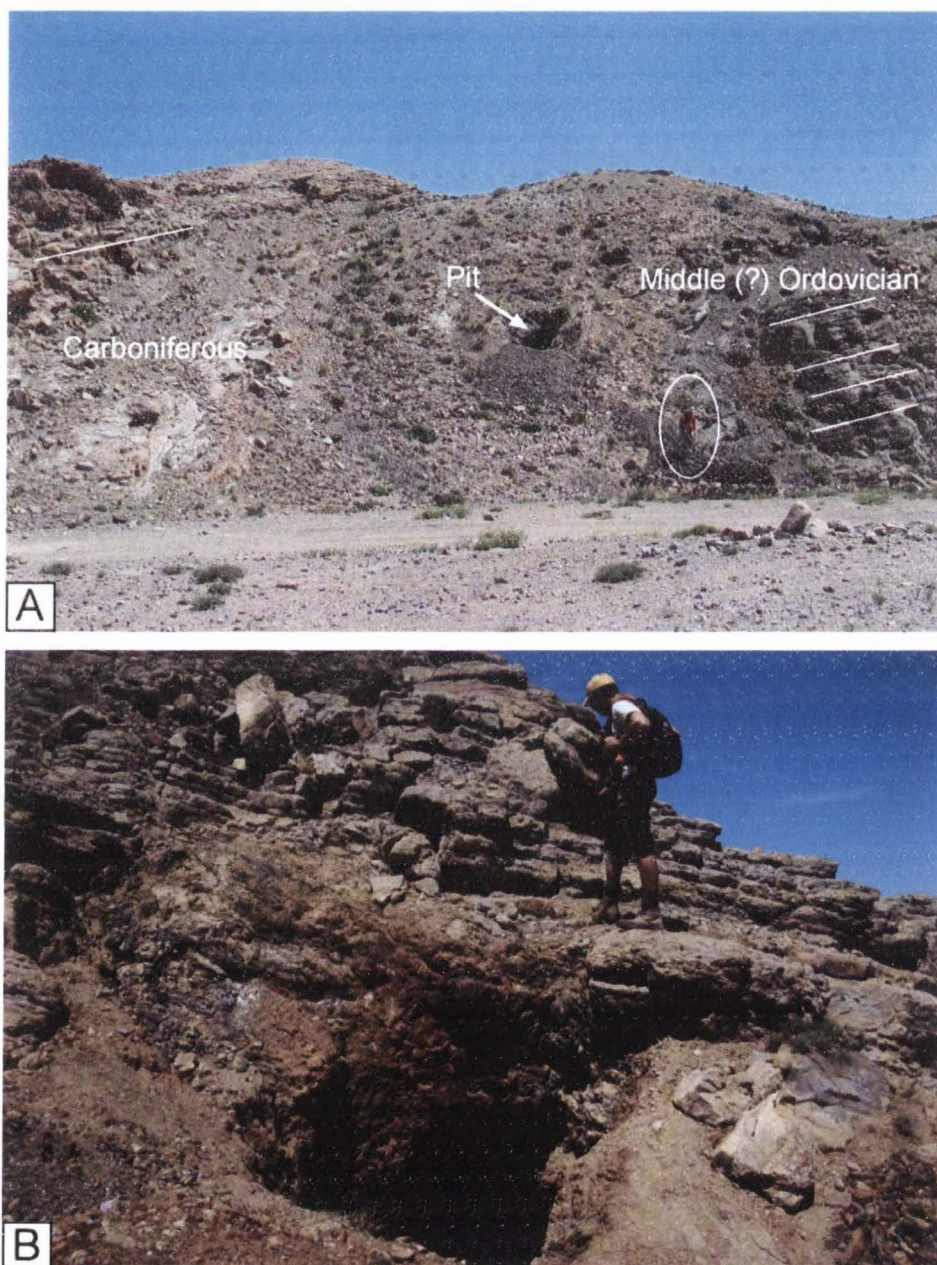


Figure 28. A) Angular relationships between Middle(?) Ordovician and Carboniferous. Kevin Randall circled for scale. B) Sub-unconformity paleokarst character showing alluvium-filled, stained pits that Chinese workers are extracting bauxite.

units. This unconformity is the represents the most missing section due to a paleokarst-related feature encountered in the Zhuozi Shan. Along the covered interval and marking the inferred contact are numerous mining pits where Chinese miners are extracting bauxite (Yang et al., 1992) from what appear to be paleocaves (Fig. 28B), some as deep as 20+ meters. Relatively large (2 m high, 1 m wide) caves are exposed lower in the Middle Ordovician section, below the unconformity, as basal collapse breccias overlain by coarse conglomerates and quartz sandstones. Several modern karst (neokarst) dissolution breccias propagating along fractures were also observed with paleokarst breccias.

Paleokarst horizons were observed most commonly in the northern-most section, Suhaitu. Paleokarst surfaces are chaotic, pebble to cobble-sized breccias, with a reddish-brown, sandy matrix. Most range in thickness from 10 cm up to 1 m thick. The upper portions of sections contain nearly all the paleokarsts present. Near the top of the Suhaitu section in the quartz sandstone and dolomitic interval is a rather large, brecciated bed of granule-to cobble-sized sandy limestone and dolomite. Also at the Suhaitu section are two horizons of large, boulder-sized breccia containing blocks of banded and bioturbated lime mudstone to wackestone, intraclastic conglomerate, biohermal limestone, fossiliferous limestone and lime mudstone. The lower interval (at approximately 320 m) caps a bed of sinuously folded, sand-sized grainstone that is bounded by truncations at the base and top. The WZA section has three exposure surfaces, none of which are very thick. The lower two exposure surfaces are pebble-sized breccias that bound a package of off lapping sandy limestone beds. This feature is interpreted as an accretion set produced by tidal

channel bar migration. Stratigraphically above is a microbially-laminated unit suggesting intertidal to supratidal deposition, and supporting shallow water deposition of this part of the section. Thin, brecciated surfaces represent relatively short periods of exposure without significant paleokarst development. The uppermost paleokarst surface at the WZA section crops out at approximately 305 m above the base of the section, and is a thin, granule-sized conglomerate composed of lime mudstone and wackestone. This unit is between a wavy-bedded, lime mudstone containing microbial mounds and possible microbial laminae, and a lower, cross-bedded fossiliferous packstone, typical of shallow, intertidal to subtidal deposition. Based upon association with shallow water facies, paleokarst development is interpreted to represent brief periods of exposure similar to those observed lower in the section. No paleokarsts or paleokarst related-features were observed in sections south of the WZA.

Interpretations

Based on the location of thinner paleokarst interbeds within the stratigraphic section, and the association of these paleokarsts with shallow-water lithofacies, these surfaces probably reflect fluctuating sea level and cave development during early Paleozoic time. Meng et al. (1997) interpret the Middle Ordovician unconformity as a post-highstand systems tract sequence boundary as Ordovician seas regressed off the craton. In northwest Ordos, the abundance of minor paleokarsts leading up to the thickest, most developed paleokarst are clues that minor sea-level regressions

exposed parts of the platform for a relatively short time periods, which were subsequently overlain by shallow-water, transgressive limestone.

DISCUSSION

Depositional Environments and Models*Late Middle Cambrian to Early Ordovician*

Based upon lithostratigraphy described above, deposition of Middle Cambrian through lowermost Lower Ordovician strata in northwest Ordos basin occurred on a storm-influenced, mixed siliciclastic and carbonate, shallow-water ramp. The fundamental quality of a carbonate ramp is low-angle geometry, which is sometimes less than 20 cm per km, without a clear break in slope (Irwin, 1965, Emery and Myers, 1996). Ramp-style geometries are distinguished from other carbonate depositional systems by the lack of seaward slope-derived facies (e.g. thick successions of slump folded deposits or breccia) (Emery and Myers, 1996), such facies are not observed in northwest Ordos. Nearshore, low-energy ramp facies are commonly separated from more distal facies by a high-energy wave barrier (i.e., shoal) (Emery and Myers, 1996). Oolitic grainstone and packstone lithofacies are common in Units A and B of the composite type section of northwestern Ordos and represent shoals (Emery and Myers, 1996).

The depositional environment of fine-grained units in northwestern Ordos basin is unclear from lithologic observations alone. Low-energy conditions required for mudstone and shale deposition exist in deep water environments (Halley et al., 1983), and shallow back reef, lagoon-type depositional environments (Enos, 1983). In order to clarify fine-grained clastic rock deposition and gain a better understanding of upsection sea-level changes, measured sections are tested against two different

depositional models. The two models of lower Paleozoic depositional environments for northwest Ordos generated for this study are based upon several published interpretations of ramp and general carbonate facies depositional environments (Fig. 29) (Enos, 1983; Halley et al., 1983; Bond et al., 1989; Tucker and Wright, 1990; James and Bourque, 1992; Liang et al., 1993; Emery and Myers, 1996). In the simple ramp model (Halley et al., 1983; Emery and Myers, 1996), shales are deposited exclusively at distal ramps settings, below storm wave base and grade into more grain-rich strata landward, without a significant barrier. The lagoonal model differs from the simple ramp model in that it contains a landward back-barrier low-energy lagoon where fine-grained clastics are also deposited. In addition, relative depth interpretations of intraclastic conglomerate packages (Liang et al., 1993) and sea-level depths of carbonate lithofacies (Bond et al., 1989) were employed in both models to generate sea-level histories.

Both the lagoonal and simple ramp models are based upon ramp and shelf carbonate model interpretations of Halley et al. (1983) and Wilson and Jordan (1983) respectively, and have unique, seaward facies transitions. In the simple ramp model, the intertidal coastal zone is characterized by tidal flat, possibly microbially-laminated muds, that grade laterally into the shallow subtidal zone, above fair weather wave-base (Halley et al., 1983). The lagoonal model is composed of a nearshore, low-energy zone, protected by a barrier of oolitic and skeletal grainstone to packstone.

Seaward of the barrier, the simple and lagoonal ramp models have similar facies transitions. Facies transitions seaward of the barrier in the lagoonal model are similar to the simple ramp model. The shallow subtidal zone is characterized by a

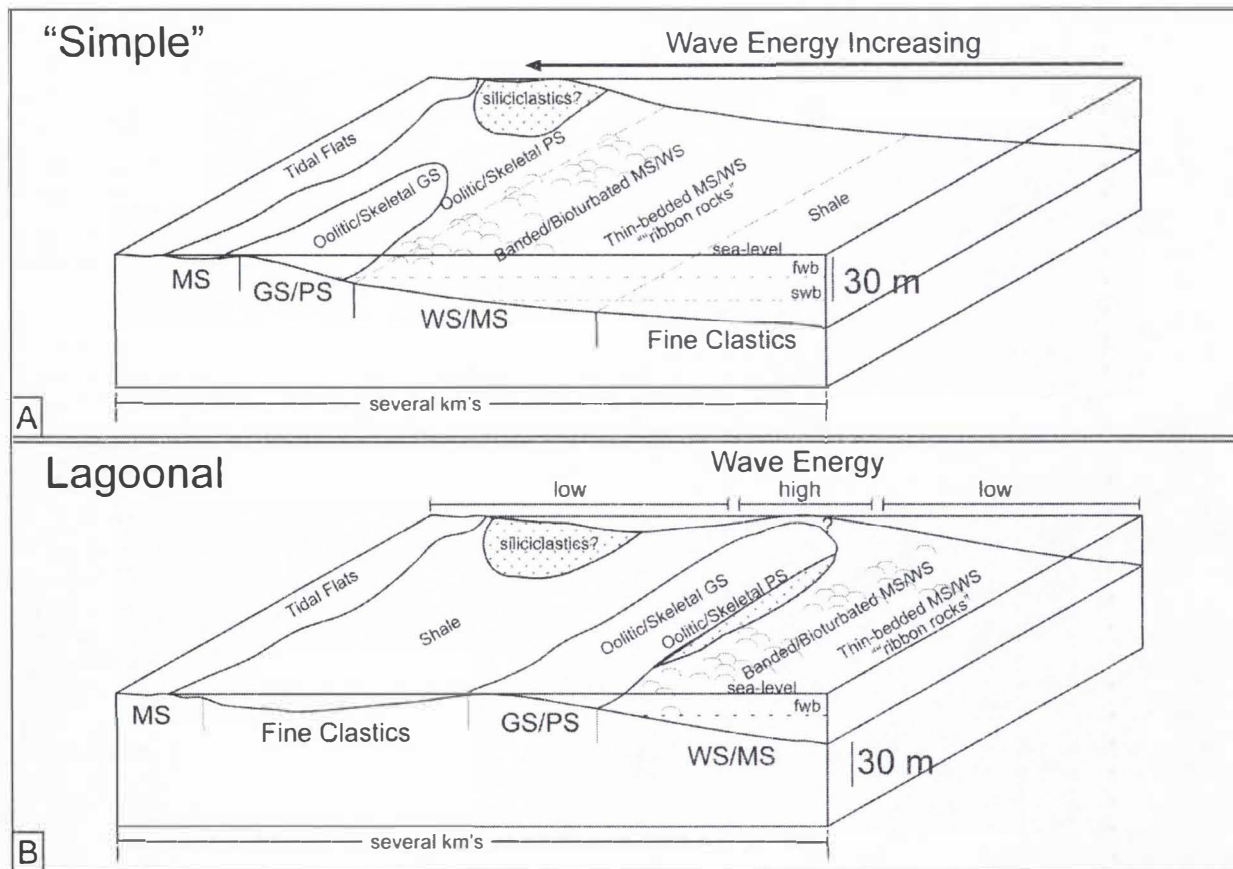


Figure 29. Depositional models proposed for carbonate ramp environments of northwest Ordos basin. A) Simple ramp profile with wave energy and grain percentage decreasing seaward. B) Lagoonal ramp model showing a high energy barrier separating a landward, low-energy lagoon (after Read, 1981; Enos, 1983; Halley et al., 1983; Bond et al., 1989; Tucker and Wright, 1990; James and Bourque, 1992; Liang et al., 1993; Emery and Myers, 1996)

abundance of cross-stratified, rounded skeletal and oolitic grains (Halley et al., 1983; Emery and Myers, 1996). Farther seaward, shallow facies grade into deep-water facies composed of packstone, wackstone and deeper subtidal ribbon-limestone and shale; sedimentary structures are limited to hummocky cross stratification and laminations (Halley et al., 1983; Emery and Myers, 1996; Tucker and Wright, 1990).

Sea-level curves for the lagoonal ramp model are presented in Plate 2, and have significant implications for shale deposition in the basal portion of measured sections. In all complete measured sections, basal shales are bounded and interbedded with lithologies interpreted to represent shallow subtidal to peritidal depositional environments. Sea-level curves generated on the assumption that shales are deposited at a deep, distal-ramp setting require several high-magnitude (30+ m) sea-level shifts. Using the lagoonal depositional model in conjunction with bounding units of the lower shale packages, shifts in sea level are reduced and are significantly lower in magnitude (< 10m) than the first model. Based upon the magnitude of facies shifts, the lagoonal model is more reasonable for deposition of lower Paleozoic shales in northwestern Ordos. Thus, only the lagoonal model is shown in Plate 2. Relative sea level curves for each section show high frequency flooding with more gradual progradation. These curves are compared to other established sea-level curves, both local (NCCP; Meng et al., 1997) and global (Vail et al., 1977; Hallam, 1992), and will be discussed later in this paper.

Enos (1983) advises that, although difficult, vertical and lateral stratigraphic transitions are crucial in distinguishing strata deposited in restricted environments in the sedimentary record. To statistically model vertical transitions, lower Paleozoic

lithofacies assemblages of northwestern Ordos were coded with numbers and entered into a Markov Chain Analysis program developed by Dan Lehrmann and Bob Goldhammer. The data set output by this program includes a lithofacies assemblage transition matrix showing the frequency of vertical transitions between coded units (Table 4). Shale to intraclastic conglomerate and shallow-water-derived oolitic grainstone is a common transition, yet shale to banded and bioturbated units and thin-bedded lime mudstone interpreted as deeper water strata, does also occur. This may imply shale deposition at both lagoonal and distal subtidal positions on the ramp.

Middle Ordovician Deposition

Upsection and lateral lithofacies assemblage contrasts indicate an upsection change in deposition in Middle Ordovician. Lithofacies assemblages of Unit D in most sections of the Zhuozi Shan are composed of lime packstone to grainstone with numerous, whole fossils, that suggest an open marine, middle to upper shelf depositional setting. Unit D is interpreted as Middle Ordovician based upon the presence of numerous *Maclurites* (sp.) gastropods (Lesueur, 1818), and brachiopods of the Rafinesquinidae family (Schuchert, 1893). Black, laminated shale rocks encountered in the southern Zhuozi Shan contain graptolitic assemblages of Middle Ordovician age, and are interpreted as deposited in a deep-water setting. This lateral contrast between similar-aged, shallow and deep-water lithofacies suggests a change in seaward slope-angle. Moreover, this change in lithofacies assemblage indicates the evolution of the late Middle Cambrian-Early Ordovician ramp system to a Middle

Table 4. Subfacies Transition Matrices

		Suhaitu subfacies transition matrix																
		to																
from		calc. ss	qtz. c ss	shale	siltstone	dolomite	int. cong.	bg. ps/gs	oolitic gs/ps	mounds	b/b ws/ps	tbfps	tblms	silty lms	arg. ls	breccia	total	
calc. ss		5	9			1					2			2	2		5	26
qtz. c ss		14	1			2	1				1		2	2			1	24
shale							5		5		1	6	3					20
siltstone																		0
dolomite		3	1								2		1	1				8
int. cong.				5			2		1		5	4	23	11			1	52
bg. ps/gs								11								3	2	17
oolitic gs/ps				5			1				1		2					8
mounds																		0
b/b ws/ps		2	2	2			6				2	5	2				3	24
tbfps							2						6					11
tblms			2	5		2	24			2	8			1				44
silty lms			2			3	11				1	1	1				1	20
arg. ls			2					2						1			1	6
breccia		2	5					3			2		1			1		14
total		26	24	20	0	8	52	16	8	0	25	11	44	20	6	14		274

		WZA subfacies transition matrix																
		to																
from		calc. ss	qtz. c ss	shale	siltstone	dolomite	int. cong.	bg. ps/gs	oolitic gs/ps	mounds	b/b ws/ps	tbfps	tblms	silty lms	arg. ls	breccia	total	
calc. ss		1	6			2		3								1		13
qtz. c ss		2		3		3	2	1								2		13
shale			3				4	1	2		3	5						17
siltstone																		0
dolomite		5	1			1							3			1		11
int. cong.				4			1		2	3	12	1	19	10				52
bg. ps/gs						1		17				1				3		22
oolitic gs/ps			2										4					6
mounds							3				2							5
b/b ws/ps		1	1				10			2	2	3	6	1				26
tbfps			6								3		1			1		11
tblms						4	22		2		4	1						33
silty lms							10				1							11
arg. ls		3	3	1				2			1							10
breccia																		0
total		11	14	17	0	11	52	23	6	5	28	11	33	11	8	0		230

		Xima subfacies transition matrix																
		to																
from		calc. ss	qtz. c ss	shale	siltstone	dolomite	int. cong.	bg. ps/gs	oolitic gs/ps	mounds	b/b ws/ps	tbfps	tblms	silty lms	arg. ls	breccia	total	
calc. ss														1		3		0
qtz. c ss			10				3		10									27
shale								10		3			3	14	2			32
siltstone								1							1			2
dolomite							13											17
int. cong.		1	9	2		1	1			8	1	6	1	88	38			156
bg. ps/gs			9					4		2					2			17
oolitic gs/ps				3				3	2	1	1	2	2	18	6			38
mounds								3		1	2	1		2				9
b/b ws/ps								9		2		1		8	2			22
tbfps				3				2		1								6
tblms				15				89		17	5	7	5	1				139
silty lms					1			38		3		5	3					50
arg. ls			3						2									5
breccia																		0
total		0	27	31	2	17	156	18	38	9	22	6	139	50	5	0		520

calc. ss=calcareous sandstone, qtz. c ss=quartz cemented sandstone, int. cong=intraclastic conglomerate, gs/ps=grainstone/packstone, bb ws/ps=banded, bioturbated wackestone/packstone, tbfps=thin-bedded fossiliferous packstone, tblms=thin-bedded lime mudstone, lms=lime mudstone, arg. ls=argillaceous limestone

Ordovician platform and shelf margin depositional system in northwestern Ordos (Fig. 30).

The Storm Sedimentation Model

The Aigner (1985) storm sedimentation model encompasses the effects of barometric pressure, wind, offshore currents and oscillatory waves (Fig. 10). During storms, bottom waters and sediments are affected by both onshore and offshore storm wave oscillations (Aigner, 1985). Storms increase barometric pressure on offshore waters and, combined with winds from storms blowing onshore, coastal water levels are raised an average of 0.5 m (Aigner, 1985). Return-flow of displaced sea-water is accommodated by offshore-directed bottom currents circulating sea-water back offshore (Aigner, 1985). Thus, this model predicts onshore sediment transport by storms in shallow water and offshore transport in deeper waters (Aigner, 1985).

Upper Cambrian and lowermost Lower Ordovician strata in northwestern Ordos support aspects of the storm sedimentation model of Aigner (1985). Fine-grained, lagoonal beds contain thin interbeds of grain-rich lithofacies, such as ooids and fossiliferous packstone, that are expected in higher energy settings. Ooid margins in samples from banded and bioturbated units at Suhaitu are noticeably pitted and pockmarked. Although northwestern Ordos lithologies record numerous diagenetic events which may be responsible for obscuring and altering grain margins, evidence suggests that some grain-rich interbeds were transported and abraded by storm activity.

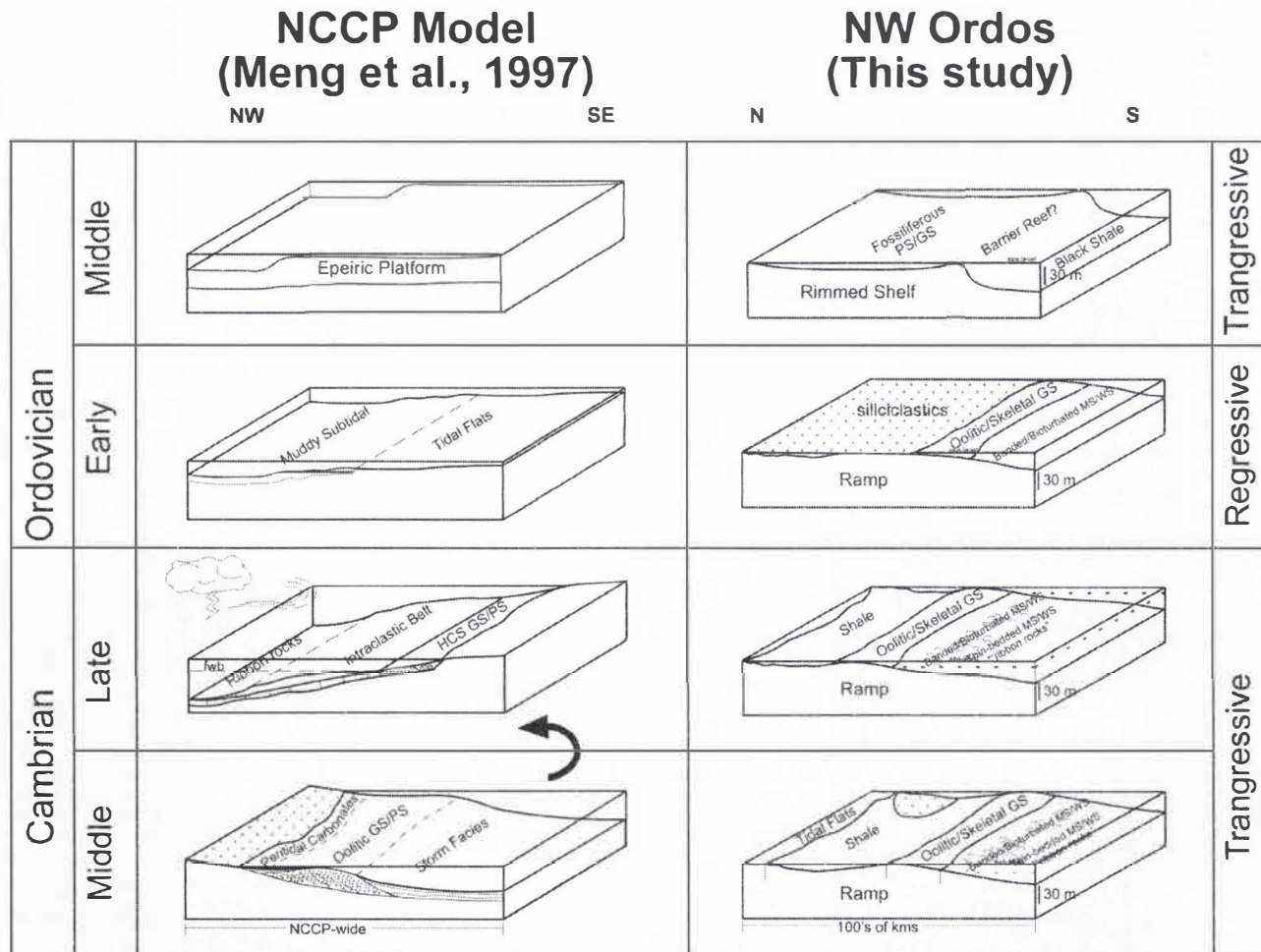


Figure 30. Block diagrams depicting depositional environments and platform architecture. Meng et al. (1997) invoke platform-wide tilting as a mechanism for Late Cambrian intraclastic conglomerate abundance, placing the ramp's windward side into the path of more frequent storm activity. The NW Ordos model is more localized and does not require tilting of the platform.

Sequence Stratigraphy

Detailed sequence stratigraphic interpretations are difficult to make without proper age constraints. However, stacking patterns of lithofacies have implications for the sea-level history of Ordos basin. Suhaitu section was first evaluated in terms of cyclicity and the location of significant flooding surfaces, and then compared to other sections of northwestern Ordos. As stated above, numerous cycles are evident. The following lower Paleozoic sequence stratigraphy of northwest Ordos is presented on relative sea-level shifts of the parasequence set (4th order) and sequence (3rd order) scales. Major sea-level changes (2nd to 3rd order scale) correspond with Units A, B, C, and D.

Unit A at the base of the Suhaitu section is composed of four, meter-scale, shallowing upwards parasequence sets. These sets consist of lower, distal carbonate rocks (e.g., banded and bioturbated mudstone to packstone) capped by mudrock and shale (e.g., mudrocks with oolitic and intraclastic interbeds) lithofacies assemblages, interpreted as lagoonally derived. The WZA section parasequence sets consist of shallow subtidal rocks, such as oolitic grainstone, grading upwards into lagoonal shale and microbially-laminated dolostone and breccia, which supports a shallow water interpretation. Unit A at Xima consists of four shallowing upward sequences, similar to those described at Suhaitu section. Unit A stacking patterns suggest two different implications for Middle Cambrian sea-level. Cambrian seas may have been transgressing and regressing at a higher frequency, causing shallowing upward sequences in the rock record. An alternative to high frequency sea-level shifts involves the interplay of sedimentation and sea-level rise. Cambrian seas may have

transgressed while carbonate deposits prograded, shown as shallowing upward sequences in the stratigraphic record, which is common in carbonate systems (Emery and Myers, 1996). North American sea-level curves suggest that global sea-level was transgressing throughout much of the Cambrian (Vail et al., 1977; Hallam, 1992), thus the progradational explanation may be more applicable to northwestern Ordos.

Unit B of Suhaitu section was deposited in deeper water relative to Middle Cambrian lithofacies of Unit A. At least four parasequence sets are recognized from Unit B, all of which are characterized by subtidal, distal carbonate rocks (e.g. banded and bioturbated lithofacies) capped by shallow-water rocks (e.g. oolitic grainstone, paleokarst). Parasequence sets in Unit B are characterized in all sections by less frequent intertidal to supratidal rocks relative to Unit A and more frequent thin-bedded lime mudstone and banded and bioturbated mudstone to wackestone. This change in deposition reflects a continued transgression during Late Cambrian and Early Ordovician times. Again, shallowing upward sequences within Unit B are likely a result of carbonate sedimentation rates outpacing sea-level, resulting in progradation of the entire system (Emery and Myers, 1996). This agrees with North American sea-level curves that suggest continued transgression during the Late Cambrian and Early Ordovician (Vail et al., 1977).

Unit C is rich in quartz sand, dolomitic mudstone and paleokarsts, and probably reflects the shallowest sea-level within the stratigraphic succession. Generally, sequences within Unit C are not apparent. Coarsening upward sequences at the sub-meter scale are exposed in quartz sandstone beds at Xima section, indicating progradation of siliciclastic systems. Relative to Unit B, Unit C represents

a sea-level regression. Sequences in Unit D are composed of quartz sandstone beds, capped by sand-rich limestone and fossiliferous packstone to grainstone. These sequences are interpreted as transgressive packages. Overall, stacking patterns in Units C and D suggest a major regression during the Early Ordovician, followed by a sea-level transgression during the Middle Ordovician. This pattern is also observed in North American lower Paleozoic sea-level curves (Vail et al., 1977; Sloss, 1988).

Thus, Cambro-Ordovician sea-level at the 2nd order scale (Plate 2) in northwestern Ordos was transgressing from the Middle Cambrian through the Lower Ordovician. Lower Ordovician seas lapped off the continent forming paleokarsts and quartz sandstone deposits, which is equivalent to the boundary between the Sauk and Tippecanoe cratonic sequences in North America (Sloss, 1988). Sea level rose again in the Middle Ordovician, as evidenced by transgressive sequences at the top of the Suhaitu, WZA and Xima sections. Middle Ordovician transgression in northwest Ordos is concordant with North American stratigraphy, as the Middle Ordovician marks the transgressive phase of the Tippecanoe 2nd order sequence (Bond et al., 1988; Sloss, 1988; James et al., 1989)

Paleogeography and Lower Paleozoic Tectonic Events

Multiple phases of tectonic and geometric evolution on the NCCP occurred during the lower Paleozoic (Fig. 30) (Meng et al., 1997). Lower Cambrian clastics, phosphorites and minor carbonates represent initial flooding and ramp initiation, capped by widespread carbonate deposition as the platform was established (Meng et al., 1997). Middle Cambrian units were deposited during the ooid-dominated stage,

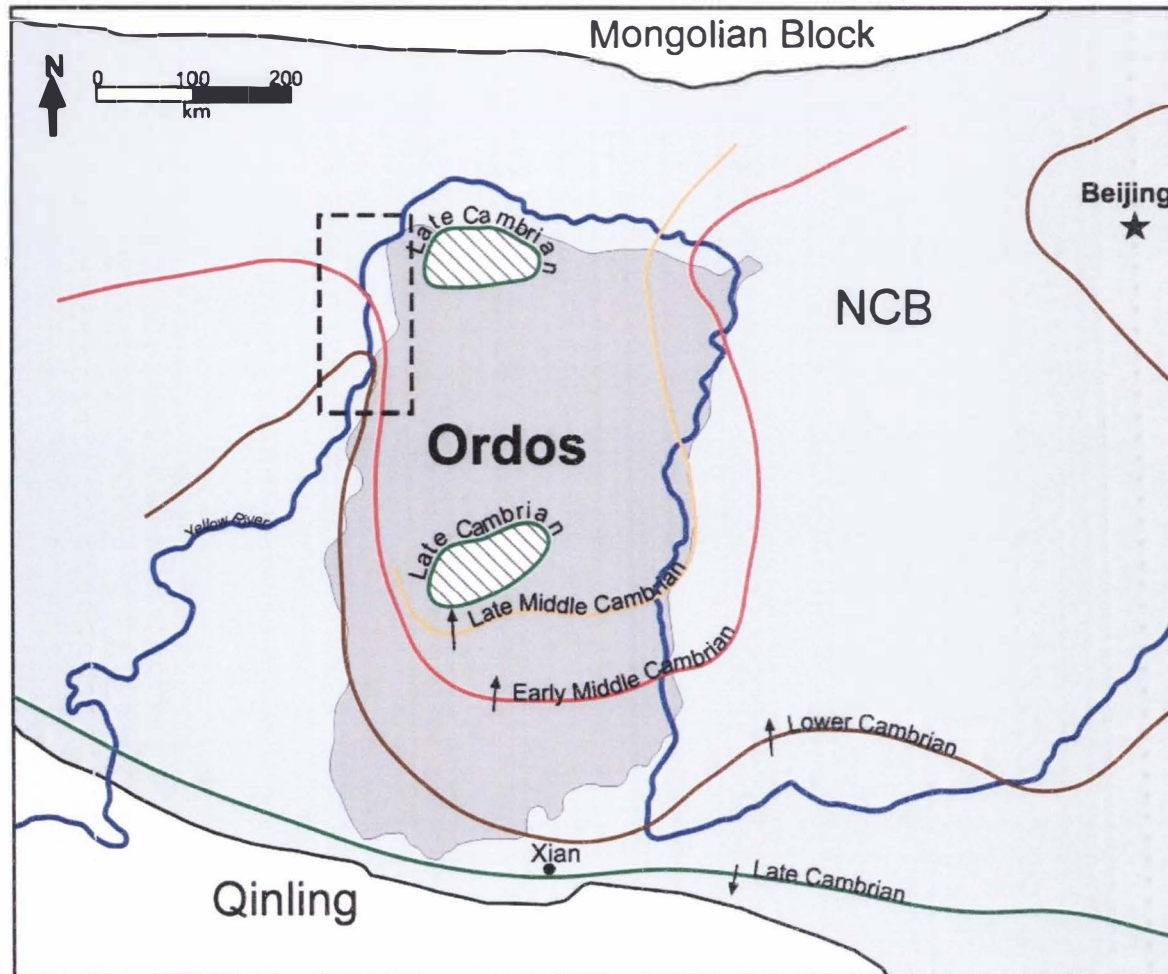


Figure 31. Map of Ordos basin showing shoreline positions through the lower Paleozoic, as interpreted from Meng et al. (1997). Arrows on shorelines indicate landward direction; diagonal pattern represents paleoislands. Note dual positions of Late Cambrian sea-level surrounding suggested paleoislands and in the southern portion of the platform, with landward direction opposite of older shorelines, post-platform tilting. (Modified from Meng et al., 1997)

while the Upper Cambrian was a time of storm-influenced deposition (Meng et al., 1997). The upper part of the Upper Cambrian through Lower Ordovician stratigraphic succession is interpreted as a result of epeiric carbonate platform deposition, later terminated by platform exposure (Meng et al., 1997).

Meng et al. (1997) state that a tilting event changed the shoreline position of the whole North China Carbonate Platform before the start of the Upper Cambrian (Fig. 31). The Middle Cambrian shoreline in western Ordos was oriented approximately NW-SE, landward to the northeast (Meng et al., 1997). The whole platform was tilted at the end of the Middle Cambrian, inverting the shoreline to a WNW-ESE position, exposing the formerly deepest parts of the basin as landward was located to the south (Meng et al., 1997). Mechanisms for tilting are described as a “collision with a marginal basin to the north and the subsequent loading and flexural response of the platform” (Meng et al., 1997). The only evidence presented for NCCP tilting is an increase in the abundance of the storm-influenced intraclastic conglomerates in the Upper Cambrian; tilting to the northwest places the platform in the path of more frequent storm currents (Meng et al., 1997). Conflicting information is presented in figure 4 of Meng et al. (1997), which shows two Late Cambrian shorelines (Fig. 31). Therefore, the following discussion examines the relevancy of both shoreline positions to Ordos in order to determine which one is most applicable.

Although an increase in intraclastic conglomerate is observed in northwest Ordos and seemingly corresponds with the boundary between the Middle and Upper Cambrian as described by Meng et al. (1997), shoreline positions are not consistent with observations from northwest Ordos. The percent of Lower Ordovician quartz

sandstone beds and thicknesses increase to the north, which suggests that the northern part of the platform was proximal to the source of siliciclastic influx. Quartz sandstone beds are composed of well-sorted, rounded quartz with carbonate cement, showing planar cross-strata and minor hummocky cross-stratification, deposited in a nearshore environment. Microbial mound trends also question the Meng et al. (1997) shoreline model, as larger mounds are found toward the south, indicating that accommodation space was greater in the southern part of the Zhuozi Shan relative to the north. Measured sections increase in thickness to the south (Plate 1), suggesting that more accommodation space was being created to the south. All of this evidence implies accommodation space in northwestern Ordos basin increased to the south and a more plausible shoreline for this area during the Cambrian and Ordovician was most likely oriented roughly E-W, with seaward to the south. An increase in intraclastic conglomerate abundance is likely attributable to climate change, as suggested for the Helan Shan by Liang et al. (1993).

Another conflict with the paleogeographic model presented by Meng et al. (1997) are paleokarst horizons. Paleokarst surfaces are exposed in the upper portion of the northernmost section, Suhaitu, while few were observed at WZA section and none were encountered at Xima. This trend suggests that northern exposed unconformities may grade into correlative conformities (Emery and Myers, 1993) farther south, further supporting that strata in the south were deposited in relatively deeper water. However, paleokarsts exposed at Suhaitu are generally thin, and similar surfaces farther south may be obscured due to poor outcrop exposure.

Shale trends are less apparent, yet the presence of black shale in the southern Zhuozi Shan may also support the proposed shoreline position herein. The only reliable signatures of black shale are low depositional energy and low oxygen conditions allowing for preservation of organic matter, conditions that occur in both deep and shallow water depositional environments (Wignall, 1994). However, Laosunmiao shale beds contain graptolites and minor chert nodules, both of which suggest deep water deposition (Bulman, 1955). Therefore, if Laosunmaio facies are assumed distal ramp, deep-water depositional facies and equivalent to the upper part of Unit D, their presence has implications in support of new paleogeographic models presented in this paper (Fig. 30). In comparison to the Middle Ordovician shallow, lagoonal to sub-tidal carbonates of Suhaitu, WZA and Xima sections, deep-water shales at Laosunmiao imply increasing of accommodation space southward (Plate 1).

Lower Paleozoic Tectonics

Numerous authors cite aulacogen subsidence (Sun et al., 1989; Yang et al., 1992; Yin and Nie, 1996; Meng et al., 1997; Darby and Ritts, 2002) in north China during the lower Paleozoic, yet the evidence to support the presence of an aulacogen is lacking. Aulacogens are thought to be major forces in Middle Ordovician tectonics, and are suggested to have accommodated greater than 2000 m thick successions of lower Paleozoic carbonates and lesser siliciclastics in the western part of Ordos (Sun et al., 1989; Yang et al., 1992; Yin and Nie, 1996; Meng et al., 1997). Deemed the Helan Aulacogen (Sun et al., 1989), this trough is interpreted to be a major factor in the structural evolution of Ordos basin not only in a depositional sense, but also as a

control on subsequent tectonic evolution. Lower Paleozoic aulacogen-controlling normal faults are cited as potential structures for re-activation during Mesozoic shortening of the WOFTB (Darby and Ritts, 2002). In spite of its importance and widespread acceptance, evidence for an early Paleozoic aulacogen is lacking. Columnar stratigraphic sections and facies distributions demonstrating thickness changes have not been published as evidence. Thus, the simple question of whether or not aulacogen-induced deposits exist in northwestern Ordos is relevant.

Evidence such as subsurface data or abnormally thick Ordovician sections are not presented in the literature supporting the presence of the Helan Aulacogen. This study did not encounter any outcrop evidence in support of the existence of lower Paleozoic aulacogens in western Ordos. It is possible that rapidly subsiding troughs such as the proposed Helan Aulacogen simply did not extend to the Zhuozi Shan. Field observations in southwest Ordos in the summer of 2004 found that thick, lower Paleozoic outcrops shown on geologic maps (NBGMR, 1991) are covered (Appendix A). It also seems plausible that western Ordos aulacogens are a product of inaccurate mapping, creating inflated stratigraphic thicknesses.

Ordovician strata encountered in the Zhuozi Shan do not exceed 300 m in total thickness. Meng et al. (1997) report thicknesses upwards of 2000 m for Ordovician units in the "Ordos area" related to aulacogen movement. Due to lack of access, sections were not measured in lower Paleozoic strata of the southern Helan Shan. Nonetheless, Helan Shan Ordovician units were observed and were not thousands of meters thick (Appendix A).

Paleokarsts

Karst reservoirs are complex features that are highly variable in both lateral and stratigraphic position. As a general rule, carbonate rocks are initially deposited with high porosity and low permeability, which can be altered by post-depositional diagenetic events, such as karstification (Selley, 1998). Porosity in karst systems is a result of dissolution, fracturing, erosion and collapse, and can be enhanced or destroyed by added dissolution, cementation or influx of detrital matrix (Esteban and Wilson, 1993). Esteban and Wilson (1993) suggest that an understanding of the location, timing and evolution of karstification processes is fundamental to predicting porosity in karst reservoirs. Furthermore, outcrop analogs allow the geometry, style and heterogeneity of paleokarst intervals to be described.

Carbonate depositional systems are sensitive recorders of sea-level changes (Emery and Myers, 1996). For example, a rapid rise in sea level during the initial, building stages of a carbonate platform may drown the system, causing carbonate production to step back to a shallower location (Emery and Myers, 1996). Fluctuations in eustatic sea level can be a product of large-scale changes in the shape of ocean basins or in the volume of water within those basins (climatic) (Emery and Myers, 1996). Therefore, sequence stratigraphic control of lower Paleozoic carbonate rocks within western Ordos Basin helps constrain global sea-level fluctuations during this period and enables additional interpretations on probable causes. Meng et al. (1997) noted major karst surfaces within the Lower Cambrian-Middle Ordovician strata of northeastern China, with a major, craton-wide unconformity separating Middle Ordovician from Middle Carboniferous strata. Pinpointing duration and extent

of subaerial exposure surfaces within marine, carbonate rocks can be useful for interpreting sea level fluctuations (Esteban and Klappa, 1983).

The thickest paleokarst exposed in northwestern Ordos basin is at the Middle Ordovician to Middle Carboniferous boundary. However, paleokarsts occur in the Lower Ordovician part of Unit B, and are concentrated along the boundary between Units C and D. Sea-level models generated for northwestern Ordos show major sea-level regressions during the upper part of the Middle Cambrian and Lower Ordovician. Thus, these parts of the section are the primary candidates for paleokarsts. Outcrops paleo-landward of lower Paleozoic units in northwestern Ordos may contain thicker, more-developed paleokarsts. Porosity in lower Paleozoic paleokarsts is enhanced by crackle and chaotic breccias, interpreted to represent dissolution and collapse of cave systems, respectively (Loucks, 1999). The major post-Ordovician paleokarst horizon shows the most evidence for porosity decrease by influx of detrital matrix as paleocaves are filled with cobble conglomerates. Paleokarsts lower than the uppermost unconformity surface are less-frequently infilled with coarse clastics, and commonly are filled with fine-grained detrital material. The next best prospect for potential hydrocarbon reservoirs within the central subsurface of Ordos basin after the Middle Ordovician-Middle Carboniferous paleokarst is in consolidation of thinner paleokarsts in Units C and D.

Comparisons to the Meng et al. (1997) Model

Lower Paleozoic sections in northwestern Ordos basin are broadly similar to those described by Meng et al. (1997). Middle and Upper Cambrian lithofacies

assemblages described by Meng et al. (1997) in the NCCP model contain numerous cycles of lower, siliciclastic-rich rocks capped by cross-stratified oolitic lithofacies. Also, for the broad NCCP model (Meng et al., 1997), Upper Cambrian cycles are similar to those in the Middle Cambrian, with a greater abundance of intraclastic conglomerate, capped by thick sequences of fenestral dolomitic mudstone and bioherms (Meng et al., 1997).

Middle and Upper Cambrian strata in northwestern Ordos, however, do not contain the abundant oolitic packages and microbially-laminated dolomitic mudstone as described from other areas of Ordos basin (Meng et al., 1997). Intraclastic conglomerate is abundant within the Upper Cambrian, but is also found in the Upper part of the Middle Cambrian in northwestern Ordos. Quartz sandstone beds are not described in Middle and Upper Cambrian strata by Meng et al. (1997), but are dominant components of the lower part of the upper Middle Cambrian section of WZA.

The Meng et al. (1997) study states that “great changes in the regional tectonic framework” occurred in Early Ordovician time in the western and southwestern margins resulting in deposition of distal, nodular, cherty limestone and mudrock within the Helan aulacogen. Lower and Middle Ordovician carbonate assemblages encountered within the Zhuozi Shan by this study show markedly different lithologies. Ordovician strata in northwest Ordos contain a significant amount of quartz sandstone and shallow-water carbonate facies. The only deep-water facies encountered in northwestern Ordos were found at Laosumiao section, in the southernmost Zhuozi Shan. This section contains thick, black shale and dark gray lime

mudstone; graptolites from this section indicate an upper Middle Ordovician age (Mitchell, pers. comm., 2005). The Middle Ordovician deep-water packages' relationship to older units is unknown since Laosumiao is an incomplete lower Paleozoic section.

Quartz sandstone encountered in the lower Paleozoic lithofacies assemblages of northwestern Ordos basin have unclear origins and implications. Quartz sandstone strata in the Lower and Middle Cambrian of northwestern Ordos are interpreted as upper shoreface deposits from their sedimentary structures and associated facies characteristics (Walker, 1979; Tucker and Wright, 1990). Rapid influx of siliciclastic material can be detrimental to carbonate systems, effectively shutting down the carbonate system through increased turbidity (James and Kendall, 1992). Since lower Paleozoic carbonate rocks in northwest Ordos are interbedded with siliciclastics, siliciclastic sedimentation is not interpreted to have been rapid enough to terminate carbonate production. Quartz sand bodies are interpreted as isolated pods, input into the system from a cratonic source and reworked by ocean currents. The abundance of quartz sand in the Ordovician may be a result of a change in sea level, or may indicate tectonic change landward, pushing alluvial systems farther seaward (Emery and Myers, 1996). The shift from carbonates to siliciclastics was not permanent, as younger carbonate strata of the Middle Ordovician overlie quartz sandstone units.

Paleogeographic reconstructions and, most specifically, shoreline trends of the NCCP model, are proved inapplicable to northwestern Ordos. The proposed Upper Cambrian shoreline orientation change of the larger NCCP model (Meng et al., 1997) does not apply to northwestern Ordos. Tilting of the NCCP and shoreline change is

evidenced by an increase in the abundance of intraclastic conglomerate across the Middle and Upper Cambrian boundary (Meng et al., 1997), an increase that is also present in northwestern Ordos. However, there is no evidence for tilting in the lower Paleozoic of northwestern Ordos. Lower Ordovician sections contain a high percentage of siliciclastic material, suggesting that northwestern Ordos was proximal to a siliciclastic source during the Ordovician. Meng et al. (1997) do provide a caveat, suggesting that patterns of sedimentation and relative sea level are influenced by local tectonics, especially in western parts of the NCCP.

Sea Level

While there are some discrepancies between this research and previous work, lower Paleozoic sea level models for northwestern Ordos are consistent with previous models and established sea level curves. At the sequence scale, sea level curves generated by this project closely resemble those of Meng et al. (1997) and the global eustatic signature work of Vail et al. (1977) and Bond et al. (1988) (Fig. 32). The lower Paleozoic lithologic stacking patterns of northwestern Ordos suggest overall sea level transgression throughout the Upper Cambrian and Lower Ordovician; Unit B was deposited in the deepest sea-level conditions. The Lower-Middle Ordovician boundary is marked by a paleokarst, implying a major regression near the top of Unit C. Shallow sand and dolomite-rich sequences grade into fossiliferous packstone and grainstone and mark the second phase of transgression. This upward progression of facies is consistent with the lower Paleozoic sea-level interpretations of North America by Vail et al. (1997) (Fig. 32) (Hallam, 1992) and lower Paleozoic sea level

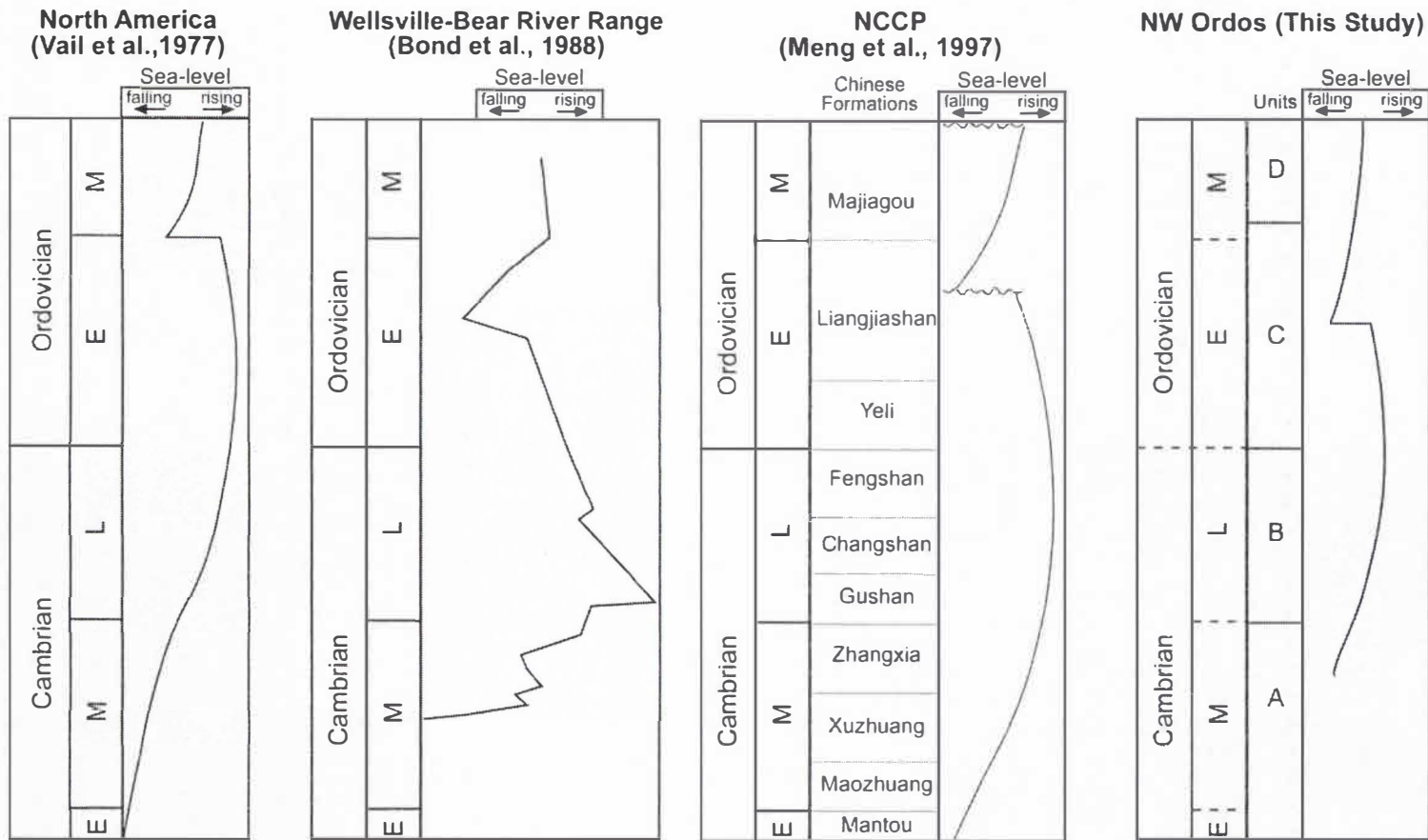


Figure 32. Comparison of 2nd and 3rd order sea-level curves of North America (Vail et al., 1977; Bond et al., 1988), the whole NCCP (Meng et al., 1997) and NW Ordos Basin. Similar trends are apparent in all three models likely indicating a eustatic sea-level signal. All curves are scaled to the 1999 GSA Geologic Time Scale.

evolution of the NCCP presented by Meng et al. (1997). While the exact placement of the Sauk and Tippecanoe boundary is variable, all North American, lower Paleozoic sea level curves recognize a major regression, interpreted to be this boundary, sometime during the Early or Middle Ordovician (Vail et al., 1977; Bond et al., 1988; Read, 1989; Hallam, 1992).

In North America, the end of the Lower Ordovician is interpreted is marked by a large-scale regression, which is interpreted to be the boundary between the Sauk and Tippecanoe cratonic sequences (Sloss, 1988; Levin, 1999). During this interval, regressive tongues of quartz sandstone traceable back to cratonic arches in the interior show up (Sloss, 1988). Consistent with North American cratonic sequences, Lower and Middle Ordovician sections in northwestern Ordos are also marked by quartz arenite, which are most likely derived from a source north of the present-day Zhuozi Shan. Similar-aged lithologies and successions are present in western North America, specifically the Lower Ordovician Garden City Formation of northern Utah (Morgan, 1988), the Upper Cambrian and Lower Ordovician Whipple Cave and House Formations in Nevada (Cook and Taylor, 1977), and the Upper Cambrian and Lower Ordovician Snowy Range Formation of Montana (Myrow et al., 2004). Stratigraphic similarities support the similar, eustatic signature between the North China Block and North America in the early Paleozoic time.

Uncertainties

A major source of uncertainty in interpreting the geologic history of northwest Ordos basin is the paucity of age control. Index fossils used in previous work (e.g.

Meng et al., 1997) for biostratigraphy included trilobites, graptolites and conodonts. Trilobites and graptolites are the most readily-preserved macrofossils that can be collected at outcrop scale. Conodont biostratigraphy sampling requires more time and laboratory preparation, taking large samples, acidizing the carbonate content, sieving and finally picking conodonts from the residue. Unfortunately, trilobites and graptolite specimens were rarely encountered; those encountered were either non-diagnostic fragments, or were transported within alluvium. Other fossils, such as brachiopods, have been used to give an estimate on age, but these samples are sporadic in distribution. Volcanic ash layers are also an effective way to date stratigraphic columns, however none were encountered in this study.

Measured sections from northwest Ordos are thick, and were measured with the intention of covering a large area within a short amount of time. The laser range finder method accurately describes the upward progression of strata for thick sections and large-scale interpretations, yet more detail can be pulled from individual formations. This research has set up a framework for the stratigraphic succession of northwest Ordos, to be built upon by future researchers examining details at a finer resolution, such as biostratigraphy, isotopic indicator and magnetostratigraphy. An important step will be to tie trends observed in the northwestern Ordos composite type section to other stratigraphic databases (e.g. SPICE isotopic excursion of Saltzman et al., 1998) in order to further investigate lower Paleozoic eustacy, global tectonics and paleogeography.

CONCLUSIONS

All lower Paleozoic measured sections in northwestern Ordos follow similar, upsection trends. The basal portion of sections is composed of shale and mudrocks of Unit A, followed by thin bedded lime mudstones and wackestones of Unit B, overlain by the sandstones and dolostones of Unit C, all capped by fossiliferous packstones and grainstones of Unit D. These upsection lithofacies patterns are generally similar to those described by Meng et al. (1997), with the exception of a higher abundance of sandstones in northwestern Ordos. Second order sea level curves suggest that sea level was transgressing during the Late Cambrian, with a transgression and regression in the Early Ordovician, followed by a Middle Ordovician transgression. This sea level history is similar to North American sea level curves of Vail et al. (1977), which suggests eustatic sea level control. Based on the stratigraphic thicknesses, tectonic changes, such as early Paleozoic aulacogen movement, and platform tilting, reported by Meng et al. (1997) in the larger NCCP model are not applicable to northwestern Ordos. Paleokarsts are concentrated in the northern part of west Ordos, suggesting early Paleozoic sea level became deeper to the present day south. The major unconformity separating Middle Ordovician carbonate rocks from Carboniferous siliciclastics is exposed in the Zhuozi Shan and is the largest paleokarst-related feature encountered in the Zhuozi Shan. Relatively large (2 m high, 1 m wide) caves are exposed lower in the Middle Ordovician section, below the unconformity, as basal collapse breccias overlain by coarse conglomerates and quartz sandstones. All stratigraphic sections in northwest Ordos basin reveal that deposition of carbonate

and lesser siliciclastic rocks occurred on a shallow water carbonate platform that was tilted to the south throughout the Lower Paleozoic. The early Paleozoic paleogeographic picture interpreted from stratigraphic evidence collected northwest Ordos differs from that of prior studies (Meng et al., 1997), showing that deposition of carbonate and clastic strata across the NCCP was dependent upon local changes in sedimentation and tectonics.

REFERENCES

- Aigner, T., 1985. Storm depositional systems: Dynamic stratigraphy in modern and ancient shallow-marine sequences. In: Friedman, G.M., Neugebauer, H.J., Seilacher, A. (Eds.), *Lecture Notes in Earth Sciences*. Springer-Verlag, Berlin, pp. 3-5.
- Boggs, S. Jr., 2001. *Principles of Sedimentology and Stratigraphy*, (3rd ed.) Prentice Hall, New Jersey, 726 pp.
- Bond, G.C., Kominz, M.A., Grotzinger, J.P., 1988. Cambro-Ordovician Eustacy: Evidence from geophysical modelling of subsidence in Cordilleran and Appalachian passive margins. In: Kleinspehn, K.L., Paola, C., (Eds.), *New Perspectives in Basin Analysis*. Springer-Verlag, New York, pp. 129-160.
- Bond, G.C., Kominz, M.A., Steckler, M.S., 1989. Role of thermal subsidence, flexure, and eustacy in the evolution of Early Paleozoic passive-margin carbonate platforms. In: Crevello, P.D., Wilson, J.L., Sarg, J.F., Read, J.F., (Eds.), *Controls on Carbonate Platform and Basin Development*. Society of Economic Paleontologists and Mineralogists Spec. Paper No. 44, pp. 39-61.
- Cook, H.E., Taylor, M.E., 1977. Comparison of continental slope and shelf environments in the Upper Cambrian and Lowest Ordovician of Nevada. In: Cook, H.E., Enos, P., (Eds.), *Deep-Water Carbonate Environments*. Soc. of Economic Paleontologists and Mineralogists Spec. Publ. No. 25, pp. 51-81.
- Darby, B.J., 2003. *Mesozoic Intraplate Deformation in the East Asian Tectonic Collage: The Enigmatic Northwest Ordos Region, China*. Ph.D. Dissertation, University of Southern California, 177 pp.
- Darby, B.J., Davis, G.A., Zheng, Y., 2001. Structural evolution of southwestern Daqing Shan, Yinshan Belt, Inner Mongolia, China. In: Hendrix, M.S., and Davis, G.A., (Eds.), *Paleozoic and Mesozoic Tectonic Evolution of Central Asia: From Continental Assembly to Intracontinental Deformation*. Geol. Soc. America Memoir 194, pp. 199-214.
- Darby, B.J., Ritts, B.D., 2002. Mesozoic contractional deformation in the middle of the Asian tectonic collage: the intraplate Western Ordos fold-thrust belt, China. *Earth and Planetary Science Letters* 205, pp. 13-24.
- Davis, G., Cong, W., Zheng, Y., Zhang, J., Zhang, C., Gehrels, G., 1998. The enigmatic Yinshan fold-and-thrust belt of northern China: new views on its intraplate contractional styles. *Geology* 26, pp. 43-46.

- Emery, D., Myers, K.J., 1996. Concepts and principles of sequence stratigraphy. In: Emery, D., and Myers, K.J., (Eds.), *Sequence Stratigraphy*. Blackwell Science, London, pp. 11-16.
- Enkin, R.J., Yang, Z., Chen, Y., Courtillot, V., 1992. Paleomagnetic constraints on the geodynamic history of the major blocks of China from the Permian to the present. *J. Geophysical Res.* 97, pp. 13953-13989.
- Enos, P., 1983. Shelf. In: Scholle, P.A., Bebout, D.G., Moore, C.H., (Eds.), *Carbonate Depositional Environments*. Am. Assoc. Petrol. Geol. Memoir 33, pp. 267-296.
- Esteban, M., Klappa, C.F., 1983. Subaerial exposure. In: Scholle, P.A., Bebout, D.G., Moore, C.H., (Eds.), *Carbonate Depositional Environments*. Am. Assoc. Petrol. Geol. Memoir 33, pp. 1-7.
- Esteban, M., Wilson, J.L., 1993. Introduction to karst systems and paleokarst reservoirs. In: Fritz, R.D., Wilson, J.L., Yurewicz, D.A., (Eds.), *Paleokarst Related Hydrocarbon Reservoirs*. Soc. Econ. Paleontol. Mineral. Core Workshop 18, pp. 1-9.
- Halley R.B., Harris, P.M., Hine, A.C., 1983. Bank margin. In: Scholle, P.A., Bebout, D.G., Moore, C.H., (Eds.), *Carbonate Depositional Environments*. Am. Assoc. Petrol. Geol. Memoir 33, pp. 463-506.
- Hallam, A., 1992. *Phanerozoic Sea-Level Changes*. Columbia University Press, New York, 225 pp.
- Heubeck, C., 2001. Assembly of central Asia during the Middle and Late Paleozoic. In: Hendrix, M.S., Davis, G.A., (Eds.), *Paleozoic and Mesozoic Tectonic Evolution of Central Asia: From Continental Assembly to Intracontinental Deformation*. Am. Assoc. Petrol. Geol. Memoir 194, pp. 1-22.
- Huang, B., Yang, Z., Otofujii, Y., Zhu, R., 1999. Early Paleozoic paleomagnetic poles from the western part of the North China Block and their implications. *Tectonophysics*, 308, pp. 377-402.
- Irwin, M. L., 1965. General theory of epeiric clear water sedimentation, Am. Assoc. Petrol. Geol. Bulletin v.49 , pp. 445-459.
- James, N.P., Bourque, P.A., 1992. Reefs and mounds. In: Walker, R.G., James, N.P., (Eds.), *Facies Models: Response to Sea Level Change*. Geological Association of Canada, St. John's, pp. 323-348.

- James, N.P., Kendall, A.C., 1992. Introduction to carbonate and evaporite facies models. In: Walker, R.G., James, N.P., (Eds.), *Facies Models: Response to Sea Level Change*. Geological Association of Canada, St. John's, pp. 265-275.
- James, N.P., Stevens, R.K., Barnes, C.R., Knight, I., 1989. Evolution of a lower Paleozoic continental-margin carbonate platform, northern Canadian Appalachians. In: Crevello, P.D., Wilson, J.L., Sarg, J.F., Read, J.F., (Eds.), *Controls on Carbonate Platform and Basin Development*. Society of Economic Paleontologists and Mineralogists Spec. Paper No. 44, pp. 123-146.
- Johnson, C.L., 2004. Polyphase evolution of the East Gobi basin: Sedimentary and structural records of Mesozoic-Cenozoic intraplate deformation in Mongolia, *Basin Research*, v. 16, pp. 77-99.
- Lee, K.Y., 1986. Geology of the coal and petroleum deposits in the Ordos basin, China. U.S. Geol. Survey Open File Report 86-278, 63 pp.
- Lesueur, C.A., 1818. Maclurites. In: Shimer, H.W., Shrock, R.R., (Eds.), *Index Fossils of North America*. Wiley, New York, p. 467.
- Levin, H.L., 1999. *The Earth Through Time*. Saunders College Publishing, Orlando, p. 270.
- Liang, C., Friedman, G.M., Zheng, Z., 1993. Carbonate storm deposits (tempestites) of Middle to Upper Cambrian age in the Helan mountains, northwest China. *Carbonates and Evaporites* 8, pp. 181-190.
- Liu, H., Lu, W., Wang, Y., 1990. Formation and deformation of fold-thrust belts in the western margin of Ordos block. In: Yang, J. (Ed.), *Petroleum and Structure of the Western Margin of Ordos Basin* (in Chinese with English abstract). Science and Technology Publishing House, Gansu, pp. 54-76.
- Liu, S., 1998. The coupling mechanism of basin and orogen in the western Ordos Basin and adjacent regions of China, *J. Asian Earth Sci.* 16, pp. 369-383.
- Loucks, R.G., 1999. Paleocave carbonate reservoirs: Origins, burial-depth modifications, spatial complexity and reservoir implications. *Am. Assoc. Petrol. Geol. Bulletin* 83, pp. 1795-1833.
- Ma, L., 2002. *Geological Atlas of China*. Geological Publishing House, Beijing, 348 pp.
- Meng, Q.R., Zhang, G.W., 2000. Geologic framework and tectonic evolution of the Qinling orogen, central China. *Tectonophysics* 323, pp. 183-196.

- Meng, X., Ge, M., Tucker, M., 1997. Sequence stratigraphy, sea-level changes and depositional environments in the Cambro-Ordovician of the North China carbonate platform. *Sediment. Geol.* 114, pp. 189-222.
- Morgan, S.K., 1988. Petrology of Passive-Margin Epeiric Sea Sediments: The Garden City Formation, North-Central Utah. M.S. Thesis, Utah State University, 168 pp.
- Myrow, P.M., Tice, L., Archuleta, B., Clark, B., Taylor, J.F., Ripperdan, R.L., 2004. Flat-pebble conglomerate: its multiple origins and relationship to metre-scale depositional cycles, *Sedimentol.* 51, pp. 973-996.
- NBGMR (Ningxia Bureau of Geology and Mineral Resources) 1991. Regional Geology Map of Ningxia Hui Autonomous Region. Geological Publishing House, Beijing, 1991.
- Pratt, B., 2002. Storms versus tsunamis: dynamic interplay of sedimentary, diagenetic, and tectonic processes in the Cambrian of Montana. *Geology* 30, pp. 423-426.
- Read, J.F., 1981. Carbonate ramp-to-basin transitions and foreland basin evolution, Middle Ordovician, Virginia Appalachians, *Am. Assoc. Petrol. Geol. Bulletin*, v. 64, pp. 1575-1612.
- Read, J.F., 1989. Controls on evolution of Cambrian-Ordovician passive margin, U.S. Appalachians. In: Crevello, P.D., Wilson, J.L., Sarg, J.F., Read, J.F., (Eds.), *Controls on Carbonate Platform and Basin Development*. Soc. Econ. Paleontol. and Mineral. Spec. Paper No. 44, pp. 147-165.
- Rigby, J.K., Kessel, B.J., Ritts, B.D., Friedman, S.J., 2006. A New Ordovician Chiasoclonellid Sponge from Inner Mongolia, China. *J. Paleontology*, (in review).
- Ritts, B.D., Hanson, A.D., Darby, B.J., Nanson, L., Berry, A., 2004. Sedimentary record of Triassic intraplate extension in north China: Evidence from the nonmarine NW Ordos Basin, Helan Shan and Zhuozi Shan. *Tectonophysics* 386, pp. 177-202.
- Ritts, B.D., Keele, D., Darby, B.J., Liu, S., 2006a. Ordos basin gas reservoir outcrop analogs: Permian braided fluvial sandstone of the Zhuozi Shan and Helan Shan, China. *Int. Geol. Review*, in press.

- Ritts, B.D., Weislogel, A., Graham, S.A., Darby, B.J., 2006b. Mesozoic tectonics and sedimentation of the giant polyphase nonmarine intraplate Ordos basin, western North China Block. In: Phanerozoic Regional Geology of the World, A. Bally and D. Roberts, (Eds.). Elsevier, in press.
- Saltzman, M., Runnegar, B., Lohmann, K.C., 1998. Carbon isotope stratigraphy of Upper Cambrian (Stepoean Stage) sequences of the eastern Great Basin: Record of a global oceanographic event. *Am. Assoc. Petrol. Geol. Bulletin* 110, pp. 285-297.
- Schoelle, P.A., Ulmer-Schoelle, D.A., 2003. A color guide to the petrography of carbonate rocks: grains, textures, porosity, diagenesis. *Am. Assoc. Petrol. Geol. Memoir* 77, p. 261.
- Schuchert, C., 1893. Rafinesquinidae. In: Kaesler, R.L. (Ed.), *Treatise on Invertebrate Paleontology, Part H (revised), Brachiopoda, vol. 2*. The Geological Society of America and University of Kansas, Boulder and Lawrence, p. 237.
- Selley, R.C., 1998. *Elements of Petroleum Geology* (2nd ed.). Academic Press, London, 470 pp.
- Sepkoski, J.J., 1982. Flat-pebble conglomerates, storm deposits, and the Cambrian bottom fauna. In: Einsele, G., Seilacher, A., (Eds.), *Cyclic and Event Stratification*. Springer-Verlag, Berlin, pp. 371-385.
- Sloss, L.L., 1988. Tectonic evolution of the craton in Phanerozoic time. In: Sloss, L.L., (Ed.) *Sedimentary Cover-North American Craton: U.S., The Geology of North America, vol. D-2*. Geol. Soc. of Am., Boulder, pp. 25-31.
- Sun, Z., Xie, Q., Yang, J., 1989. Ordos basin-A typical example of an unstable cratonic interior superimposed basin. In: Zhu, X. (Ed.), *Sedimentary Basins of the World*. Elsevier, Amsterdam, pp. 63-75.
- Tucker, M.E., 2001. *Sedimentary Petrology: An Introduction to the Origin of Sedimentary Rocks* (3rd ed.). Blackwell Science, Oxford, 262 pp.
- Tucker, M.E., Wright, V.P., 1990. *Carbonate Sedimentology*. Blackwell Scientific, Oxford, 482 pp.
- Vail, P.R.J., Mitchum, R.M., Todd, R.G., Widmier, J.M., Thompson, S., Songree, J.B., Bubb, J.N., Hatlelid, W.G., 1977. Seismic stratigraphy and global changes in sea-level. *Am. Assoc. Petrol. Geol. Memoir* 26, pp. 49-212.
- Walker, R.G., 1979. Shallow marine sands. In: Walker, R.G., (Ed.), *Facies Models*. Geoscience Canada, Ontario, pp. 75-89.

- Wang, B., Al-Aasm, I.S., 2002. Karst-controlled diagenesis and reservoir development: Example from the Ordovician main-reservoir carbonate rocks on the eastern margin of the Ordos basin, China. *Am. Assoc. Petrol. Geol. Bulletin* 86, pp. 1639-1658.
- Wignall, P.B., 1994. *Black Shales*. Clarendon Press, Oxford, 127 p.
- Wilson J.L., Jordan, C., 1983. Middle shelf. In: Scholle, P.A., Bebout, D.G., Moore, C.H., (Eds.), *Carbonate Depositional Environments*. *Am. Assoc. Petrol. Geol. Memoir* 33, pp. 298-299.
- Yang, J., Li, K., Zhang, D., Zhang, S., Liu, S., 1992, *Petroleum Geology of China, Changqing Oil Field*, Vol. 12, Petroleum Industry Publishing House, Beijing, 490 pp.
- Yang Y., Li, W., Ma, L., 2005. Tectonic and stratigraphic controls of hydrocarbon systems in the Ordos basin: A multicycle, cratonic basin in central China. *Am. Assoc. Petrol. Geol. Bulletin* 89, pp. 255-269.
- Yin, A., Nie, S., 1996. A Phanerozoic palinspastic reconstruction of China and its neighboring regions. In: Yin, A., Harrison, T.M. (Eds.), *The Tectonic Evolution of Asia*. Cambridge University Press, Cambridge, pp. 442-485.
- Zhao, G., Sun, M., Wilde, S.A., 2003. Correlations between the Eastern Block of the North China Craton and the South Indian Block of the Indian Shield; an Archaean to Palaeoproterozoic link. *Precambrian Res.* 122 , pp. 201-233.
- Zhao, M.W., Behr, H.J., Ahrendt, H., Wemmer, K., Ren, Z.L., Zhao, Z.Y., 1996. Thermal and tectonic history of the Ordos basin, China: evidence from apatite fission track analysis, vitrinite reflectance, and K-Ar dating. *Am. Assoc. Petrol. Geol. Bulletin* 80, pp. 1110-1134.

APPENDICES

APPENDIX A-SOUTHWEST/SOUTHERN ORDOS RECONNAISSANCE

The original field plan in the summer of 2004 was to measure complete lower Paleozoic sections along the roughly 700 km of the entire western margin of Ordos basin. This work started in the Zhuozi Shan in the north, and moved south into the Helan Shan and Liupan Shan towards Xian, where relatively complete, lower Paleozoic sections are shown on the geologic map (Ma, 2002). There were several problems encountered south of the Zhuozi Shan, which included lack of outcrop access, vegetation cover and structural complexities. Although sites were visited along the western margin of Ordos, south of the Zhuozi Shan, data from this part of the basin are sparse, and difficult to correlate to other areas of west Ordos (e.g. Zhuozi Shan). This section presents observations from the western margin of Ordos basin, south of the Zhuozi Shan.

Helan Shan

Both the northern and central Helan Shan contain exposures of lower Paleozoic rocks. In the central Helan Shan west of Yinchuan (Fig. A1), canyons expose stratigraphic sections from the Proterozoic-Cambrian boundary through the Ordovician (Fig. A2A) (Ma, 2002). Unfortunately, these outcrops are part of a nature reserve and Chinese authorities deny foreign access to them. However, initial reconnaissance work was conducted in the summer of 2004, described in the following lithofacies assemblage observations.

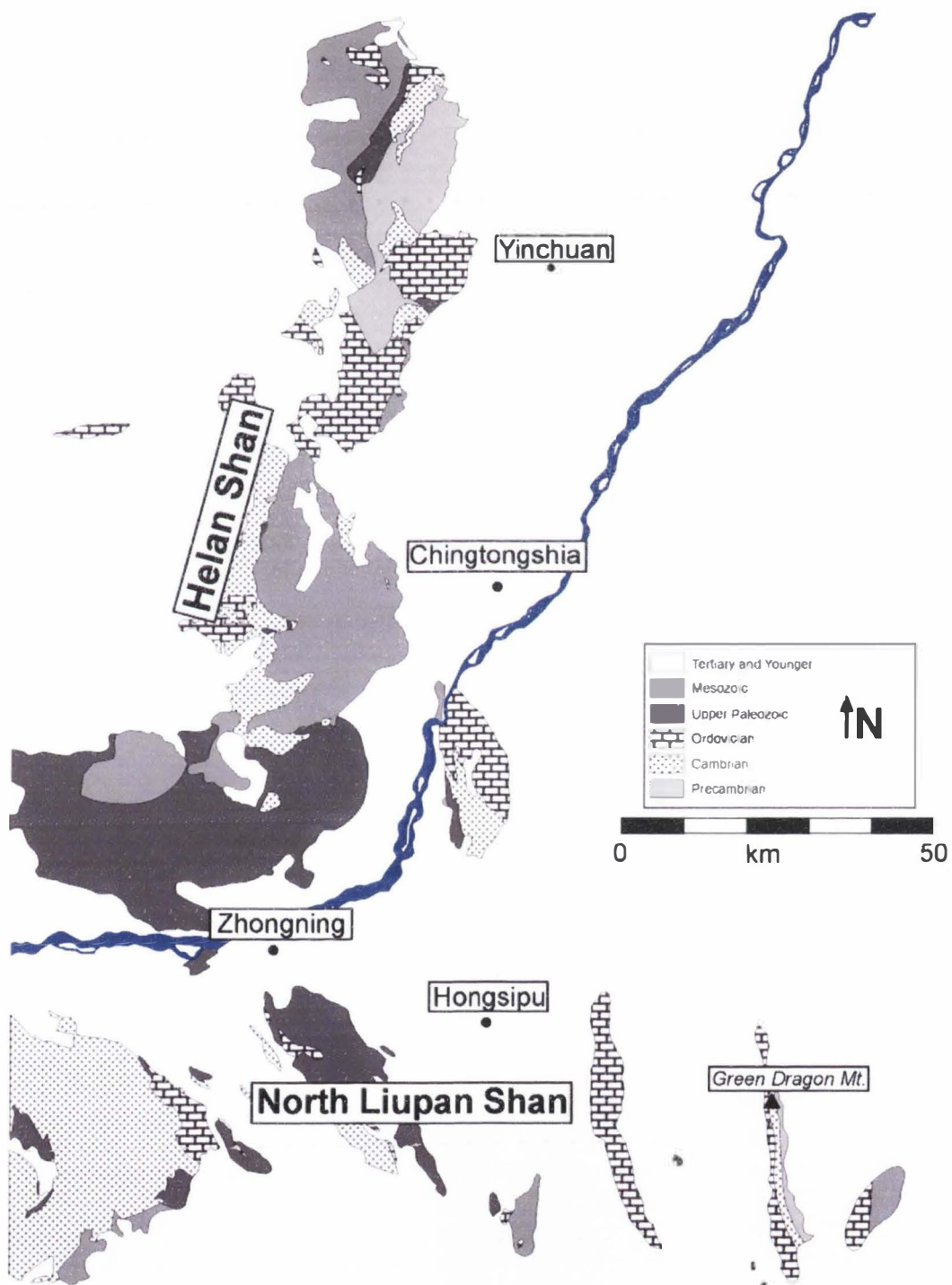


Figure A1. Geologic map of the central and southern Zhouzi Shan and Liupan Shan (Modified from Ma, 2002).

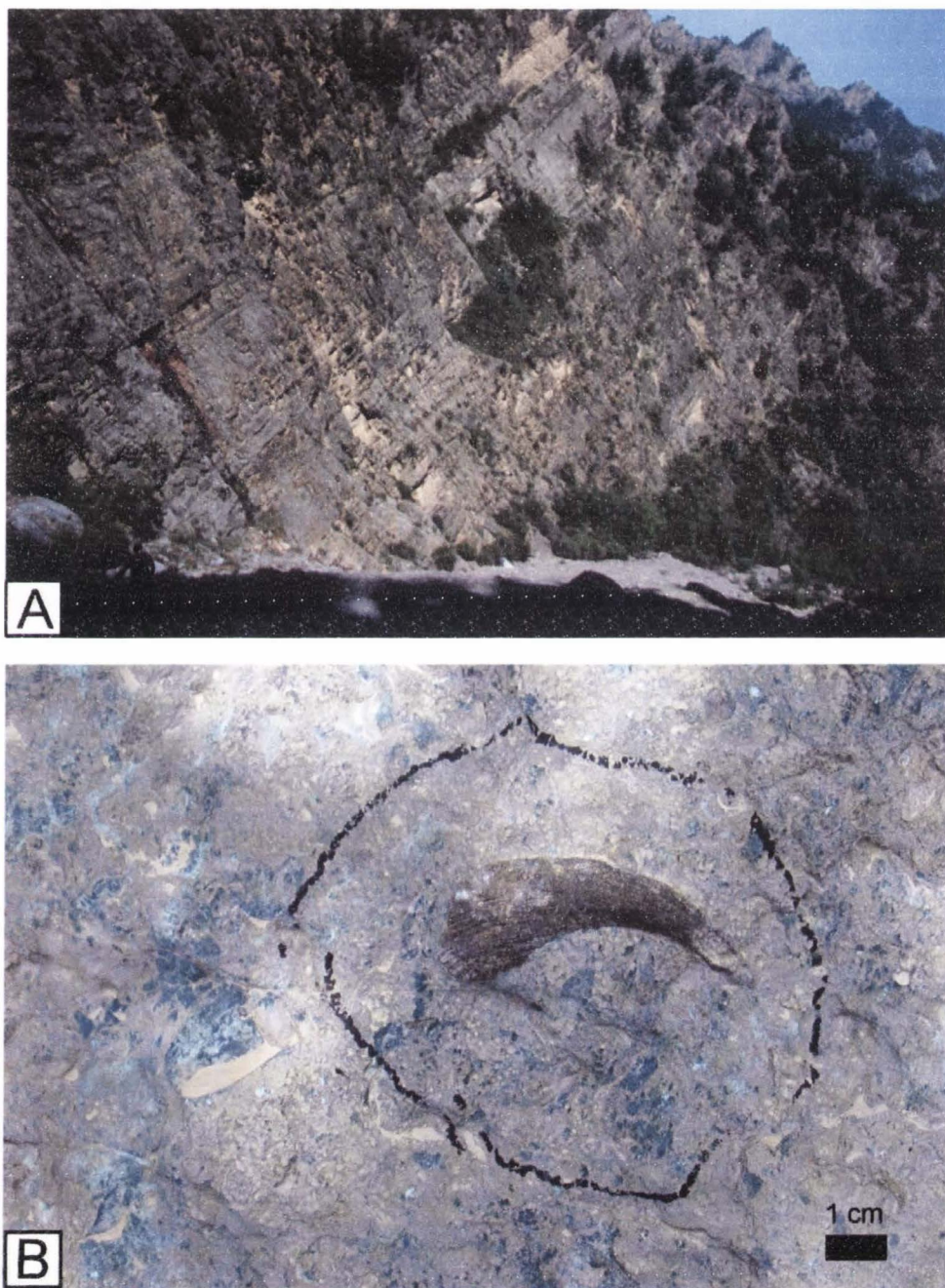


Figure A2. A) Ordovician strata exposed in Helan Shan. Note person in lower left for scale. B) Rugose coral in Ordovician blue-gray fossiliferous packstone in the Helan Shan

The Proterozoic west of Yinchuan is characterized by banded, cherty grayish-black lime mudstone and dolomitic lime mudstone containing mounds and laminations.

The Proterozoic-Cambrian contact was not observed. The lower part of the lower Paleozoic section is composed of green shale, siltstone, oolitic grainstone and flaggy lime mudstones. Near the top of the section, lime mudstones are more massive and seem to become more fossil-rich with gastropods, rugose corals (Fig. A2B) and burrows. This part of the section also contains interbedded green shale and intraclastic conglomerate. Although this section was not measured, it is likely not more than 1000 m thick from the basal Proterozoic contact.

Southwest of Chingtongsha in the southern Helan Shan (Fig. A1), lower Paleozoic sections are poorly exposed and most outcrops are cut with complex fractures and faults. Outcrops mapped as Lower Cambrian (Ma, 2002) in this area are breccias and conglomerates, with clasts of lime mudstone, sand-rich limestone and quartz arenite. Less than 5 km south of the breccia and conglomerate, outcrops are heavily faulted and contain greenish-black, laminated, silt-rich mudstones, some of which are metamorphosed. Approximately 25 km south-southwest of Chingtongsha (Fig. A1) is a pod of well-exposed Lower Ordovician thin-bedded lime mudstones, siltstones and mudstones. Access to stratigraphic sections in this area is difficult and is further complicated by military training exercises, and quarrying.

Northern Liupan Shan

Lower Paleozoic sections near the city of Zhongning (Fig. A1) in the northern Liupan Shan are heavily faulted and fractured. 40 km southeast of Zhongning is an interesting locality, mapped as Cambrian in unconformable contact with Silurian rocks (Ma, 2002). These outcrops contain poorly exposed thin-bedded quartzite and red shale; the Cambro-Silurian contact was not exposed. Another interesting contact is mapped 20 km due south of Zhongning mapping Ordovician rocks in contact with Silurian rocks (Ma, 2002). This contact is exposed as a thrust fault, placing Ordovician dark gray, lime mudstones over Silurian (Fig A3A), pink and purple feldspathic sandstones (Ma, 2002). Numerous faults cut this section making a measured section impossible. 30 km southwest of Zhongning, one small Ordovician section was measured. The lower portion of the section is composed of thin bedded to massive, dark gray lime mudstone, with brachiopod, gastropod and bivalve fragments. Higher up in the section are sand-rich limestones and bioturbated, massive packstone containing gastropods (Fig A3B), brachiopods and trilobite fragments. Outcrops mapped as Ordovician contain sparse, coherent pieces of section, characterized by thin to thick beds of gray to dark gray lime mudstone to wackestone with minor packstone. This section seems to coarsen upward, and may represent a shallowing upward cycle in the Ordovician. However, several faults and fractures slice through these rocks making interpretations unreliable.

50 km southeast of Hongsipu is Green Dragon mountain (Fig. A1), where some of the best exposures of lower Paleozoic rocks of the Liupan Shan are contained. Numerous faults cut this section, some omitting as much as 50 m of

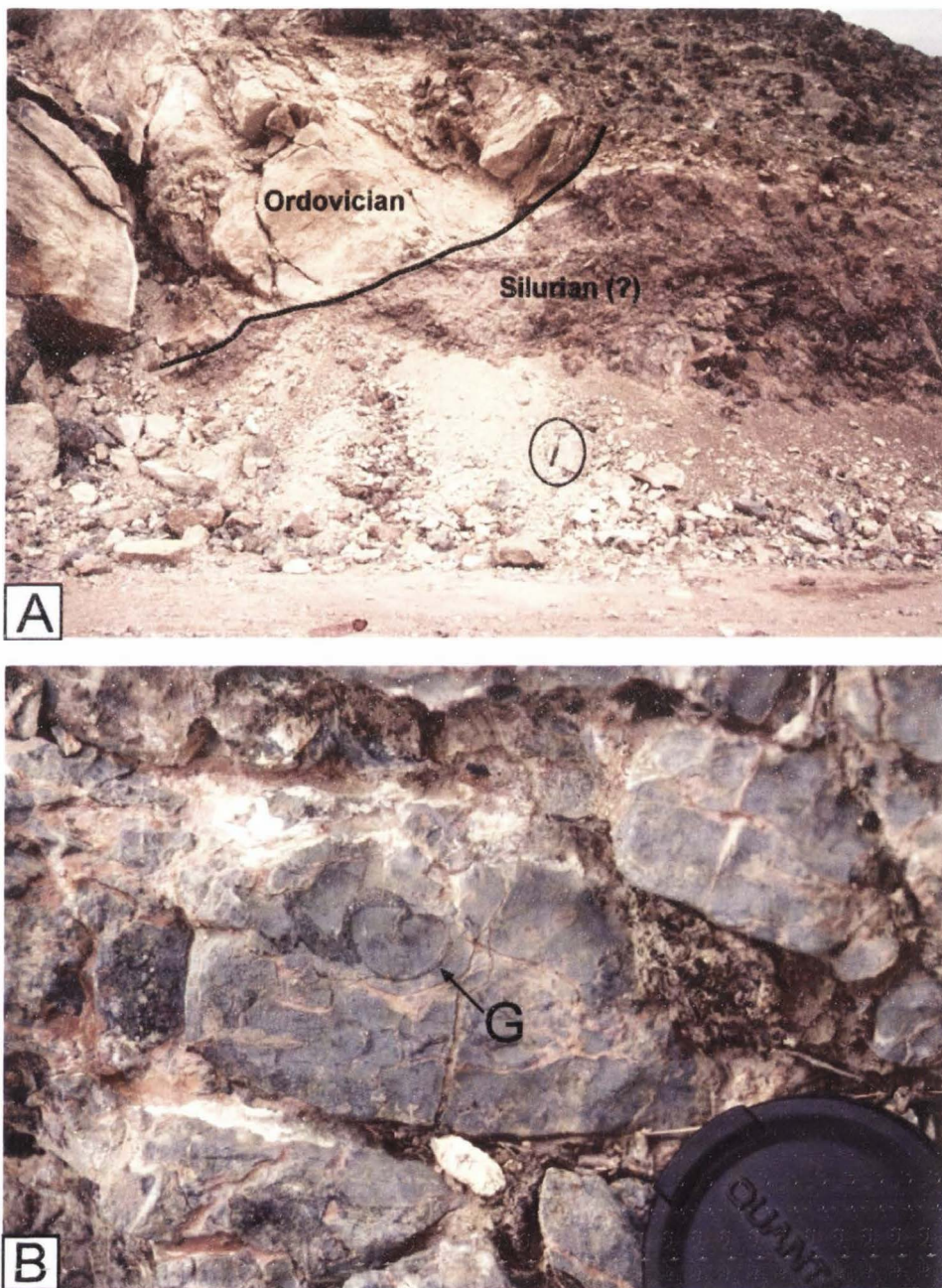


Figure A3. A) Thrust contact juxtaposing Ordovician limestone on top of Silurian (?) sandstone near Zhongning. B) Blue gray fossiliferous packstone lithofacies assemblage containing gastropod shells (G) near Zhongning

section, which make its significance as a primary source of data questionable. Green Dragon section is mapped as spanning the Lower Cambrian through the Lower Ordovician (Ma, 2002), and follows the northwestern Ordos type section described in this paper. Unit A is characterized by thick packages of red to green mudrock and shale, interbedded with thin fossiliferous grainstone, intraclastic conglomerate, and sandstone. These clastic and carbonate rocks are capped by several, thick beds of planar cross-stratified, oolitic lime grainstone. In Unit A, there are at least 3 cycles of lower mudrock and shale, capped by oolitic lime packstone and grainstone; oolitic rocks increase in abundance upward (Fig A4A). Above the shale and oolitic beds of Unit A, rocks change to thin-bedded lime mudstone, argillaceous limestone, intraclastic conglomerate and cross stratified oolitic grainstone (Fig. A4B) interbedded with thin shale, which marks the change to Unit B. The upper portion of Unit B contains thin-bedded lime mudstone with mounds, and intraclastic conglomerate, capped by a major thrust fault. Unit C is missing from the Green Dragon section; a large thrust fault of unknown offset caps the top of Unit B at Green Dragon section, which is the likely cause. Unit D strata are exposed near Green Dragon Mountain and are dark gray-to-gray, thin and thick-bedded dolomitic lime mudstones and lime mudstones, which are frequently bioturbated. Lithofacies get more grain-rich near the top of the section and contain gastropods, nautiloids, brachiopods and sponges (*Craterospongiella sinica*). The top of this section is covered by Quaternary rocks. Unit D strata are darker in color, and less grain-rich compared to those in the Zhuozi Shan, supporting the south-dipping ramp model.

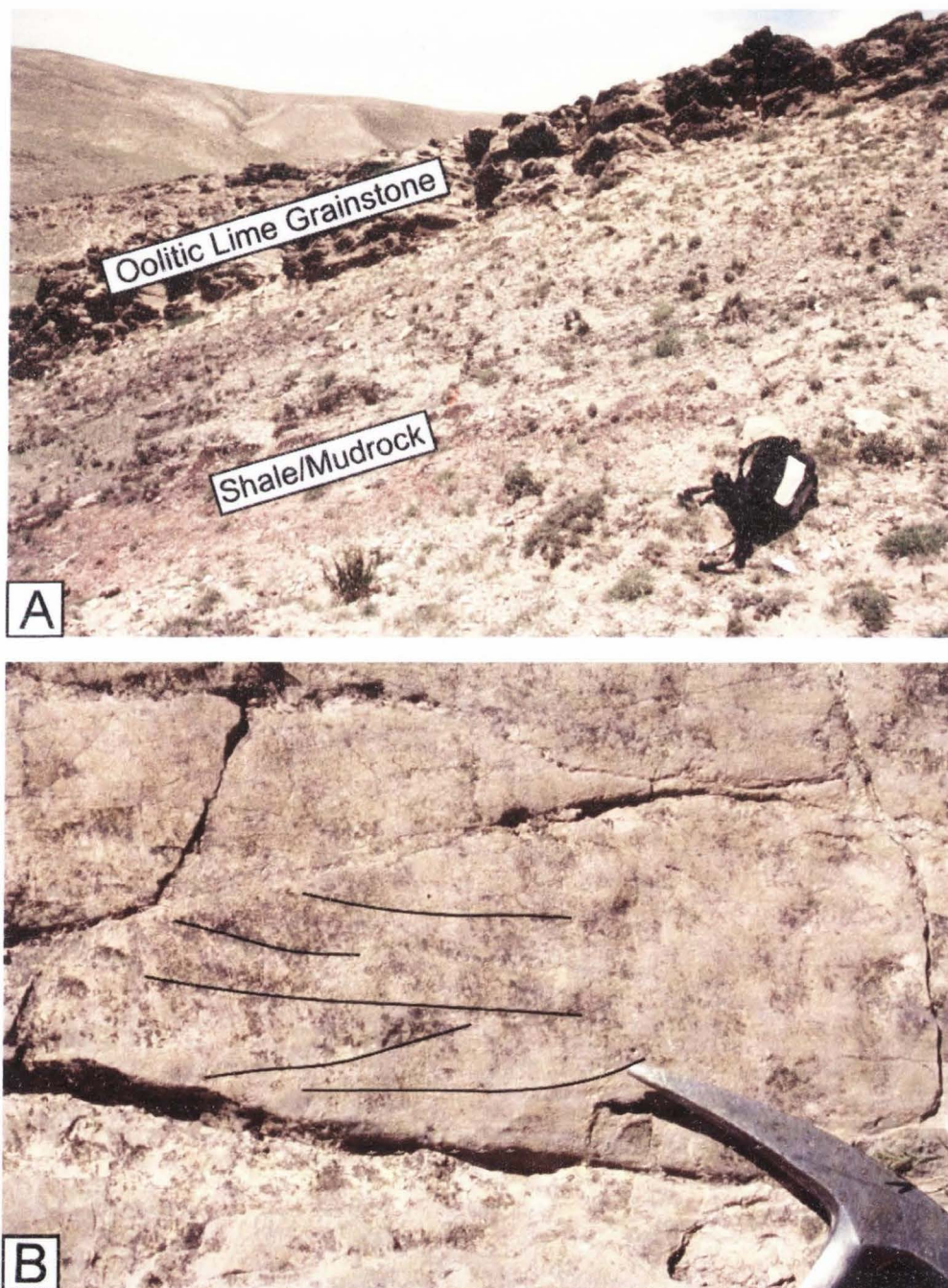


Figure A4. A) Shale and mudrock lithofacies capped by cross-stratified oolitic grainstone in Unit A at the Green Dragon section. B) Cross-stratified oolitic grainstone.

25 km west of the Green Dragon Mountain is an outcrop of Middle Ordovician (Ma, 2002) rocks (Fig. A6). Exposure is poor in this region and sections are complicated by faults of unknown offset. Rocks exposed at this outcrop are brown-green cherts and siltstones. It is interesting to note that other Chinese maps (e.g. NBGMR, 1991) trace the Ordovician part of Green Dragon section to these Middle Ordovician beds as a single coherent outcrop. Most of the portion between Green Dragon and the Middle Ordovician is covered, thus the data supporting this linkage is unknown.

Southern Liupan Shan

Outcrops in the southern Liupan Shan are heavily faulted and covered by dense vegetation. Some fragments of lower Paleozoic section were observed in small quarries and roadcuts no complete stratigraphic sections were recorded. In the Pinaliang area (Fig. A6), units mapped as Cambrian (Ma, 2002) are composed of argillaceous limestone, thin-bedded lime mudstone, interbedded with thin, calcareous siltstone, intraclastic conglomerate and oolitic lime grainstone. Most lower Paleozoic outcrops near Pingliang shown on the geologic map (Ma, 2002) were either covered or dangerous due to active quarrying. One Cambrian section was measured approximately south of Pingliang, approximately 20 km northwest of Langshia. However, this section was abruptly terminated by a fault of unknown offset. The portion measured contains silty, argillaceous, lime mudstone with hummocky cross-stratification, capped by thicker, oolitic lime grainstone beds with planar cross-stratification; oolitic beds thicken upsection. These strata are similar to Unit A

lithofacies observed in the north. 15 km northwest of Langshia are outcrops of Lower and Middle Ordovician rocks. These rocks are generally more siliciclastic, composed of thin beds of green, shale, siltstone, thick packages of calcareous cemented quartz arenite and feldspathic arenite. One measured section in Middle Ordovician(?) rocks in this area is made of gray, brown and green shale and mudrock, calcareous sandstones, and thin lime mudstones (Fig A5A). All beds are thin (less than 20 cm); siltstones and sandstones are frequently rippled. As in other parts of the southern Liupan Shan, this area contains numerous faults of unknown offset (Fig. A5B) and dense vegetation obscuring exposure.

Southern Ordos/Zhangjia Shan

This region of Ordos basin is densely covered by vegetation. Several outcrops visited 5-10 km southwest of Qianyang yielded no complete stratigraphic sections. Sporadic exposures yielded dark gray, thin-bedded, bioturbated lime mudstones, light gray lime wackestones, calcareous siltstones, argillaceous lime mudstones and dolostones. 10 km north of Qishan (Fig. A6) is mapped as a continuous, lower Paleozoic section. A road cut through this area exposes a thick succession of faulted, Proterozoic dolomites, yet all lower Paleozoic strata on this road are covered by a combination of loess and vegetation. Other road cuts through this region do expose what appear to be lower Paleozoic carbonate rocks; however, numerous, large faults of unknown offset cut these strata, making measured sections impossible to record. Lithofacies observed in this area are thin and thick beds of light gray to gray, lime mudstone with no apparent fossil material. In the Zhangjia Shan (Fig. A6), a nearly

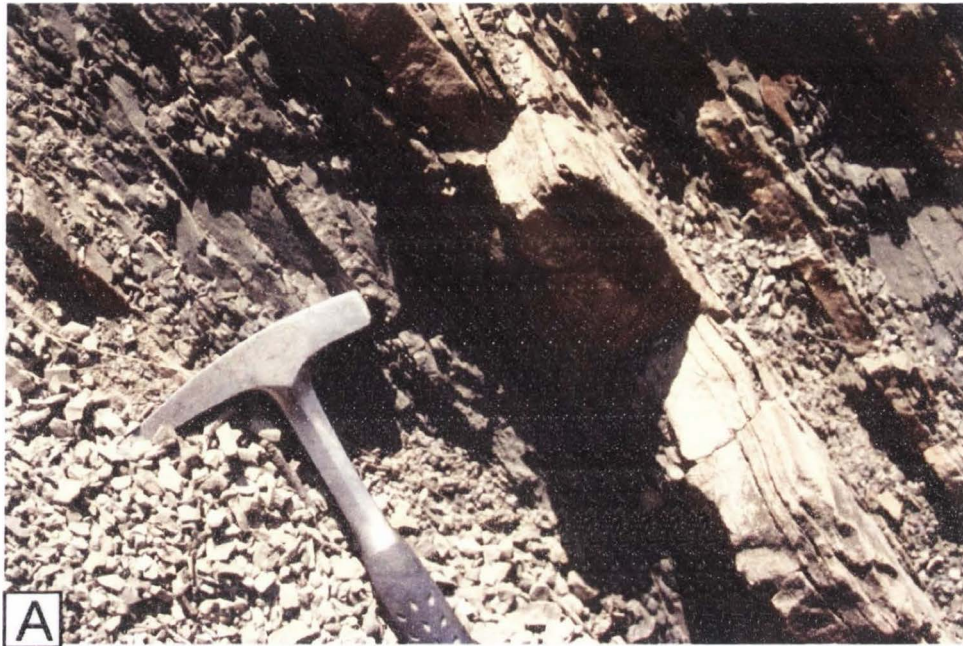


Figure A5. A) Lower and Middle Ordovician dark brown shales and fine sandstones exposed near Langshia in the southern Liupin Shan. B) Folded and faulted Ordovician strata, west of Langshia

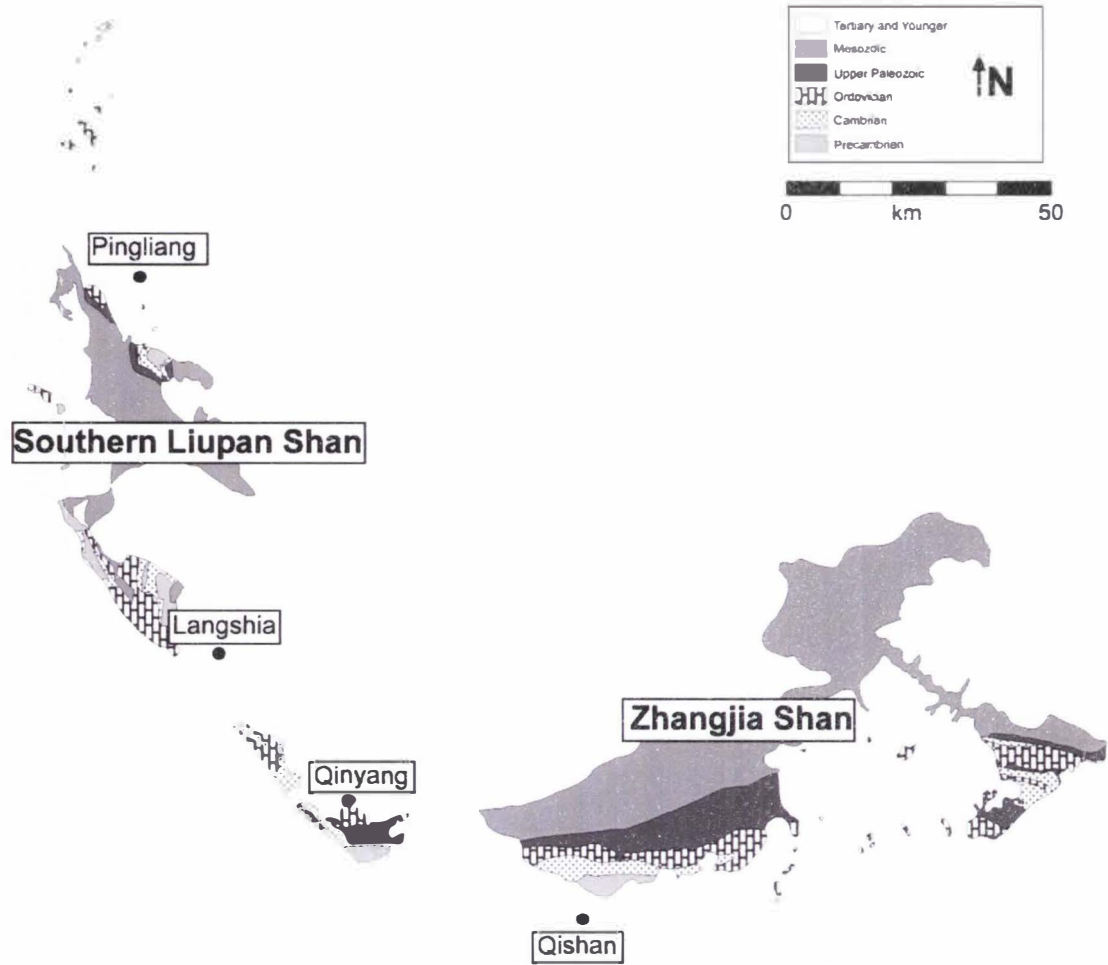
























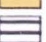




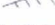




Figure A6. Geologic map of the southern Liupan Shan and Zhangjia Shan in southwestern Ordos (Modified from Ma, 2002).

conformable section of thin, dolomitic limestones mapped as Upper Cambrian (Ma, 2002) is exposed above a large quarry. Again, large faults with unknown offset pierce the exposed section; exploration in other parts of this area is difficult due to extremely rough terrain and quarry operations.

APPENDIX B-DETAILED STRATIGRAPHIC COLUMNS

Key

	Breccia		Crinoid
	Quartz Cemented Quartz Arenite		Gastropod
	Calcareous Cemented Quartz Arenite		Rugose Coral
	Shale		Trilobite
	Siltstone		Cephalopod
	Dolomite		Oncoid
	Intraclastic Conglomerate		Bivalve
	Massive Fossiliferous Lime Packstone/Mudstone		Brachiopod
	Oolitic Lime Grainstone		Bryozoan
	Mounded Strata		Burrow
	Banded/Bioturbated Wackestone/Packstone		Ooid
	Thin-bedded Fossiliferous Packstone		Ripples
	Thin-bedded Lime Mudstone		Laminations
	Argillaceous Limestone		Wavy laminae
	Sand-Rich Limstone		Cross stratification
			HCS Hummocky Cross Stratification
			Mudcrack
		sh	Shale
		ms	Lime Mudstone
		ws	Lime Wackestone
		ps	Lime Packstone
		gs	Lime Grainstone
		ic	Intraclastic Conglomerate

Suhaitu 1

	Sample	Photo	Comments/Description		
200	04BOZ-15	OBK4-1	Outcrop becomes more resistant; "flaggy" banded and bioturbated units become more abundant		
190					
180					
170					
160					
150					
140				OBK3-6,7,8,9	Tan, recessive shale
130					Red-green shale
120				OBK3-6,7,8,9	Red-brown calcareous shale with mudcracks, microbial laminae
110					Oxidized, bored rims on intraclasts
100	04BOZ-14	OBK3-3,4,5	Numerous cycles of thin, argillaceous limestone, interbedded with greenish-white calcareous siltstone gapped by intraclastic conglomerate		
90					
80					
70					
60	04BOZ-14	OBK3-1	Argillaceous limestone Tan to brown shale		
50					
40	04BOZ-13	OBK2-32, 33	Cross-bedded, reddish-purple oolitic grainstone with glauconite		
30					
20	04BOZ-12	OBK2-30, 31	Fissile, green to brown micaceous shale with interbedded thin shell hash limestones with hummocky cross strata Dark gray and red banded and bioturbated lime mudstone to wackestone		
10					
		OBK2-27,28	Cycles of shale, thin-bedded lime mudstone and shale		
		OBK2-25, 26	Laminations evident Proterozoic quartzite		

sh ms ws ps gs lc

Suhaitu 2

	Sample	Photo	Comments/Description
400	04BOZ-24		Dolomitic lime packstone with sand grains, oncoids, and bioturbation
390			
380	04BOZ-21, 22, 23	OBK4-8, 9	Well-rounded, calcareous cemented medium sand-sized sandstone
370			
360	04BOZ-19		Laminations evident in reddish, bioturbated mudstone
350			
340	04BOZ-18	OBK3-22, 23, 24, 25, 26	Breccia overlies sinuously-folded, strata-bounded grainstone
330			
320	04BOZ-17		Sand-rich dolomitic mudstone
310			
300	04BOZ-16	OBK3-18, 19, 20, 21	Erosive, argillaceous lime mudstones ~2 m of chaotic, boulder to pebble-sized clasts in a reddish, sandy matrix
290			
280	04BOZ-15	OBK3-15, 16, 17	Bioturbated Recessive, argillaceous lime mudstones
270			
260	04BOZ-16		Digitate stromatolite on top of mound
250			
240	04BOZ-16		Heavily bioturbated bedding planes; burrows are cross-cut by smaller, mineralized burrows
230			
220	04BOZ-15	OBK3-11, 12, 13	
210			
200			

sh ms vs ps ga ic

Suhaitu 3

Sample	Photo	Comments/Description	
540		04BOZ-38 OBK6-1415 16	Generally finer/muddier in texture near the top of the section
530		04BOZ-37 OBK6-9,10, 11,12, OBK6-5,6,7, OBK6-2,3,4	Extremely fossiliferous with thin interbedded oolitic grainstones; articulated crinoid calyx Numerous <i>Craterospongia sinica</i> individuals observed forming small buildups; first appearance
520		OBK4-28,29, 30,31	Thin-bedded, blue-gray lime packstone to grainstone with interbedded, thin (~20 cm) sandy limestones
510		OBK4-33	Thin, pebble breccias and minor conglomerate; thickness seems to increase to the north
500		OBK4-26,27	Thick, reddish-brown, gravel-to-cobble sized, breccia
490		04BOZ-26 OBK4-24	Thin, pebble-sized, reddish-brown, breccia
480		OBK4-22,23	Brecciated horizon with basal scoured contact
470		04BOZ-25	Brecciated horizon with basal scoured contact
460			Brecciated horizon with basal scoured contact
450			Brecciated horizon with basal scoured contact
440			Brecciated horizon with basal scoured contact
430			Brecciated horizon with basal scoured contact
420			Brecciated horizon with basal scoured contact
410			Brecciated horizon with basal scoured contact
400			Brecciated horizon with basal scoured contact

WZA 1

Sample	Photo	Comments/Description
	<p style="text-align: center;">OBK5-28</p> <p style="text-align: center;">OBK5-22,23,24,25</p> <p style="text-align: center;">OBK5-21</p> <p style="text-align: center;">OBK5-7,8</p> <p style="text-align: center;">OBK5-5,6</p>	<p>Heavily bioturbated, recessive outcrop profile</p> <p>Trilobite pygidia within float</p> <p>Large mounds</p> <p>Bioturbated grainstone</p> <p>Finely laminated sandy siltstone, possible mudcracks</p> <p>Purple-green shale, interbedded nodular limestone</p> <p>Shell-hash topped by ripples</p> <p>Green, micaceous shale interbedded with lime mudstones and minor siltstone</p> <p>Microbial laminae</p> <p>Strata-bounded folds Sand infilling burrows</p> <p>Sandy dolomite</p> <p>Sand infilling burrows</p> <p>Green/brown silty shale</p> <p>Thin bedded calcareous, wavy bedded sandstone</p> <p>Microbial laminae</p>

sh ms sv ps gs lc

WZA 3

Sample	Photo	Comments/Description
<p>550 540 530 520 510 500 490 480 470 460 450 440 430 420 410 400</p> <p>sh ms ws ps gs ic</p>	<p>OBK5-29</p>	<p>Heavily bioturbated, with chert nodules</p> <p>Numerous concavo-convex brachiopods within recessive sandy limestone</p> <p>Gradational contact between medium bedded, brownish-gray dolomitic mudstones and thin bedded lime mudstone</p>

Xima 1

Sample	Photo	Comments/Description	
200		Argillaceous lime mudstone; less resistant profile	
190		Change from more shaley to more resistant, "flaggy" outcrop profile	
180		OBK7-30	Change from more shaley to more resistant, "flaggy" outcrop profile
170		OBK7-29	Burrow mottled; sand infilling burrows; iron nodules Interbedded yellow-brown mudstone, and bioturbated, thin-bedded lime mudstone
160		OBK7-27,28	Burrow mottled; sand infilling burrows; iron nodules Interbedded yellow-brown mudstone, and bioturbated, thin-bedded lime mudstone
150		OBK7-25,26	Thin ooid grainstones interbedded with thin lime mudstones, heavily bioturbated, burrows filled with yellow, silty interbeds
140		OBK7-24	Crumbly, burrowed lime mudstones interbedded with more resistant intraclastic conglomerates, and oolitic grainstones
130		04BOZ-48	Oolitic units are thin (.2-.8 m); oncoids with brachiopod nucleus, interbedded with thin lime mudstones
120		OBK7-23	Thin-bedded, heavily rippled, thin-bedded lime mudstones, with interbedded tan/brown, massive shale and banded, bioturbated lime wackestones
110		04BOZ-46	Thin-bedded, heavily rippled, thin-bedded lime mudstones, with interbedded tan/brown, massive shale and banded, bioturbated lime wackestones
100			
90			
80			
70			
60			
50			
40			
30			
20			
10			

sh ms vs ps gs ic

Xima 2

	Sample	Photo	Comments/Description						
400	04BOZ-51								
390									
380									
370									
360									
350									
340									
330									
320				OBK8-3,4		Basal, crumbly mudstones grade upwards into more resistant bioturbated lime wackestones			
310									
300				OBK8-1 OBK7-35,36		Resistant, cliff-forming beds of banded, bioturbated lime mudstone to wackestone and intraclastic conglomerate.			
290									
280				OBK7-33,34 OBK7-32					
270									
260									
250									
240									
230							OBK7-33,34		Intraclastic conglomerates usually capped by thicker oolitic grainstones
220									
210							OBK7-32		More resistant
200									

sh ms vs ps ga ic

Xima 3

Sample	Photo	Comments/Description
	04BOZ-55	Dolomitized intraclastic conglomerate
	OBK8-10 OBK8-9	Tan to brown, well-rounded, calcareous, fine sand-sized quartz arenite
		Medium to thin bedded, heavily fractured, fine sand-rich, dolomitic lime mudstones with burrows
		Calcareous sandstone
		Thin-bedded, green, calcareous siltstone, interbedded with intraclastic conglomerate
		Thin-bedded, green, calcareous siltstone, interbedded with intraclastic conglomerate
		Smaller mounds
	OBK8-6,7	Large mounds; 2-3 m high, 1.5-2 m wide, numerous individuals

Xima 4

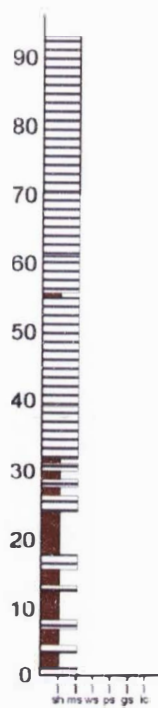
Sample	Photo	Comments/Description
<p>690 680 670 660 650 640 630 620 610 600</p> <p>sh ms ws ps ga ic</p>	<p>04BOZ-58</p> <p>OBK8-13,14</p> <p>OBK8-12</p> <p>OBK8-17,18</p>	<p>More massive beds of blue-gray, fossiliferous packstone</p> <p>Interbedded thin, blue-gray, fossiliferous packstones, sand-rich limestones and sandstones</p> <p>Rafinesquinidae brachiopod-rich grainstone</p> <p>Cross-bedded, medium to coarse sand-sized quartz arenite composed of rounded quartz grains; bioturbated</p> <p>Cross-bedded, fine to medium sand-sized quartz arenite composed of rounded quartz grains</p>

Chipanjing Section

	Sample	Photo	Comments/Description
200	04BOZ-79	OBK9-9,10	Blue-gray, mottled lime wackestone to packstone; abundant gastropod fossils (OBK9-11 to 16)
190			
180		OBK9-8	More massive sandstones relative to other sections, calcareous sandstone, abundant x-bedding
170			
160			Interval covered by sandstone boulders
150			Greenish-yellow siltstone with thin-bedded lime mudstone interbeds
140		OBK9-6	Sandy, biotubated dolomitic lime mudstone to wackestone Silty/argillaceous limestones
130			
120			Similar reddish, glauconitic/oolitic interbeds as Suhaitu section
110			Shale interbedded with thin-bedded fossiliferous grainstones
100	04BOZ-76	OBK8-35,36 OBK9-1,2,3	Abundant oncoids with reddish fringes
90			
80			Green calcareous siltstone
70			Interbedded, medium sand-sized, well-cemented, calcareous sandstones, green shales and skeletal packstones
60			
50			
40			
30			
20			
10			

Laosunmiao

Sample	Photo	Comments/Description
		Thin, bioturbated beds
	OBK2-15,16	Thicker lime mudstone beds
04BOZ-8,9, 10		Fewer shale beds
04BOZ-6,7	OBK2-10,11, 12,14 OBK2-5,6,7, 8,9	Thin bands of black chert Abundant graptolites Heavily fractured
04BOZ-1,2, 3, 4, 5	OBK1-35,36	Interbedded black shales and dark, laminated lime mudstone-graptolites Samples for source evaluation



Shitanjin 1

Sample	Photo	Comments/Description
04BOH-5		<p>Resistant</p> <p>Erosive</p> <p>OBK10-7,8,9 Large dunes</p> <p>Resistant</p> <p>Green, fissile shale Red siltstone Green limestone color</p> <p>OBK10-1,2,3 Microbial laminae</p> <p>OBK9-33,34,35,36 Bioturbated</p> <p>OBK9-31,32 Large storm channels, with trilobite fragment hash</p> <p>OBK9-30</p> <p>More recessive</p> <p>Individual bed thicknesses range from 1-40 cm thick</p>

Shitanjin 2

Sample Photo Comments/Description

Sample	Photo	Comments/Description
		Slope forming

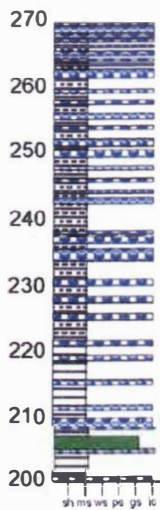
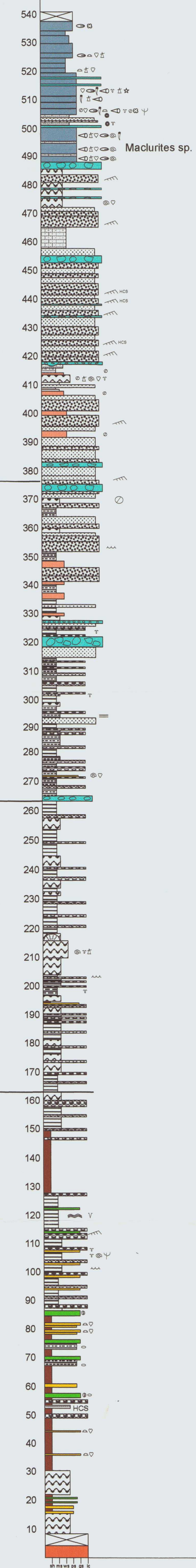


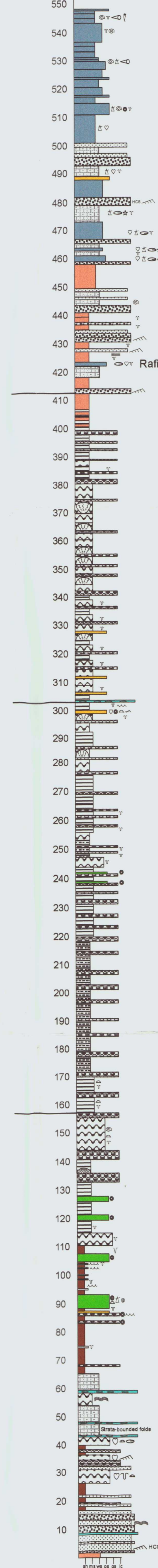
Plate 1-Stratigraphic Columns of NW Ordos

NE

Suhaitu

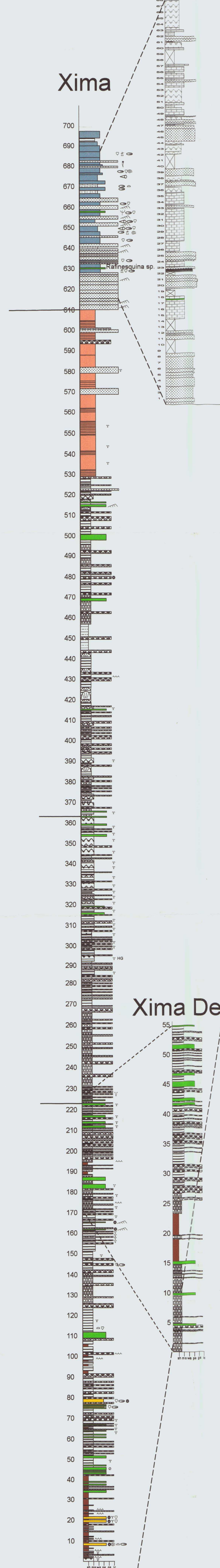


WZA

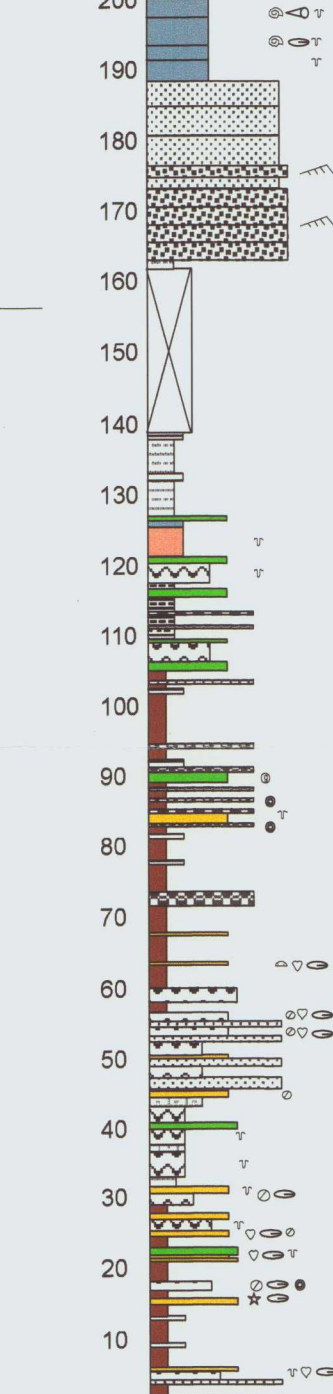


Xima Detailed 2

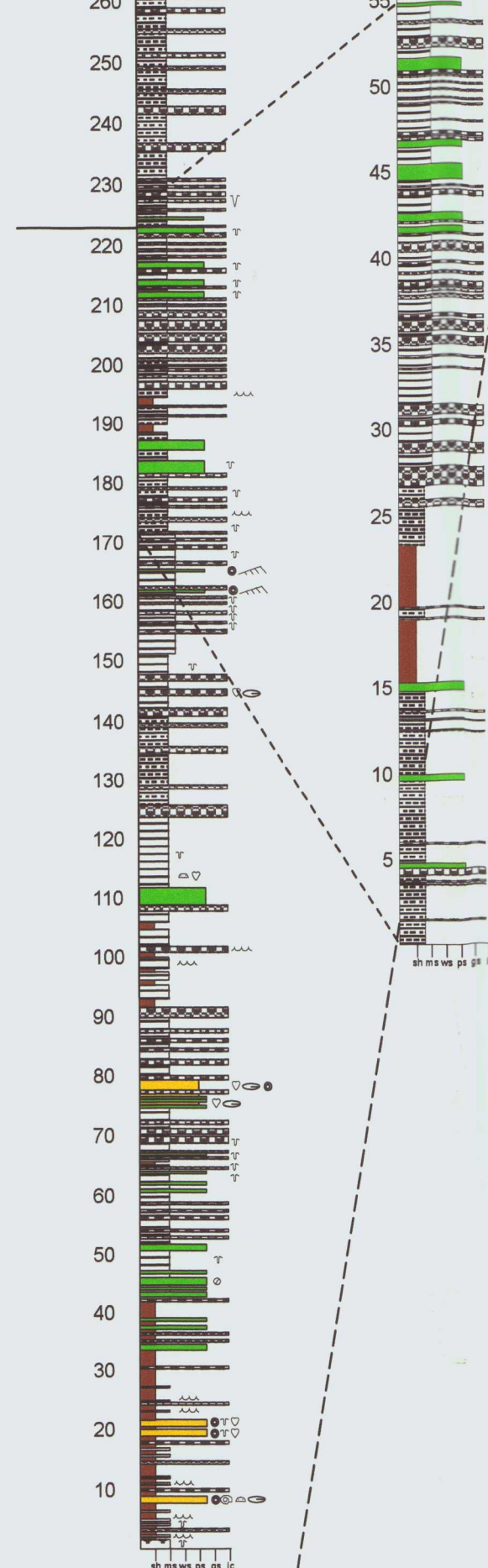
Xima



Chipanjing

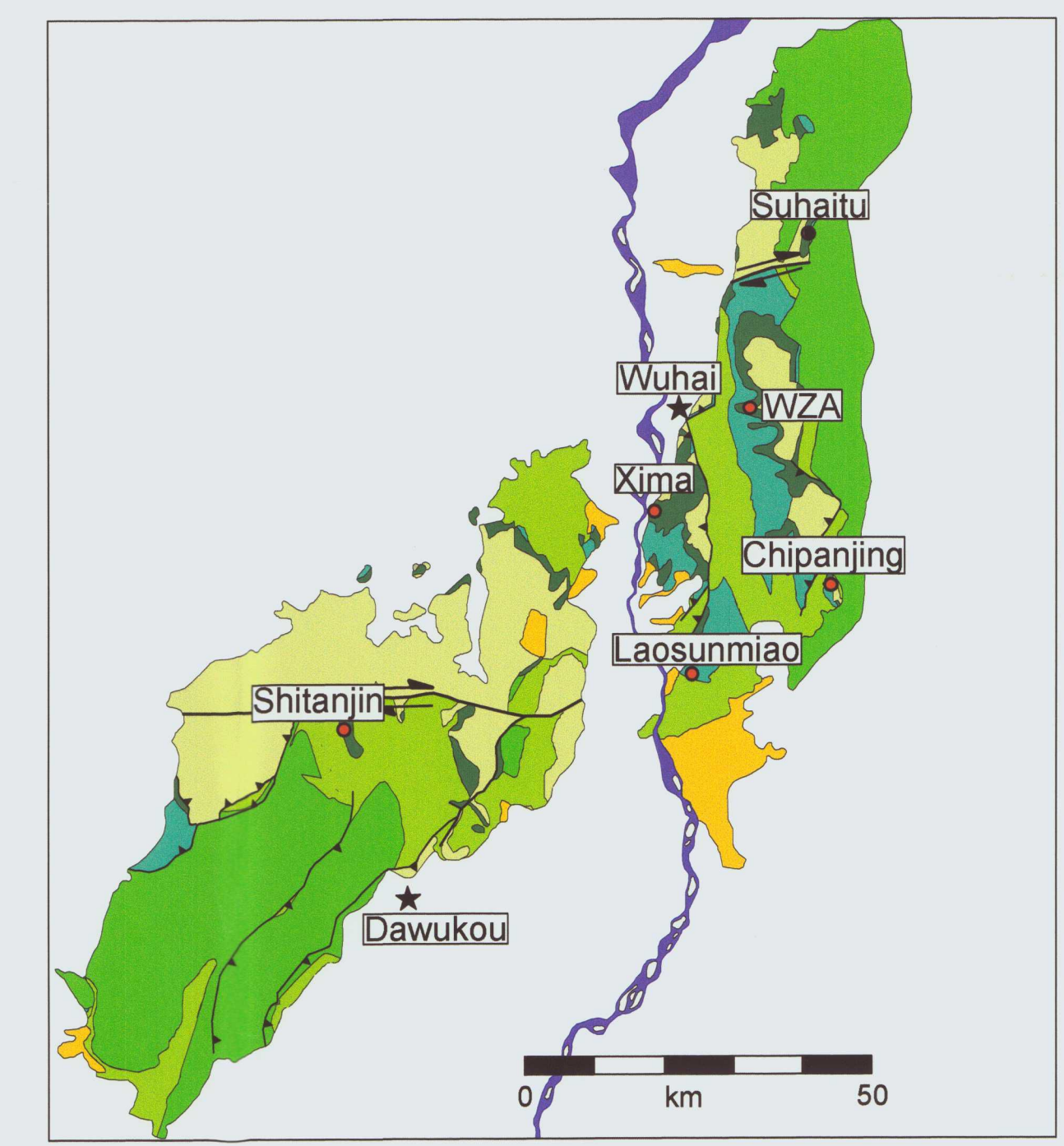
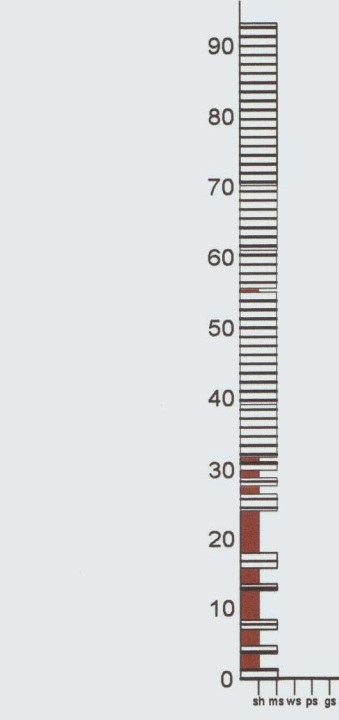


Xima Detailed 1

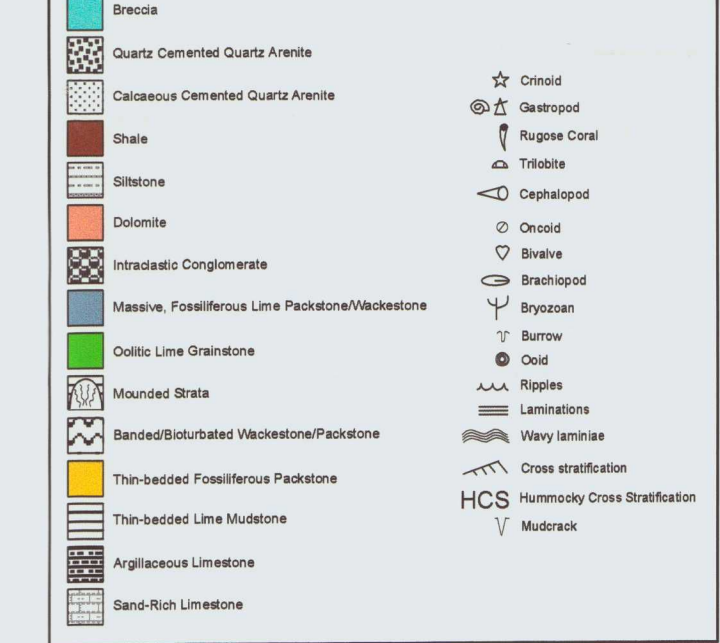


SW

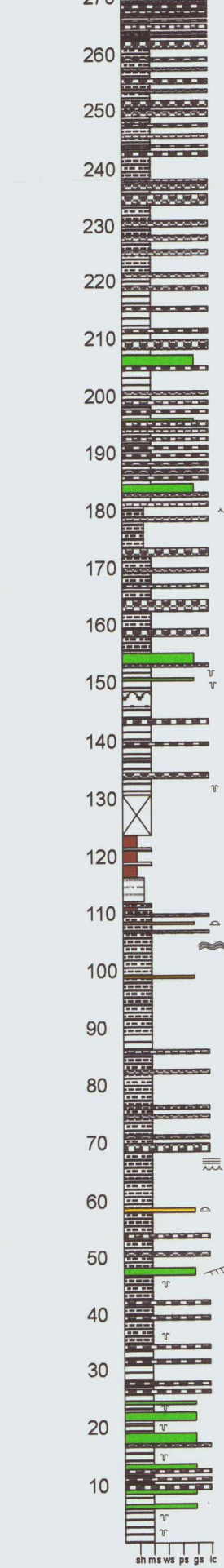
Laosunmiao



Stratigraphic Key



Shitanjin



26 km

19 km

2 km

18 km

24 km

Plate 2-Relative Sea-Level Curves for Primary Stratigraphic Sections in NW Ordos

